LBL PUB-5244
SLAC-352
CALT-68-1589

FEASIBILITY STUDY
for an
ASYMMETRIC B FACTORY
BASED ON PEP

October 1989

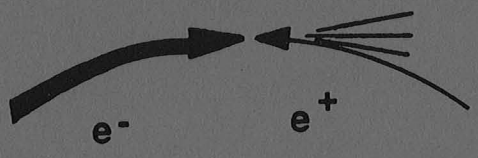

Prepared for the U.S. Department of Energy under Contract Numbers DE-AC03-76SF00098, DE-AC03-76SF00515, and DE-AC03-81-ER40050.

LBL PUB-5244
SLAC-352
CALT-68-1589

FEASIBILITY STUDY for an ASYMMETRIC B FACTORY BASED ON PEP

October 1989

Lawrence Berkeley Laboratory
1 Cyclotron Road
Berkeley, California 94720

Stanford Linear Accelerator Center
Stanford University • Stanford, California 94305

California Institute of Technology
Pasadena, California 91125

Prepared for the U.S. Department of Energy under Contract Numbers DE-AC03-76SF00098, DE-AC03-76SF00515, and DE-AC03-81-ER40050.

CONTENTS

Executive Summary

This report addresses the feasibility of designing and constructing an asymmetric B-factory—based on the PEP storage ring at SLAC—that can ultimately reach a luminosity of 1×10^{34} cm^{-2} s^{-1}. Such a facility, operating at the $\Upsilon(4S)$ resonance, could be used to study mixing, rare decays, and CP violation in the $B\bar{B}$ system, and could also study tau and charm physics. The essential accelerator physics, engineering, and technology issues that must be addressed to successfully build this exciting and challenging facility are identified, and possible solutions, or R&D that will reasonably lead to such solutions, are described. Based on this study, it can confidently be concluded that:

- Using state-of-the-art storage ring technology, careful engineering, and a well-thought-out design philosophy, it is possible to begin immediately to design and then construct an asymmetric B-factory that can be commissioned, a few years from now, at an initial luminosity of at least 10^{33} cm^{-2} s^{-1}

- By keeping the design flexible and providing sufficient "parametric reach" it will be possible for the collider to reach its ultimate luminosity goal of 1×10^{34} cm^{-2} s^{-1}

The investigations performed to date have been quite encouraging. A study of those issues that pertain to the high beam current requirements indicates that the anticipated problems are amenable to well-understood, albeit difficult, engineering solutions; no new phenomena have been uncovered that would lead to the need to develop entirely new technologies. A scheme for separating the closely-spaced beam bunches at the IP has been worked out in detail for the case of head-on collisions and shown to be feasible, and an alternative scheme based on a finite crossing angle scenario with crab-crossing also shows promise. Feasibility proofs for new rf cavities and feedback systems have been worked out, and the vacuum and heat load issues have been demonstrated to be solvable by straightforward application of modern storage ring vacuum system technology. The injection system requirements could be easily met by the present SLC injector complex. If that is not available, a newly built, similarly designed conventional system would be adequate.

To successfully reach our design goal, R&D efforts in a few specialized areas will be required. The primary topics that deserve further study include: high-power windows for delivering the rf power to the smallest possible number of rf cavities; high-power feedback systems to suppress multibunch instabilities; means to remove higher-order modes from the rf cavities and the power deposited into them; vacuum chamber designs capable of providing good vacuum in the presence of high synchrotron radiation power; and compact, high-gradient superconducting quadrupoles. In addition to these technology issues, there are several accelerator physics issues where further work is needed. Foremost among these is the continuation of our efforts to understand quantitatively the behavior of the beam-beam interaction for asymmetric beam conditions.

The PEP storage ring is an ideal platform from which to launch an asymmetric B-factory facility, having a well-designed, flexible lattice with suitably long straight sections, a tunnel that would permit the siting of a new low-energy storage ring, thereby avoiding extensive conventional facilities construction, and potential access to a powerful injector. These advantages, coupled with the existence—in close proximity—of a highly qualified and enthusiastic team of physicists from SLAC, LBL, LLNL, Caltech, and various university campuses, make this an ideal project for the SLAC site.

The design concept presented here provides an unprecedented opportunity for SLAC to extend the cutting edge of high-energy physics research and collider technology worldwide, and would make an ideal use of the PEP storage ring far into the future.

Foreword

This document represents the outcome of studies that were carried out at irregular intervals over the past 18 months, and which culminated in a series of meetings held jointly at LBL and SLAC during the summer of 1989. These and related gatherings bear witness to the enthusiasm and hard work contributed by a number of physicists and engineers from a variety of institutions listed on the following page.

The design of a high-luminosity collider, such as we are considering in this report, demands the very best and most innovative work in *all* of the areas that make up an operating high-energy physics laboratory, including high-energy experimentalists, accelerator physicists, and engineers. The design of an asymmetric B factory demands a true synthesis of the various disciplines. Unquestionably, the success of the machine will depend in large measure on the ability of these groups to establish a symbiotic relationship among themselves that will build on the strengths of each. In reading this document, it will become clear that this symbiosis has already begun.

The study reported on here, and the B Factory Collider Group Meetings that led to it, were coordinated by S. Chattopadhyay (LBL). This report was prepared under the scientific editorship of S. Chattopadhyay and M. Zisman (LBL); the technical editor was J. Chew (LBL).

Participants

- **California Institute of Technology**
  D. Hitlin; F. Porter

- **Lawrence Berkeley Laboratory**
  S. Chattopadhyay; Y.H. Chin; D. Dell'Orco; E. Forest; M. Furman; A.A. Garren; E. Hoyer; K. Kennedy; G. Lambertson; C.C. Lo; H. Nishimura; P. Oddone; M. Ronan; A. Sessler; B. Taylor; C. Taylor; M. Zisman

- **Lawrence Livermore National Laboratory and University of California at Los Angeles**
  W. Barletta

- **Stanford Linear Accelerator Center**
  M. Allen; E. Bloom; D. Burke; M. Cornacchia; W. Davies-White; H. Destaebler; M.H. Donald; J. Dorfan; G. Feldman; J. Rees; H. Schwarz

- **IIRPA/University of California at San Diego**
  M. Sullivan

- **LBL Visitors**
  B. Autin (CERN); J. Tennyson

- **SLAC Visitors**
  B. Brabson (Indiana University); K. Oide (KEK)

1. Introduction

The study of rare and CP-violating B-meson decays holds great promise as a fundamental probe of the Standard Model and whatever new physics may lie beyond it. An ideal way to carry out such a study would be to construct a high-luminosity electron-positron collider to serve as a "B factory." The physics potential of such a facility is discussed in detail in a companion paper.[1]

There are various possible approaches to the design of such an electron-positron collider, including storage-ring, linac-on-linac, and linac-on-storage-ring scenarios. At the present time, the linac-based approaches must be considered to be more speculative, since the technologies of linear colliders and high-power, high-repetition-rate, high-brilliance linacs are still in their infancy. Moreover, in the energy range of interest for a B factory, such alternatives do not seem to offer any significant advantages over storage-ring colliders, which correspond to a more straightforward extrapolation of the present state of the art. Consequently, the many major laboratories worldwide that are now enthusiastically pursuing the design of a high-luminosity B-factory, e.g., CESR at Cornell,[2] KEK in Japan,[3] INP at Novosibirsk,[4] Paul Scherrer Institute in Switzerland,[5] and DESY in Germany,[6] have uniformly focused on storage-ring colliders.

Because of the rare decay modes that must be observed with good statistics to study CP violations, luminosity is of paramount importance in B-meson physics. The required luminosity for observing CP violation depends on several parameters of the Standard Model that are in a continuous state of refinement. This is discussed in some detail in Chapter Two of the companion report.[1] It appears that a luminosity in the range of 10^{33}–10^{34} $cm^{-2}\,s^{-1}$ is sufficient for asymmetric storage rings at the $\Upsilon(4S)$ resonance.[1,7]

A luminosity of 1×10^{34} $cm^{-2}\,s^{-1}$ is approximately two orders of magnitude beyond that provided by existing electron-positron colliders, so a colliding-beam storage ring complex designed to reach luminosities in the range of 10^{33} to 10^{34} $cm^{-2}\,s^{-1}$ is a bold venture. It sets goals well beyond those that have been approached before, and naturally suggests the question: Is it

plausible that a machine with such high performance can be realized with storage ring technology as we now understand it? We believe the answer is yes. The task confronts us with challenges of many kinds, but we think we understand them well enough to attack them with a good hope of success.

1.1. Luminosity Requirements and Feasibility

The history of colliding-beam storage rings, since its inception in the 1950s, has offered a mixed bag of successes and disappointments. Many of the machines have reached their beam-energy goals, but some have fallen well short of their luminosity goals. On the other hand, most of the recent electron-positron rings have approached their design luminosities; CESR and BEPC (in a remarkably short time) have even exceeded their design luminosities. Most of these machines are of the single-ring variety in which one or a few bunches are stored in each beam and collide at a few interaction regions.

We recognize, of course, that the few attempts to use double rings and multiple bunches have been disappointing. Most relevant, perhaps, is Doris as it was originally built at DESY. When Doris came on line in 1973, difficulties were encountered due to the finite beam crossing angle (i.e., the beams met at an angle rather than head-on) and the large number of bunches in each beam. Although these problems were never completely overcome, and in the end Doris was converted to a single-ring system, it is noteworthy that currents up to 0.75 A had been successfully stored in a single ring and currents of several hundred mA had been collided in the double-ring configuration. In interpreting these historical data, it is also important to remember the circumstances at the time. SPEAR had been running since 1972 and churning out data in an energy region that turned out to be exceptionally important; the "November revolution" was in the offing and the users at Doris wanted to get on with the physics. Perhaps a more sustained effort could have solved more of the multibunch problems; we shall never know.

In any case, the physics of B mesons, and especially of their charge- and parity-violating decays, demands that colliding-beam systems of unprecedentedly high luminosity be created for their study. The laws of storage ring behavior force us to use large numbers of bunches in double rings whether we require

asymmetric collisions or not. Thus, we are on the luminosity frontier rather than the energy frontier. SPEAR, Doris, Petra, PEP, and LEP have pushed forward the energy frontier for electron-positron collisions; a B factory would drop back from the energy frontier but push forward the luminosity frontier.

Great strides have been made in the physics of beam instabilities and current limitations in the last decade, and we believe that there is a good chance that we can achieve the demanding goals of B-meson physics. In this document we will show that—with innovative design approaches and suitable R&D efforts—*it is possible to design a collider that has sufficient design flexibility to begin with an initial luminosity of at least* 1×10^{33} cm^{-2} s^{-1}, *to grow quickly to* 3×10^{33} cm^{-2} s^{-1}, *and to ultimately reach* 1×10^{34} cm^{-2} s^{-1}. With progressive R&D and with state-of-the-art technology applied in the initial implementation, construction of such a collider could begin immediately.

1.2. APIARY: PEP plus a New 3.1-GeV Ring

We have conducted preliminary investigations of a design for a B factory to be sited at SLAC. The specific scenario we consider, APIARY (Asymmetric Particle Interactions Accelerator Research Yard), involves a high-luminosity, asymmetric, 9 GeV $\times$ 3.1 GeV electron-positron collider with a high-energy storage ring based on PEP and a newly constructed low-energy ring. For the purposes of this report, we have considered two scenarios for siting the low-energy ring: one in which it has one-third the circumference of PEP and is housed in a separate tunnel, and another in which it has the same circumference as PEP and is housed in the PEP tunnel. Both options are intended merely to serve as "proofs of principle."

Since the separate-tunnel scenario has presently been explored in more detail, we have emphasized the complete description of this case. *We stress, however, that a scenario involving a larger ring in the PEP tunnel is the preferred choice*, for reasons that will become clear later in this report. Thus, in the future, the conceptual design of the APIARY facility will focus on that case—a large low-energy ring that coexists with the high-energy ring in the existing PEP tunnel.

It is somewhat arbitrary which ring contains the electrons and which contains the positrons; we will assume that the positrons reside in the low-energy ring. The rationale for this choice is that any problems that might arise from trapped ions in the electron ring will likely be less severe if the electron beam has the higher energy. Further, if the low-energy ring has a smaller circumference than the high-energy ring, it will require fewer particles to reach a given beam current. This fact would also favor putting positrons (which are more difficult to produce) in the smaller ring. Of course, having fewer particles in the low-energy ring would imply a poorer luminosity lifetime, so this choice is not without some drawbacks.

The PEP storage ring is well suited to its role in the APIARY collider, needing only straightforward hardware upgrades to achieve the requisite luminosity capability. Moreover, the operating PEP ring provides an ideal test-bed for the R&D activities that will be required to realize the full luminosity potential of the facility. The high-luminosity APIARY collider, operating at the $\Upsilon(4S)$ resonance, could be used to study mixing, rare decays, and CP violation in the $B\overline{B}$ system, as well as tau and charm physics. These possibilities have been discussed in detail elsewhere.[1]

The choice of an *asymmetric* collider in this energy range gives certain quantitative advantages from the detector and machine-design viewpoints. The companion paper describes the detector advantages.[1] At the $\Upsilon(4S)$ resonance, the minimum acceptable asymmetry is 1:3, with a rather broad optimum between the low end of the range of possibilities (9 GeV $\times$ 3.1 GeV) and the high end (12 GeV $\times$ 2.3 GeV). From the accelerator point of view, a lower asymmetry eases some of the difficulties associated with the disparity in energy between the two rings. For this reason, we have settled on beam energies in the APIARY collider of 9 GeV and 3.1 GeV for the high-energy and low-energy rings, respectively. A distinct advantage of an asymmetric design is that it allows high collision frequencies (up to 100 MHz) in a head-on colliding mode based on magnetic separation.

To accomplish the design of a high-luminosity, asymmetric B factory, two major classes of technical problems have to be addressed: issues related to achieving high luminosity, and issues associated with heteroenergetic colliding beams.

The high-luminosity issues are generic to all B-factory designs, and imply the need for high average and high peak currents in the collider. The current requirements are another reason (besides the energy asymmetry) for using two separate storage rings, as opposed to the typical collider design in which electron and positron beams are counter-rotating in a single ring. Difficulties associated with high beam currents include:

- Beam lifetime degradation arising from synchrotron-radiation-induced gas desorption from the walls
- Longitudinal and transverse coherent beam instabilities (both single-bunch and multibunch)
- Synchrotron radiation power dissipation in the vacuum chamber walls

The second set of issues—the one associated with heteroenergetic colliding beams—is unique to the asymmetric scenario. Areas of concern include:

- Complications arising from the physics of the beam-beam Coulomb interaction between heteroenergetic beams that may limit the intrinsic luminosity
- Beam separation requirements, which imply constraints on the choice of interaction region (IR) parameters and the design of the collision optics
- Detection system requirements, such as the need for a small beam pipe radius—on the order of 3 cm at the interaction point (IP)—for determining vertices

Given the many challenges that must be met to achieve our ultimate luminosity goal of 1×10^{34} cm^{-2} s^{-1}, *the approach we have followed here is aimed at maintaining the maximum possible flexibility and "parametric reach" for our design.* We believe that this philosophy will ensure reaching our design goals in the minimum possible time.

2. Collider Design Issues

In this section we discuss machine physics and engineering issues, as summarized previously, that guide and constrain the APIARY design.

2.1. Luminosity

The general expression for luminosity in an asymmetric collider is cumbersome, involving various parameters of both beams at the IP. To simplify the choices, and to elucidate the general issues of luminosity for all B factories, it is helpful to express the luminosity in an energy-transparent way. Here we express luminosity in terms of a single, common beam-beam tune shift parameter, ξ, along with a combination of other parameters taken from *either* the high-energy (e^-) or the low-energy (e^+) ring, irrespective of energy.

With a few plausible assumptions (e.g., complete beam overlap at the IP and equal beam-beam tune shifts for both beams in both transverse planes) such parameters as energy, intensity, emittance, and the values of the beta functions at the IP may be constrained to satisfy certain scaling relationships. (Details on our approach are presented in Appendix A.) It then becomes possible to express luminosity in a simple, energy-transparent form:[8]

$$\mathcal{L} = 2.17 \times 10^{34}\, \xi\, (1 + r) \left(\frac{I \cdot E}{\beta_y^*} \right)_{+,-} \quad [\mathrm{cm}^{-2}\, \mathrm{s}^{-1}] \qquad (2.1\text{–}1)$$

where

- ξ is the maximum saturated dimensionless beam-beam interaction parameter (the same for both beams and for both the horizontal and the vertical transverse planes)
- r is the aspect ratio characterizing the beam shape (1 for round, 0 for flat)
- I is the average circulating current in amperes
- E is the energy in GeV
- β_y^* is the value of the beta function at the IP in cm

The subscript on the combination $(I \cdot E/\beta_y^*)_{+,-}$ means that it may be taken from either ring.

In this report, the scaling relations derived in Appendix A are used to produce self-consistent sets of parameters. After a few basic parameters are chosen, such as the energies, the currents, the aspect ratios, and the lowest beta value at the IP for either ring, most of the other parameters, including the luminosity $\mathcal{L}$, will follow. To a certain extent, the choice of which parameters should be specified and which should be derived is somewhat arbitrary. Nonetheless, as discussed below, there are many practical considerations that limit the degrees of freedom in maximizing the luminosity.

Energy. The energies, $E_{+,-}$, are not entirely free parameters; they are constrained kinematically. To take advantage of the cross section enhancement at the $\Upsilon(4S)$ resonance, the collider center-of-mass energy must be 10.58 GeV. Precise determination of the interaction vertex with a reasonable detector geometry then limits the energy ratio to the range of about 1:3 to 1:5. Considerations of the beam-beam interaction (see below) argue for approximately equal damping time per collision ("damping decrement") in the two rings, which is more easily accomplished when the energy asymmetry is reduced. Taken together, these considerations lead to an optimum energy of the high-energy beam of $E \approx 8$–12 GeV, and the corresponding energy of the low-energy beam is thus $E \approx 2.3$–3.5 GeV. For this design study, we have adopted a low asymmetry, that is, $E_- = 9$ GeV and $E_+ = 3.1$ GeV.

Beam-beam tune shift. The beam-beam tune shift parameter ξ is not really a free parameter; it is determined intrinsically by the nature of the beam-beam interaction. The range of maximum beam-beam tune shifts achieved in existing equal-energy e^+e^- colliders is $\xi \approx 0.03$–0.07. A typical—perhaps conservatively optimistic—choice would be $\xi = 0.05$; this value is the basis of our luminosity estimates. Insofar as higher tune-shift values than this have already been observed at PEP, we consider this value to be quite justifiable. There is evidence from computer simulations[9] that ξ may depend intrinsically on the beam aspect ratio; in other words, that $\xi = \xi(r)$. This is a controversial issue, now being debated, but it is known that an enhancement in ξ (for round beams) of at best a factor of two can be obtained. In the luminosity estimates made here, we did not take this possible enhancement into account; that is, we took $\xi = 0.05$, independent of r.

One implication of this tune-shift limitation is that increased luminosity must perforce come from decreasing the bunch spacing s_B —that is, increasing the number of bunches. The push towards small bunch spacing has a significant impact on the design of the IR, which must separate the beams sufficiently to avoid unwanted collisions, and it also exacerbates the problem of coupled-bunch beam instabilities.

Beam aspect ratio. The aspect ratio, r, is free to the extent that one can create round beams. However, the physics of the beam-beam interaction is sensitive to the method (coupling resonances, vertical wigglers, etc.) that is used to make the beams round. Although the use of coupling resonances is a straightforward way to obtain a round beam, it is not clear that applying such a constraint in tune space—where the nonlinear effects of the beam-beam interaction manifest themselves—is the best thing to do. The use of vertical wigglers offers the potential advantage of giving round beams via a noiselike excitation that should not correlate with the subtleties of the nonlinear tune-space behavior. In the low-energy ring, one might imagine the practical use of vertical wigglers to create a large vertical emittance corresponding to $r = 1$.

In the case of the high-energy ring, where the synchrotron radiation emission in the horizontal bending magnets is already very large, the addition of sufficient vertical wigglers (in an intentionally created vertically dispersive region) to produce a round beam is nontrivial but is certainly possible. This technique may, however, be impractical from the viewpoint of synchrotron radiation power. If so, optics changes (via skew quadrupoles) may be the preferable way to create round beams in the high-energy ring. In any case, the maximum enhancement from the use of round beams is by a geometric factor of two—that is, $r = 1$ gives $(1+ r) = 2$ in Eq. (2.1–1).

Beam intensity. The average beam current, I, is a relatively free parameter, but not absolutely so. It is determined by various current-dependent coherent effects. The storage rings will have to accept the chosen current, given a certain impedance in the

paths of the beams. There are several intensity-dependent issues with which we must be concerned:

- Longitudinal microwave instability, which causes individual beam bunches to grow both in length and in momentum spread; both the resultant center-of-mass energy spread and the increased bunch length can reduce the luminosity
- Transverse mode-coupling instability, which limits the maximum current that can be stored in a single beam bunch
- Touschek scattering, which causes particle loss (from large-angle intrabeam scattering) and reduces the beam lifetime
- Coupled-bunch instabilities, which, unless controlled by feedback, can lead to unstable longitudinal or transverse motion and thus to either beam loss or luminosity loss
- Synchrotron-radiation-induced gas desorption, which can lead to very high background gas pressure and thus to beam losses from gas scattering
- Synchrotron radiation heating of the vacuum chamber wall, which can lead to melting of the chamber if the power density is sufficiently high

Based on our present estimates, the issues of most concern to the APIARY design are coupled-bunch instabilities (driven by parasitic higher-order modes of the rf system); synchrotron-radiation heating; and synchrotron-radiation-induced gas desorption. To deal with the first issue, we propose a modern, low-impedance rf cavity design (either superconducting or room temperature). The problems arising from synchrotron radiation will require innovations in vacuum chamber design, but should be manageable if sufficient care is taken in engineering. These problems will be discussed later in this document.

Beta function at the IP. The beta function at the IP, β_y^*, is a free parameter and is easily variable down to a few centimeters, subject to the bunch-length condition $\sigma_\ell \leq \beta_y^*$. As the beta functions are reduced, however, it becomes more difficult to maintain the required short bunches. Either the rf voltage becomes excessive or the IR optics become unmanageable due to the difficulty of refocusing the beam quickly enough to avoid

very large beta functions elsewhere in the ring. For this stage of the design, we consider a bunch length of $\sigma_\ell = 1$ cm to be a sensible target value, which then restricts the value of β_y^* to the range of 1–2 cm.

From Eq. (2.1-1), it is clear that the luminosity is maximized by high currents, low β_y^*, and round beams. What are the implications regarding these parameters for a luminosity goal of 1×10^{34} cm^{-2} s^{-1} ? Following the conservative route, we plan to use a typical low β_y^* of a few centimeters; $\xi \approx 0.05$; and round beams ($r = 1$). These choices imply an average circulating current, I, of several amperes. This is the approach we recommend at this point. If the intrinsic maximum tune shift were truly enhanced for round beams, another twofold improvement in luminosity could be expected.

An alternative—and much more speculative—approach could employ an extremely low β_y^* of a few mm, implying the need for a beam current of only a few hundred mA to reach our luminosity goal. The hardware issues involved in producing such a low β_y^* are nontrivial. More importantly, submillimeter bunch lengths would be needed as well, since the luminosity degrades unless $\sigma_\ell \leq \beta_y^*$. One way of producing ultrashort bunches is to use a zero-momentum-compaction ($\alpha = 0$) isochronous ring in which the particle path length is independent of energy.[10,11] Bunch length is then determined solely by injection conditions. However, one needs not only a very precise "zero" value for the momentum compaction, but also good control of the effects of higher-order, nonlinear momentum-compaction coefficients. To build such a ring would be quite challenging, requiring substantial technology R&D in precise control of magnetic fields. Studies along these lines are under way, but for now we favor the more traditional and conservative approach outlined above.

2.2. Beam-Beam Interaction

The attainable luminosity in the APIARY collider will be determined to a large extent by the physics of the beam-beam interaction. Very little is known experimentally about the "beam-beam tune-shift limit" under asymmetric energy conditions. The situation is complicated, since two beams with unequal energies naturally tend to behave differently. Indeed, what is often observed in computer simulations is that one beam blows up badly while the other beam suffers practically no blowup. This is a serious problem, since the significant blowup in the weaker beam imposes an unnaturally low beam-beam tune shift limit on the stronger beam.

Probably the best cure is to bring the beam-beam interaction into the "strong-strong" regime where the two beams blow up in a similar manner, reducing the beam-beam force on both beams simultaneously. In this way—putting the two beams on an equal footing as far as transverse dynamics is concerned—we might expect to reach the same maximum beam-beam tune shift limit set by nature in equal-energy colliders. Such circumstances, if they can be created, would provide the best possible rationale for the design of an asymmetric collider based on the only fact we know about the actual behavior of the beam-beam effect under symmetric conditions—the beam-beam tune shift limit, ξ, in equal-energy electron-positron colliders.

The beam-beam interaction in the strong-strong regime is not well understood in a quantitative sense at present. The only systematic tool to understand it is provided by computer simulations. Consequently, one must allow for the maximum possible flexibility and freedom in adjusting those parameters which, as indicated by numerical simulations and critical wisdom, will affect luminosity. Such parametric flexibility will be essential in tuning the collider to the highest tune-shift limit and therefore the highest luminosity. One may need to vary the beam emittances, sizes, and shapes (aspect ratios), as well as the damping decrement (damping rate per collision), in order to optimize luminosity.

Numerical simulations suggest that an asymmetric collider should have a parametric reach up to the "asymmetric energy transparency domain," where both beams have identical values for each of the parameters listed below.

1. Linear beam-beam tune shift parameter:

$$\left(\frac{\beta^-}{\beta^+}\right) \cdot \left(\frac{\gamma^+ N^+}{\gamma^- N^-}\right) = 1 \qquad (2.2\text{–}1)$$

2. Cross sectional area at the IP:

$$\sigma^+ = \sigma^- \qquad (2.2\text{–}2)$$

(and possibly equal emittance values also).

3. Radiation damping decrement per collision:

$$\lambda^+ = \lambda^- \qquad (2.2\text{–}3)$$

where the damping decrement, $\lambda = \gamma_{SR}\tau_C$, is defined as the product of the absolute radiation damping rate γ_{SR} (s^{-1}) and the time interval τ_C (s) between collisions.

4. Betatron phase modulation due to synchrotron motion:

$$\left(\frac{\sigma_\ell Q_s}{\beta_y^*}\right)^+ = \left(\frac{\sigma_\ell Q_s}{\beta_y^*}\right)^- \qquad (2.2\text{–}4)$$

where σ_ℓ is the rms bunch length and Q_S is the synchrotron tune.

With parameters constrained by these four conditions, the two unequal-energy beams behave identically as far as beam-beam effects in the transverse plane are concerned—they evolve dynamically in a similar manner and saturate to the same ξ value. If the conditions above are not satisfied, the two beams settle quickly to a "weak-strong" situation.

To demonstrate the validity of these criteria by showing that they maintain symmetric behavior in the case of asymmetric beam energies, we apply a modified version of Yokoya's beam-beam simulation program[12] to a situation in which a PEP beam at 12 GeV collides with a 2 GeV beam from a small ring. (This scenario, an early version of the present design, is referred to as APIARY-I.) Yokoya's program tracks particles in a bunch subjected to various localized disturbances, including rf energy kicks; radiation losses; random energy kicks due to photon emission; and a series of motions representing one turn around the storage ring—a linear rotation of betatron phase in a half-arc, followed by a thick-lens nonlinear beam-beam kick in the transverse plane (derived from the integrated force of a Gaussian beam), and again a half-arc of linear betatron phase rotation (thus completing the full-turn map).

For the studies reported here, Yokoya's program has been modified to track unequal-energy beams and to include a thick-lens beam-beam force in its simulations. The thick-lens modification was motivated by Siemann's recent finding[9,13] that the betatron phase advance during the collision may give non-negligible effects in beam blowup when the beta function at the interaction point, β^*, becomes comparable to the bunch length. He concluded that it is necessary to treat the beam-beam interaction as a thick element. We incorporate this thick-lens approximation into Yokoya's program by distributing beam-beam kicks into five longitudinally different positions and letting particles drift between them. The rms beam sizes of the incoming beams are assumed to be unchanged during the collision in this approximation.

Simulation Results

The main parameters of the original APIARY-I lattice (used in the simulations described in this section) are shown in Table 2.2–1 below.

Table 2.2–1
Main parameters of the original APIARY-I collider

	Low energy	High energy
Energy, E [GeV]	2	12
Circumference, C [m]	155.3	2200
Number of bunches, k_B	6	81
Emittance, ε_x [nm·rad]	300	100
Bunch length, σ_ℓ [mm]	27.7	16.2
Transverse damping time, $\tau_{x,y}$ [ms]	16.3	15.6
Beta functions at IP		
β_x^* [cm]	25.4	76.2
β_y^* [cm]	2.54	7.62
Bunch current I_b [mA]	89.1	3.3
Nominal beam-beam tune shift		
ξ_{ox}	0.05	0.05
ξ_{oy}	0.05	0.05
Luminosity, $\mathcal{L}$ [$cm^{-2}\,s^{-1}$]	5×10^{32}	

These parameters satisfy the four important criteria discussed earlier. The next few pages discuss how each criterion is satisfied.

Criterion 1: same cross-sectional area at IP:

$$\sigma_{x,-} = \sigma_{x,+}$$

$$\sigma_{y,-} = \sigma_{y,+} \ .$$

Criterion 2: same nominal beam-beam tune shift:

$$\xi_{ox,-} = \xi_{oy,-} = \xi_{ox,+} = \xi_{oy,+} \ ,$$

where the quantities of the low and the high energy rings are denoted by the subscripts + and -, respectively.

With these parameters, the beam-beam kicks are equalized in the two rings; any difference in beam dynamics should come from the difference of beam parameters elsewhere in the rings. The computer simulation results for this case are summarized in Figs. 2.2–1 and 2.2–2.

Note that a subscript of zero beneath the tune shifts and beam sizes denotes a *nominal* value determined at the input of the simulation program, in the absence of the beam-beam interaction. The beam-beam simulation modifies these parameters, which settle down to their saturated values. These saturated values, which we refer to as the *dynamic* tune shifts and beam sizes, are written without the subscript zero.

Figure 2.2–1a shows the rms beam sizes as a function of the nominal beam-beam tune shift, ξ_0. One can see that the low-energy beam blows up badly in the vertical plane, while the high- energy beam is practically unperturbed.

Fig. 2.2–1b shows the dynamic beam-beam parameter, ξ, as a function of ξ_0. Reflecting the vertical blowup of the low energy beam, the tune-shifts ξ_- of the high energy beam are suppressed to small values, e.g., $\xi_{y,-} < 0.008$. Note that, at low tune shifts, the luminosity goes up in proportion to the square of the beam current; this phenomenon is followed by a linear rise before saturation.

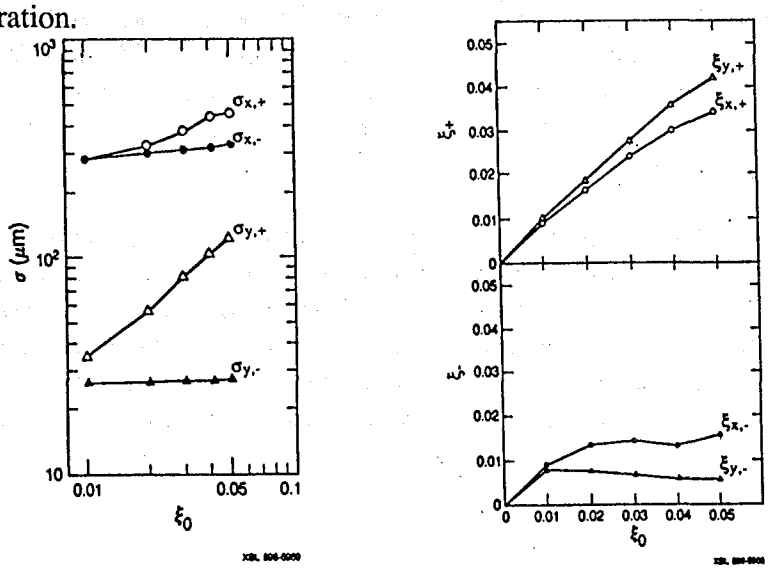

Fig. 2.2-1a (left)
RMS beam sizes predicted for nominal APIARY-I parameters.
Fig. 2.2–1b (right)
Dynamic beam-beam parameters ξ as a function of ξ_0 for the original APIARY-I lattice parameters.

The actual luminosity at $\xi_0 = 0.05$ drops by a factor of 5 from the design value, as shown in Fig. 2.2–2 below.

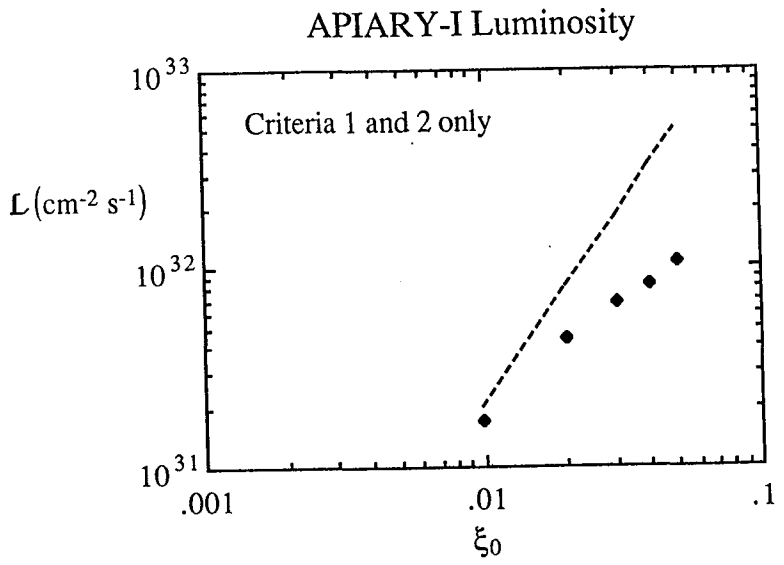

Fig. 2.2–2
Luminosity as a function of ξ_0 for the original APIARY-I lattice parameters.

In Quest of the Strong-Strong Situation

In the course of numerous simulations we achieved—by trial and error—identical behavior of two beams with unequal energies. Because we do not have enough space to describe all the attempts, we present here only the main results that lead to the asymmetric energy transparency condition.

Criterion 3: same damping decrement.

Synchrotron-radiation damping is an important effect that suppresses external perturbations of beams. There is some evidence[14] that the larger the damping rate, the larger the beam-beam limit will be. From Criterion 2, the strength of the beam-beam kick per turn is equal in the two rings. However, the number of kicks *per damping time* is different for the nominal APIARY-I parameters: the low-energy beam receives about 14 times more kicks than the high-energy one. Therefore, the low-energy beam is subjected more to the beam-beam interaction, which may partially explain the asymmetric behavior of the two beams shown in Fig. 2.2–1.

Figure 2.2–3a shows the rms beam sizes when the damping decrement of the low-energy beam is increased to the same value as that of the high-energy beam. Now, the vertical blowup of the low energy beam is reduced significantly compared with that in Fig. 2.2–1. The dynamic beam-beam parameters, ξ_+ and ξ_-, are plotted in Fig. 2.2–3b as a function of ξ_0. The horizontal ξ values behave almost identically, and the saturating value of $\xi_{y,-}$ is increased to about 0.017. The luminosity is shown in Fig. 2.2–4 as a function of tune shift; although improved, it still falls short of the design luminosity.

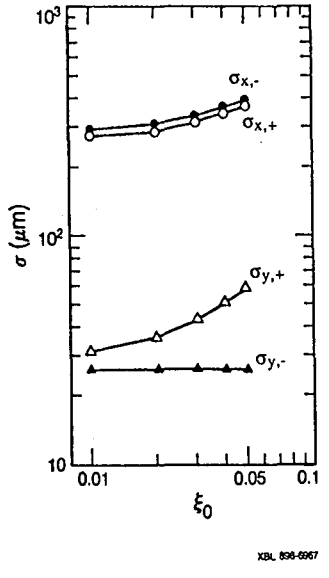

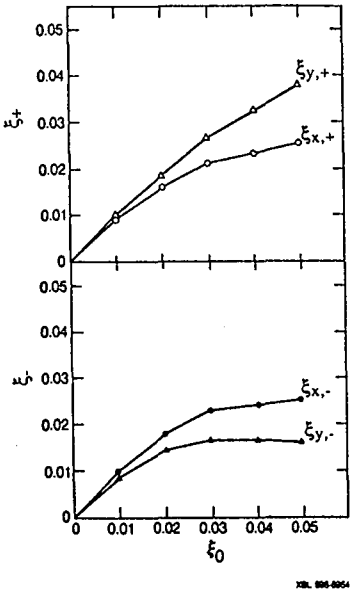

Fig. 2.2-3a (left) *RMS beam sizes when the two rings have the same damping decrement.*

Fig. 2.2–3b (right) *Dynamic beam-beam parameters ξ as a function of ξ_0. The two rings have the same damping decrement.*

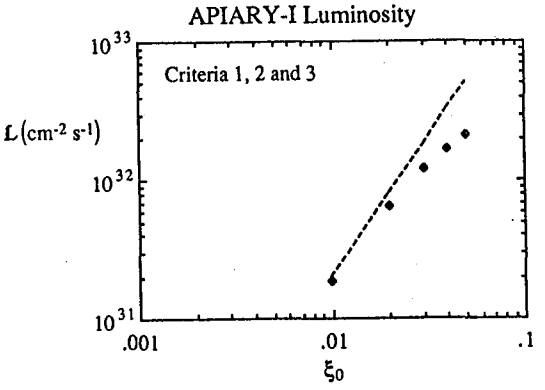

Fig. 2.2–4
Luminosity as a function of tune shift for the original APIARY-I lattice parameters.

Criterion 4: Same betatron phase modulation due to synchrotron motion (with possibly the same synchrotron tune).

A particle with a longitudinal displacement s from the center of the beam collides with the center of the incoming beam not at the designed IP but at a position longitudinally shifted by s/2. This actual collision point moves, turn by turn, because the particles execute synchrotron oscillations. Thus, the betatron phase advance per turn is also oscillating. This may excite synchrobetatron resonances, which may reduce the beam-beam limit substantially when β^* becomes comparable to the bunch length σ_ℓ. The amplitude of the tune modulation is given[15] by $\sigma_\ell Q_s/\beta^*$, where Q_s is the synchrotron tune. Figure 2.2–5 shows the simulation results when the values of $\sigma_\ell Q_s/\beta^*$ are equalized in the two rings by adjusting σ_ℓ and Q_s. The betatron tunes and Q_s are also set equal in the two rings. From Fig. 2.2-5b, it can clearly be seen that the beam behavior has been almost equalized. Now, the beam-beam tune shift limit comes horizontally, but no saturation of ξ_x is observed.

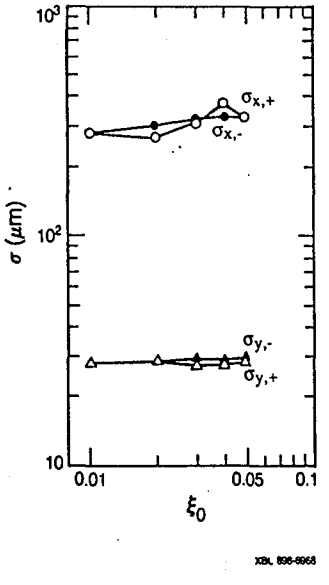

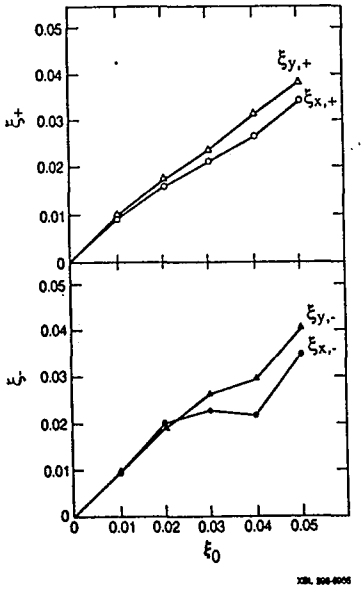

Fig. 2.2-5a (left)
RMS beam sizes when all four criteria have been satisfied.
Fig. 2.2–5b (right)
Dynamic beam-beam parameters ξ as a function of ξ_0 when all four criteria have been satisfied.

Figure 2.2–6 shows the corresponding luminosity trend, which nearly reaches the design luminosity at $\xi = 0.05$.

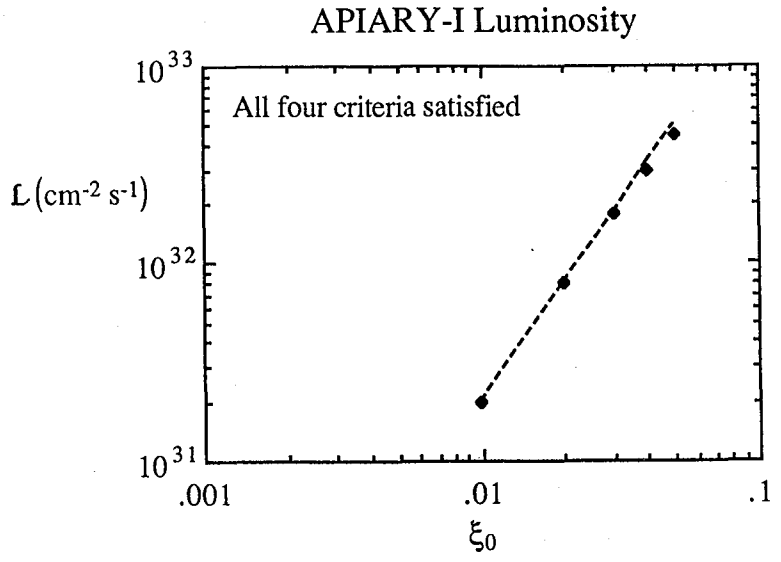

Fig. 2.2–6
Luminosity as a function of ξ_0 when all four criteria have been satisfied.

Coherent Effects

Thus far, we have studied the incoherent effects of the beam-beam interaction upon the colliding beams. However, beam-beam interactions can also excite *coherent* beam oscillations, which may become unstable in some regions of the tune diagram ("stopbands"). The dominant coherent effect is dipole motion of the center-of-mass of the beam;[16] the existence of this phenomenon has been well established experimentally. It leads to instability under any of the following resonance conditions:

$$(k_{B,+}\nu_+ + k_{B,-}\nu_-) = \text{integer},$$
$$2\nu_- = \text{integer},$$
$$2\nu_+ = \text{integer}.$$

Here, k_B is the number of bunches in the ring, ν is the betatron tune, and the subscripts + and - indicate which ring is being referred to. (A common factor has been removed from these equations.)

Figures 2.2–7a and 2.2–7b show the stopband in (ν_+,ν_-) tune space due to coherent dipole oscillations for the cases $(k_{B,+},k_{B,-}) = (1,1)$ and (1,3), respectively. The beam-beam tune shift parameter is set equal to 0.05. Numbers mark the pairs of tunes where the growth rate of the most unstable dipole mode exceeds the radiation damping rate; the blank areas denote stable

regions. Note that the case $(k_{B,+},k_{B,-}) = (1,1)$ gives the largest stable area (55% of the total tune space), but that the case $(k_{B,+},k_{B,-}) = (1,3)$, corresponding to the present APIARY design, provides stable areas large enough—45% of the total tune space—to allow scanning of the operating point without difficulty.

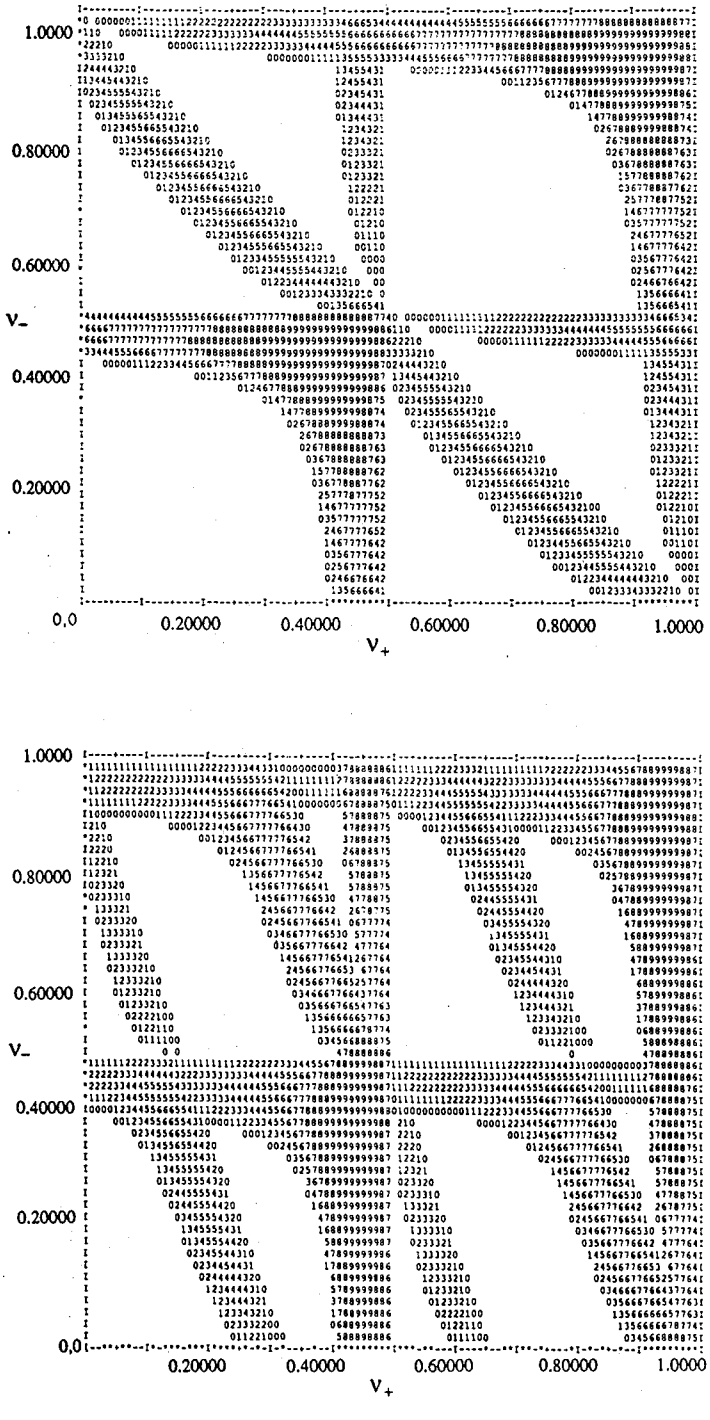

Fig. 2.2-7
The stopbands for coherent dipole beam-beam modes in the tune space of the collider for (a, top) equal numbers of bunches in both rings and (b, bottom) three times as many bunches in the high-energy ring.

2.3. Summary of Beam-Beam Studies and their Implications

We have shown that, if the four criteria given here are all satisfied, two beams of unequal energies should evolve in a similar manner dynamically. It may also be desirable to equalize other parameters, like the emittances and the beta functions at the IP, to ensure full overlap of the bunches in the interaction region. We note that if the synchrotron radiation takes place only in the normal bending magnets of the lattice, the same emittance cannot be compatible with the same damping decrement. A solution to this dichotomy, which is also desirable from the vacuum and beam lifetime points of view, is to use a "wiggler lattice," in which wigglers are distributed along the ring to produce and control the synchrotron radiation.

The simulations described above argue for the idea of symmetrizing both the lattices and the beams of an asymmetric collider, and they show how this regime should be within the parametric reach of the design in order to credibly ensure its performance. At present, when there are no existing asymmetric colliders, it is not known how strictly the four criteria outlined above must be satisfied, or how much they can be relaxed in real machines. For example, the question arises whether one could relax such strong constraints by compensating for one asymmetry with another (e.g., compensating for unequal damping decrements with unequal beam intensities). The answer is not straightforward. While such a scenario might be plausible, we raise several concerns:

- More current would have to be put into the low-energy beam in the ratio of the damping decrements. This is undesirable from a coherent-stability point of view.

- There is evidence[17] that the stability of such a delicately compensated beam-beam mode would be unpredictable. The situation is expected to be "touchy" and could bifurcate easily into a weak-strong situation at high tune shifts.

- Beam intensity is not really a "knob" that can be adjusted freely and easily. The rings must be designed to accept the desired currents.

For these reasons, we consider the flexibility of symmetrization of both the lattice and the beam to be a safer path towards optimizing the luminosity. Therefore, the wiggler lattice concept, which allows for extra flexibility in adjusting the lattice parameters, should be adopted. Elsewhere in this report we present such a lattice and justify its selection for the APIARY design.

It is clear that the conclusions from these beam-beam simulations will have major implications for the design of the low-energy ring. It is natural, then, to question the credibility of the simulation. To address this question, we have simulated—without prior knowledge of the actual experimental results—various known luminosity configurations of PEP with various sets of conditions given to us by the PEP machine group.

As an example, we studied the particular PEP configuration summarized in Table 2.3–1. We find that our luminosity prediction agrees with the measured value to within 10%. In fact, our results are actually pessimistic compared with the observed result, that is, our simulation predicts a value 10% *below* the observed luminosity. We also predict from the simulations that there will be no saturation of the dynamic beam-beam tune-shift parameter, ξ, up to a beam current of 30 mA—again in agreement with experimental observations. Calculations for other PEP configurations yield more or less equivalent agreement with the observed luminosities.

Insofar as the simulation predictions are consistent in trend with the actual PEP observations (and are even slightly pessimistic), we feel that they have withstood at least some test of fidelity.

Betatron tunes	
Horizontal	21.2962
Vertical	18.2049
Beta functions at IP	
Horizontal [m]	1.342
Vertical [m]	0.053
Dispersion at IP	
Horizontal [m]	0.00049
Emittances	
Horizontal [nm·rad]	99.6
Vertical [nm·rad]	3.96
Synchrotron tune	0.043
Beam current [mA]	18.85
Nominal beam-beam parameter, ξ	
Horizontal	0.04653
Vertical	0.04653
Luminosity	
Nominal [$cm^{-2}\ s^{-1}$]	5.07×10^{31}
Observed [$cm^{-2}\ s^{-1}$]	4.80×10^{31}
Simulation[b] [$cm^{-2}\ s^{-1}$]	4.34×10^{31}

Table 2.3–1
PEP Parameters Used in Simulation Comparison[a]

a) Data from E. Bloom and M. Donald.
b) Using same simulation code used here for estimates for the APIARY collider.

2.4. Constraints on the Low-Energy Ring Design

A number of constraints are imposed upon the design of the low-energy ring by various beam-dynamics and technological issues. The constraints would be particularly severe if the design were based on bending magnets and focusing elements alone. The damping decrement (damping time per collision), which should be kept as large as possible, varies with E^3/ρ, where ρ is the bending radius. For a 3:1 energy asymmetry, requiring the low-energy ring to have the same damping decrement as the high-energy ring leads to a low-energy ring with a very small bending radius and thus a very high bending field. Although the bending field (up to 1.8 T for a 300-m, 3-GeV ring in a typical PEP-based scenario) is achievable, such a design has some severe drawbacks:

- A pure bending magnet design gives up crucial flexibility with regard to adjusting the damping decrements and the beam emittance, both of which are largely fixed by the lattice. This inflexibility contradicts a basic premise of our design approach

- If the high-energy ring is quite large and the low-energy ring is small, there is a great disparity in the number of beam bunches in the two rings. According to our understanding of the coherent dipole beam-beam modes, this situation could lead to instabilities and must therefore be avoided

- The synchrotron radiation power density on the vacuum chamber wall along the path of the beam's synchrotron radiation fan can reach 10 kW/cm^2 in a small ring—more than an order of magnitude beyond the value tolerated by any existing vacuum chamber design. It is not clear that there is any straightforward means of dealing with such a high power density without risking severe damage to the chamber. Degradation of the vacuum under these conditions is also a serious concern

- The luminosity lifetime in a small ring is lower than in a bigger ring producing the same luminosity, because the number of particles (which are unavoidably lost at a constant rate because of the beam-beam collisions themselves) is reduced

In order to deal with the issues above, it is necessary to enlarge the low-energy ring. By doing so, we can load the two rings with more nearly comparable numbers of bunches, thus avoiding difficulties with coherent beam-beam modes. The

larger ring permits a lower bending magnet field and a larger circumferential length over which the synchrotron radiation power is absorbed by the vacuum chamber, thus reducing the power density to manageable levels. If nothing else were done, however, the price of going to a larger ring would be a lower radiation damping decrement, which is undesirable.

For these reasons, we have adopted here an alternative that should give the best of both worlds—we utilize a reasonably large low-energy ring, and then provide both horizontal and vertical wigglers to permit independent control of the damping decrement and the horizontal and vertical emittances. Indeed, in our design, the "natural" properties of the low-energy ring lattice (emittance, momentum spread, radiation damping times) are *dominated* by the wiggler parameters. The wigglers provide the flexibility to adjust beam parameters as needed to give the highest possible luminosity. In addition, the synchrotron radiation power is now concentrated in a few areas that can be suitably engineered to deal with the power density locally.

2.5. Issue of Equal-Sized Rings

There are certain advantages to having a low-energy ring identical in radius to the high-energy ring. These include:

- Luminosity lifetime from beam-beam particle interactions is improved, since individual bunches from the low-energy ring collide less frequently
- At only a moderate loss in luminosity—by a factor of about $\sqrt{2}$ —there could be two IPs
- If gaps must be imposed in the bunch trains to avoid ion trapping, the gaps could be matched in both rings so that anharmonic beam-beam effects are totally avoided
- Coherent dipole beam-beam stability is most favorable, as discussed in Section 2.2
- Vacuum-chamber design and vacuum issues are further simplified, since radiation is distributed over a longer circumferential length

Note that a proportionately larger number of wigglers would not be needed, compared with a smaller low-energy ring, because the synchrotron radiation aspects would in any case be dominated by wigglers.

A potential disadvantage to this approach, of course, is the possible additional cost of a very large low-energy ring. In the case of installing the ring in a preexisting tunnel, however, as could be done with PEP, there are significant offsetting savings that make the idea well worth exploring in detail. A preliminary effort in this regard is outlined in Appendix B, which considers the case of a second ring in the PEP tunnel with collision optics based upon a nonzero crossing angle using "crabwise" crossing. The crossing-angle scenario is provided merely as an example that has been studied in some detail at present; the alternative of head-on collision optics, using vertical bends, is also feasible for a low-energy ring in the PEP tunnel and will be studied by us as well.

3. Design Example

In Section 3, we discuss a specific design example for the APIARY collider that is capable of achieving a luminosity of 1×10^{34} cm^{-2} s^{-1}. We envision that the collider would begin operation at a more modest luminosity of 3×10^{33} cm^{-2} s^{-1} and then, with suitable improvements, would reach its ultimate luminosity goal. What we describe here is not yet a fully optimized design, but rather should be viewed as a "proof of principle."

From the viewpoint of lattice design, the challenging aspects of the APIARY collider involve meeting the following requirements:

- Achieving low beta functions ($\beta^* = 2$ cm for the low-energy ring, 6 cm for the high-energy ring) in both planes at the IP
- Separating closely spaced beam bunches to avoid unwanted collisions
- Storing a substantial beam current stably and with a reasonable lifetime
- Achieving a set of "energy transparency" conditions (as discussed in Section 2)
- Making round beams

There are several possible configurations that could be chosen to achieve our luminosity goal. We describe here a rather conventional choice in which the two beams collide head-on. Major parameters for the two rings are summarized in Table 3–1, and a site layout is shown in Fig. 3–1.

To indicate the range of possibilities, a second alternative, in which the two rings are of the same circumference and the beams collide at a finite crossing angle (making use of the crab-crossing technique) rather than head-on, is described in Appendix B. In that alternative case, we examined a design in

which the two rings coexist in the PEP tunnel. This is possible because the tunnel was originally designed to accommodate a second ring. Potential advantages to siting the low-energy ring this way were discussed in Section 2.4. Of course, it is equally possible to site the low-energy ring in the PEP tunnel if a head-on collision scheme is adopted, simply by expanding the arc sections in the sample low-energy ring design described in Section 3.1.

Table 3–1
Main parameters of the APIARY collider.

	Low-energy ring	High-energy ring
Energy, E [GeV]	3.1	9
Circumference, C [m]	733.3	2200.0
Number of bunches, B	288	864
Emittance,[a] ε_x [nm·rad]	123	41
Bunch length, σ_ℓ [mm]	14	10
Transverse damping time		
$\tau_{x,y}$ [ms]	12.3	36.8
Beta functions at IP		
β_x^* [cm]	2.0	6.0
β_y^* [cm]	2.0	6.0
Total current, I [A]	3.0	3.0
Nominal beam-beam tune shift		
ξ_{ox}	0.05	0.05
ξ_{oy}	0.05	0.05
Luminosity, $\mathcal{L}$ [cm^{-2} s^{-1}]	1×10^{34}	

[a] Equal horizontal and vertical emittances.

Specific topics of discussion in the remainder of Section 3 (in order of appearance) are:

- Lattices and Collision Optics
- Beam-Beam Dynamics
- Intensity-Dependent Collective Effects
- RF Systems
- Feedback Systems
- Synchrotron Radiation and Vacuum
- Synchrotron-Radiation Masking and Beam-Pipe Cooling
- Beamstrahlung
- Injection System
- Special-Purpose Hardware

Fig. 3.1–1
Schematic of overall ring configuration (not to scale). The ring has six straight sections, six arcs, and one interaction region.

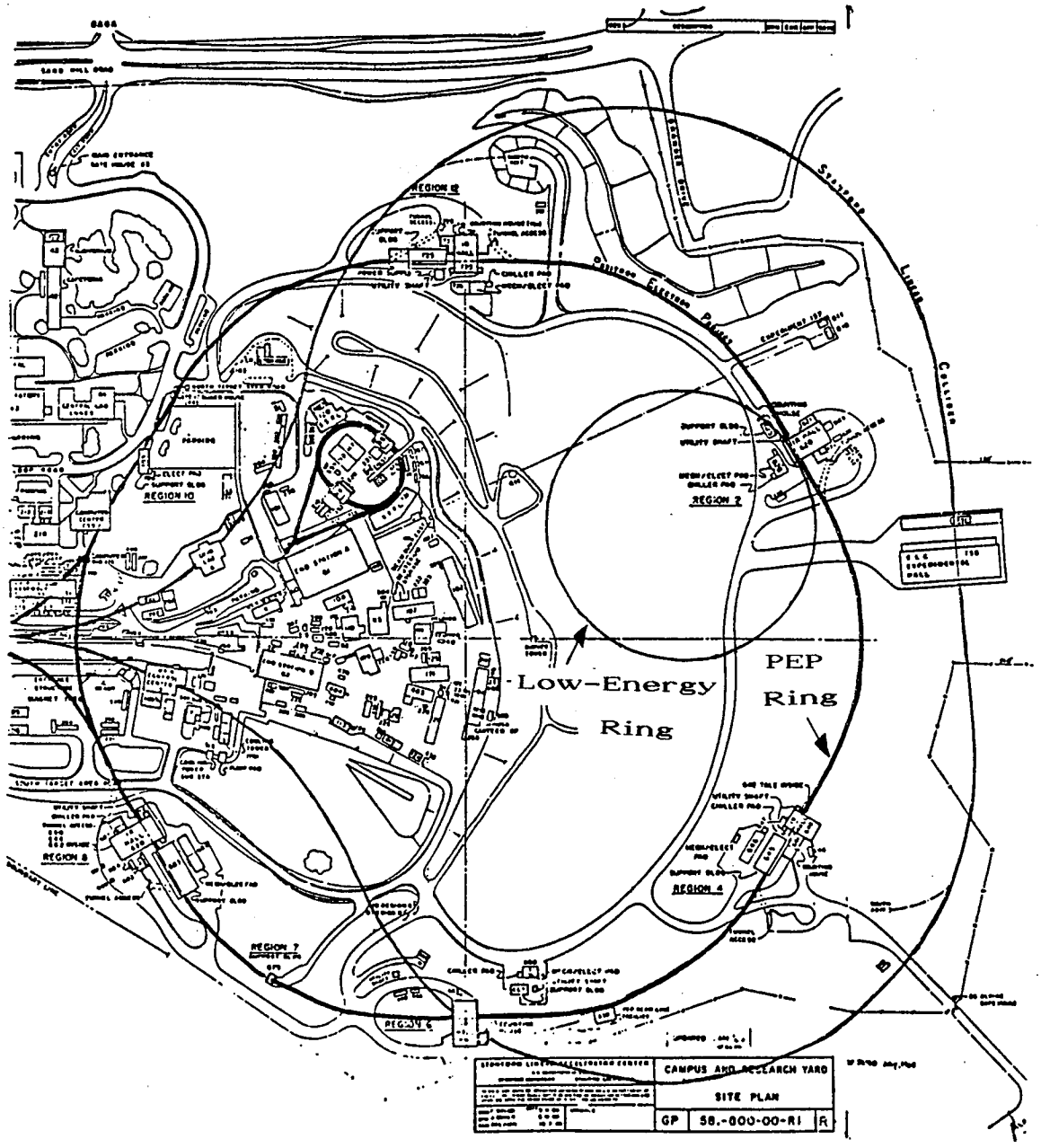

3.1. Lattices and Collision Optics

In this section we describe the two rings that make up the APIARY collider discussed in our example. As mentioned in Section 2, we used the scaling rules outlined in Appendix A to fix the relative parameters of the two rings. For our assumed tune-shift parameter of $\xi = 0.05$, and with the use of round beams in both rings, we can rewrite Eq. (2.1–1) as

$$\mathcal{L} = 2.17 \times 10^{33} \left(\frac{I \cdot E}{\beta_y^*} \right)_{+,-} \quad [\mathrm{cm}^{-2}\,\mathrm{s}^{-1}] \qquad (3.1\text{–}1)$$

where I is in amperes, E is in GeV, β^* is in cm, and numerical values are used for the remaining factors. With our present approach, the beta functions in the two rings scale proportionately to the beam energy (that is, the β_y^* value in the low-energy ring is approximately 1/3 of that in the high-energy ring). This choice makes the beam currents in the two rings identical. Since $E/\beta_y^* = 1.5$, we require a beam current of $I = 900$ mA in each ring to reach an initial luminosity of 3×10^{33} cm^{-2} s^{-1}. A current of $I = 3$ A in each ring is needed to reach the ultimate luminosity goal of 1×10^{34} cm^{-2} s^{-1}.

Low-Energy Ring

We consider here a scheme in which the low-energy ring has one-third the circumference of PEP. As we have shown in Section 2, this choice leaves a large area of tune space available—sufficient space to avoid difficulties with coherent beam-beam modes while easily remaining within parametric range of equal damping decrements, as needed to maintain the "energy transparency" condition between the two rings.

Key features of the low-energy ring include:

- Head-on collision optics
- $\beta^* = 2$ cm in both planes, using superconducting quadrupole doublets
- Zero dispersion in both planes at the IP
- Bunch separation of 2.5 m
- Beam separation in the IR first horizontally and then vertically
- Wigglers to permit adjustments of emittances and damping times
- Round beams

Overall Ring Configuration. The low-energy ring has a circumference of 733.3 m and is designed to operate at 3.1 GeV. As illustrated schematically in Fig. 3.1–1, the ring has a roughly hexagonal shape, with six straight sections and six arcs. Of the six straight sections, two are longer than the others. The first of these long straight sections contains the interaction region (IR) with its low-beta optics; on the opposite side of the ring is a utility straight section (U) for injection, rf, etc. The utility straight section is presently configured as six "empty" FODO cells (i.e., cells without dipoles). Between the IR and U straight sections there are four additional, shorter straight sections (W), two on each side of the ring, that contain horizontal and vertical wiggler magnets. The ring is reflection-symmetric about a line joining the centers of the IR and U straight sections.

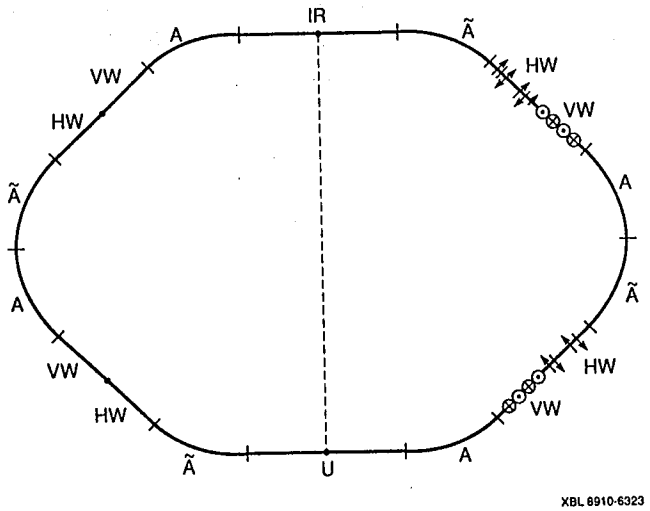

Fig. 3.1–1
Schematic of overall ring configuration (not to scale). The ring has six straight sections, six arcs, and one interaction region.

Arc section and dispersion suppressor. The six arc sections of the ring are of three different types. Each arc is a combination of some number of regular FODO cells, or half-cells, sandwiched between two dispersion suppressors. Figure 3.1–2 shows the layout and lattice functions of half of a reflection-symmetric superperiod. The lengths of all functional elements are specified in units of the standard half-cell length, $L_{1/2}$ = 5.0926 m, or 1/144 of the total ring circumference.

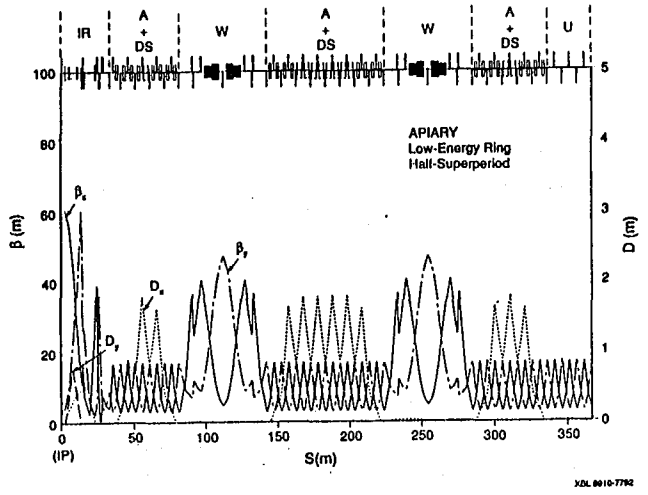

Fig. 3.1–2
Layout and lattice functions of half a reflection-symmetric superperiod in the low-energy ring.

The FODO half-cells contain one 3.26-m dipole and one 0.5-m quadrupole. The optics of a single FODO cell, shown in Fig. 3.1–3, are adjusted to give a phase advance of 90° in each transverse plane. The arcs that join the IR and W straight sections contain one half-cell in the center; those that join the U and W straight sections contain one full cell in the center; and those between two W straight sections contain four full cells in the center. Dispersion suppressors consist of two cells identical to normal cells except that they contain half-length (1.63-m) dipoles.

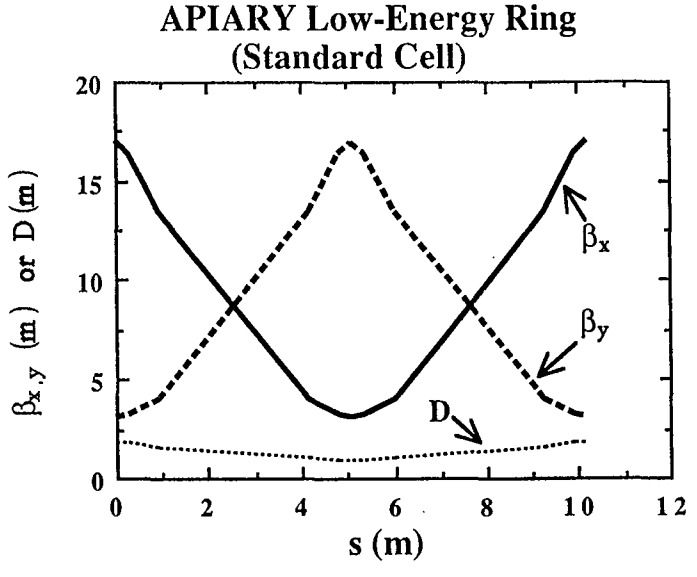

Fig. 3.1–3
Optics of a standard FODO cell.

Wiggler section. The straight sections adjacent to the arc cells are designed to accommodate wigglers in both the horizontal and vertical planes, as was indicated in Fig. 3.1–2. In the present design, wigglers have a period length of 1 m and a maximum field of 1.28 T; they are used in units of five periods, i.e., in 5-m sections. The lengths and strengths have not been optimized, but the chosen values should be more than sufficient to obtain equal damping decrements for the low- and high-energy rings. (To obtain equal damping decrements in the present example requires a 1.1-T wiggler field. The total synchrotron radiation power in this case would be shared roughly equally between the lattice bending magnets and the wigglers.) On each side of the wigglers, there are four quadrupoles whose function is to match the four lattice parameters (β_x, α_x, β_y, and α_y) into the arc optics. These optics give the flexibility to interchange the vertical and horizontal wigglers as needed.

Interaction Region and Beam Separation. The most difficult aspect of a high-luminosity collider, from the viewpoint of the lattice design, is the interaction region. Because of the energy asymmetry between the two rings, and the need to collide closely spaced bunches, the beam separation must be handled carefully . Figure 3.1–4 shows the separation optics of the IR.

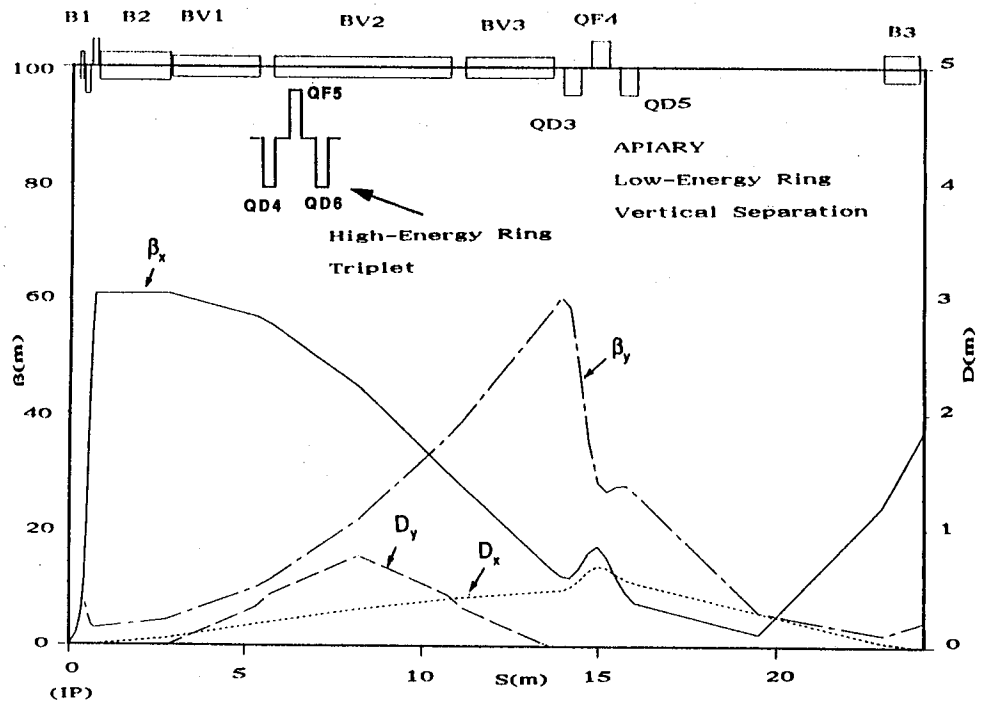

Fig. 3.1–4
Separation optics for the low-energy ring.

Reaching a design luminosity of 1×10^{34} cm^{-2} s^{-1} requires a bunch separation distance of 2.546 m, corresponding to $3\lambda_{RF}$ at 353.2 MHz. The chosen separation scheme must be capable of separating the two beams rapidly enough to avoid unwanted collisions in places other than the IP. The technique being used, which employs both vertical and horizontal bends, is described below. In brief, the idea is to keep the low-energy ring in the same horizontal plane as the high-energy ring, except for a short vertical "bypass" region.

Starting at the IP, shown in Fig. 3.1–5, with $\beta_x^* = \beta_y^* = 2$ cm, the low-energy beam is focused by a superconducting quadrupole doublet (QD1, QF2). This doublet produces essentially point-to-parallel optics, preventing substantial beam blowup over the roughly 13 m until the next focusing quadrupoles.

Fig. 3.1-5
IP optics.

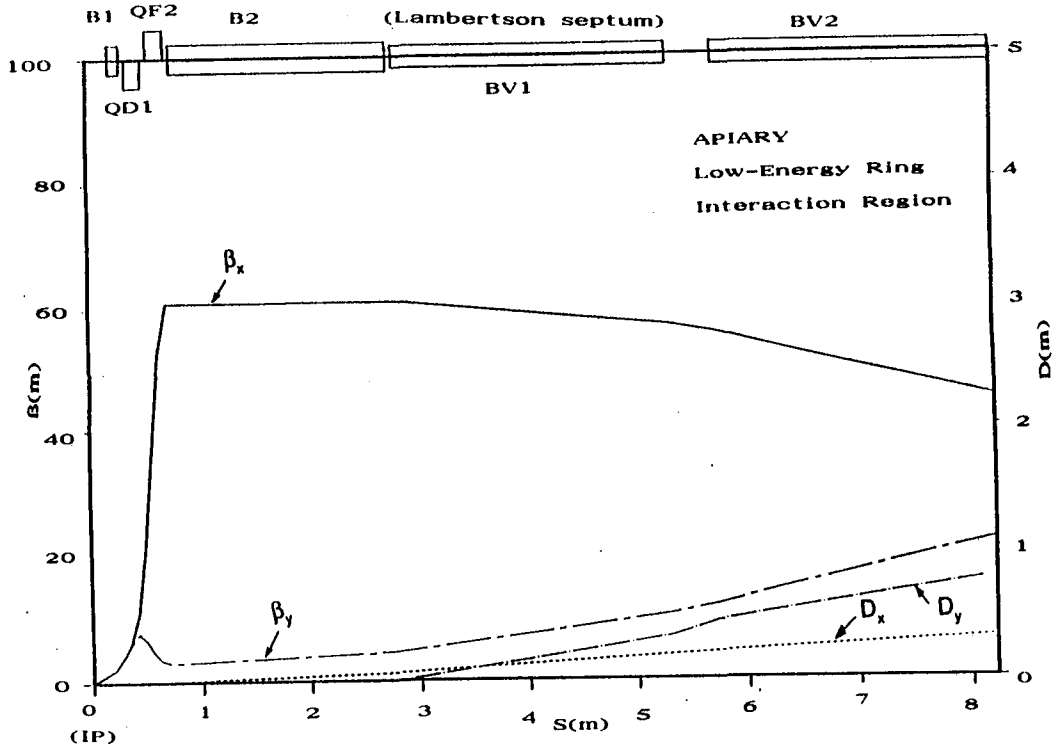

Because the process of beam separation must begin as soon as possible after leaving the IP, a small horizontal bending magnet, B1 (10 mrad), is located upstream from the superconducting quadrupole doublet, 20 cm from the IP itself. Immediately downstream of the doublet, a second horizontal bending magnet, B2 (50 mrad), continues the horizontal separation of the two beams sufficiently to permit the low-energy beam to enter the magnetic channel of a Lambertson septum, BV1 (15.75°), where it is deflected vertically upwards, away from the high-energy beam.

As shown schematically in the elevation view of Fig. 3.1–6, the low-energy beam is then transported vertically by BV2 (-31.5°) and BV3 (15.75°), in a three-magnet "compensated bump" configuration, such that it passes over the top of the superconducting quadrupole triplet required by the high-energy ring to produce its required β^* values. At the exit of BV3, the low-energy beam is again back in its original horizontal plane, and the vertical dispersion created by the various bends has been cancelled.

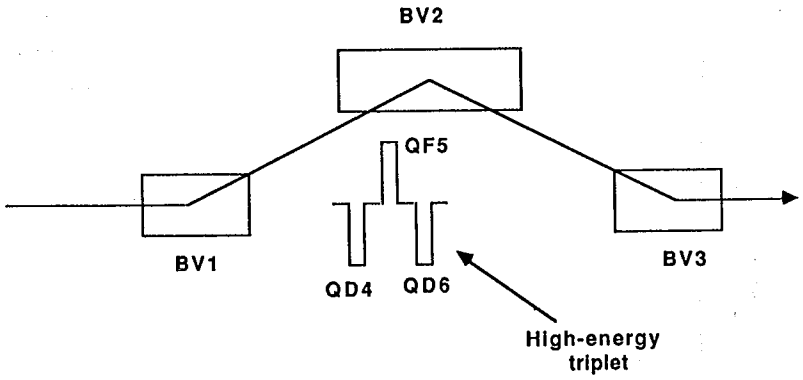

Fig. 3.1–6
Elevation view of separation scheme.

As can be seen in Fig. 3.1–7, after returning to the original horizontal plane, the low-energy beam passes through a quadrupole triplet (QD3, QF4, QD5) which, together with another horizontal bending magnet, B3 (71 mrad), returns the horizontal dispersion function and its slope to zero. Finally, the beta and alpha functions and dispersion values are matched into the standard FODO optics by means of the set of quadrupoles (QF6, QD7, QF8, QD9, QFA).

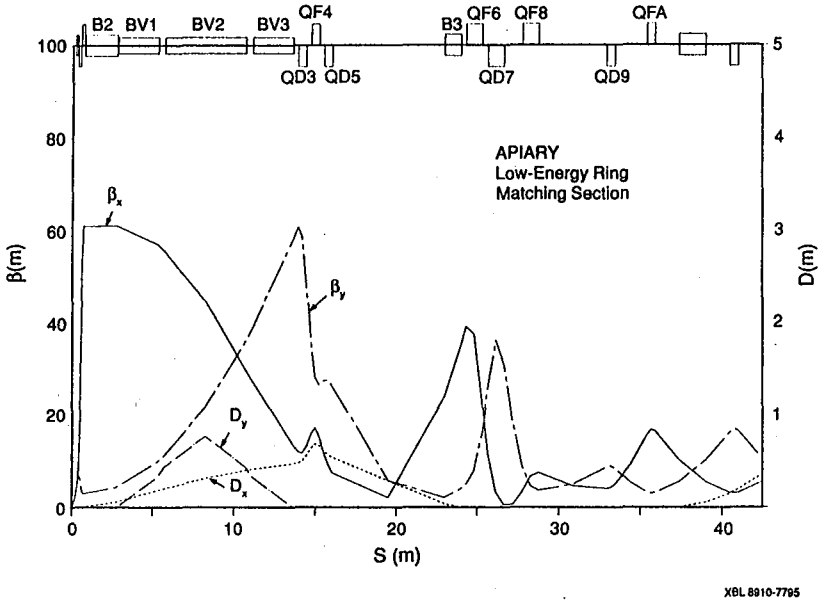

Fig. 3.1–7
Final matching back into FODO optics after IR.

Issues for Further Examination. Although the separation scheme presented here is clearly workable, there are several issues that would benefit from additional study during the optimization phase:

- The high-energy beam is slightly offset radially in the superconducting quadrupole doublet (QD1, QF2). This offset causes deflection of the beam, introduces dispersion at the IP that must be compensated, and could give masking difficulties
- The space available in the region near the IP is very tight
- The dipole B1 is close enough to the IP to possibly cause masking problems.

To deal with the first issue, it will be worthwhile to see whether it is practical to align the quadrupole doublet such that it is on-axis for the beam going towards the IP, but slightly off-axis for the outgoing beam. If the downstream optics are manageable, this could mitigate the masking problems for the detector.

The second issue, hopefully, will be amenable to clever engineering solutions. As one example, it will be necessary to use C-magnets for at least some of the IR dipoles, which should permit additional room for pumps and diagnostic equipment.

With regard to the third issue, it presently appears (see Section 3.6) that the radiation from B1 is not a severe problem for the detector compared with the quadrupoles and the B2 dipole, which is further from the IP. It will be worthwhile to examine the possibility of increasing the strength of B1 and decreasing that of B2.

High-Energy Lattice

The design of the high-energy ring is based upon the existing PEP lattice. PEP has a FODO lattice with six long (117-m) straight sections, and can operate at energies up to 15 GeV. Although the basic lattice hardware is sixfold-symmetric, the addition of a low-beta insertion in one region (Region 2) reduces the actual lattice periodicity to one. Nonetheless, the arc optics retain the symmetry of the hardware rather well, so the periodicity is violated mainly in the single IR straight section.

The basic design requirements for the high-energy ring of the APIARY collider are similar to those for the low-energy ring described above. They include:

- Achieving low beta functions ($\beta^* = 6$ cm) in both planes at the IP
- Separating closely spaced beam bunches to avoid unwanted collisions
- Storing a substantial beam current stably and with a reasonable lifetime
- Making beams as round as is practical

Given the optics configuration for the interaction region from the low-energy ring, the lattice design for the high-energy ring is already somewhat constrained. In our case, we start from an existing ring, so the technical challenge at hand is to adjust the lattice suitably "without touching anything." The high-energy lattice parameters and optics are based primarily on the standard PEP collider optics. To obtain the appropriate emittance, the standard cells are adjusted to a phase advance of 60°.

Interaction Region and Beam Separation. Figure 3.1–8 shows the IR optics as seen by the high-energy beam. (Note that, because of the large range of beta-function values for the high-energy ring, we will plot $\beta^{1/2}$ rather than β itself.) Common elements with the low-energy ring include the two horizontal dipoles (B1 and B2) and the superconducting quadrupole

doublet (QD1 and QF2). Because the high-energy beam has three times the energy, it is relatively unaffected by any of these common magnets, so it passes the Lambertson septum magnet (BV1 in Fig. 3.1–4) in the field-free region.

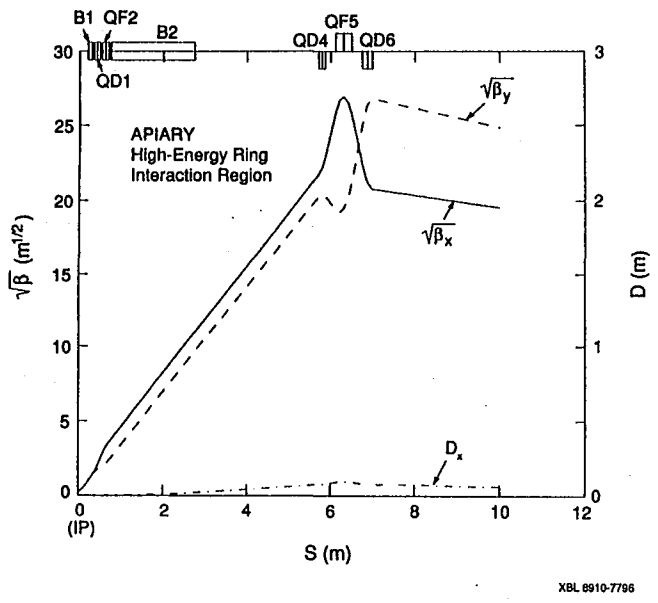

Fig. 3.1–8
IR optics for the high-energy ring.

It is clear from Fig. 3.1–8 that the principal challenge for the high-energy optics is to capture the beam from the IP with focusing quadrupoles before it gets too large. The combined horizontal-vertical separation scheme described above is an attempt to get the superconducting triplet needed for the high-energy beam as close as possible to the IP. Despite this approach, the triplet cannot be located much closer to the IP than about 6 m. The beta functions from the IP will grow as

$$\beta_{x,y}(s) = \beta^*_{x,y} + \frac{s^2}{\beta_{x,y}} \qquad (3.1\text{–}2)$$

so we expect beta functions on the order of 600 m at 6 m from the IP, in agreement with Fig. 3.1–8.

Arc Cells. As shown in Fig. 3.1–9, once the beam is past the superconducting quadrupole triplet of the high-energy ring, it drifts essentially to the end of the straight section, where it is matched to the FODO optics by means of two quadrupoles, Q3R and QF1R. The dispersion matching here requires only the single bend magnet BLM, whose position is adjusted to achieve the matching.

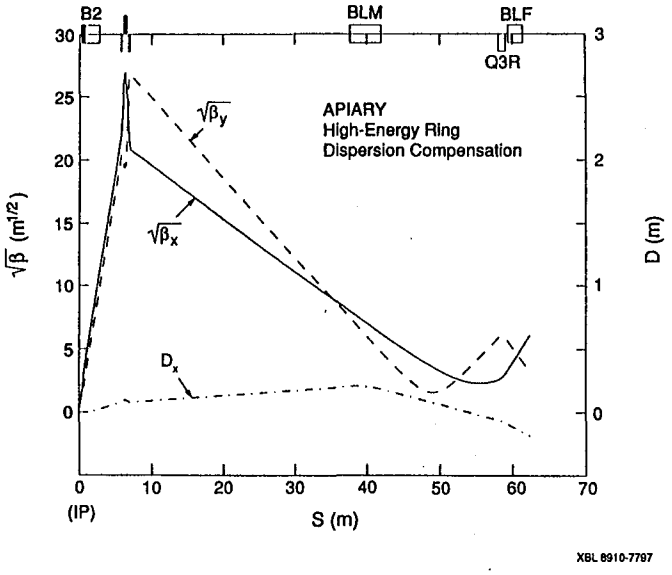

Fig. 3.1–9
Matching of the high-energy beam into the FODO optics after the IR.

Although it is not obvious from the drawing, it is important to note that adjusting the position of the dispersion-suppression bend magnet has the effect of moving the IP by 0.675 m outwards from the center of the PEP ring. If this proved inconvenient, a different matching scenario (including quadrupoles) could be explored.

In Fig. 3.1–10 we show the optics functions for 1/12 of the PEP ring (including half of the arc section adjacent to the IR). As can be seen, the matching is easily accomplished.

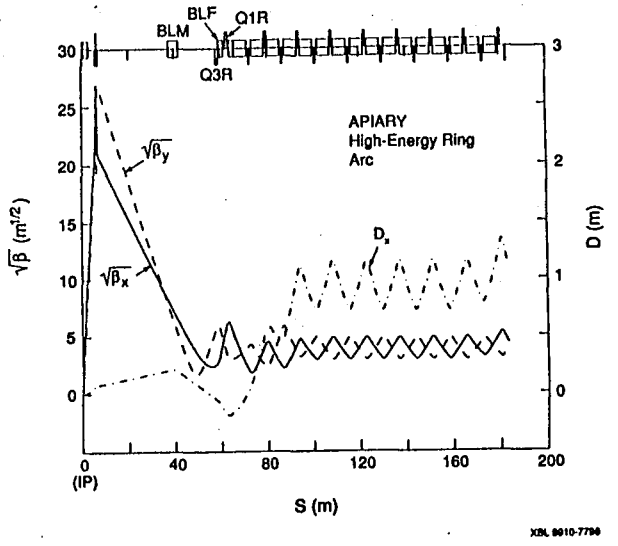

Fig. 3.1–10
Optics functions for one-twelfth of the PEP ring.

To minimize the global chromaticity of the lattice, the optics functions for the remaining long straight sections are adjusted to give large beta functions (weak focusing), as shown in Fig. 3.1–11. This optics configuration has already been tested successfully at PEP as part of a program to explore the use of PEP as a synchrotron radiation source.

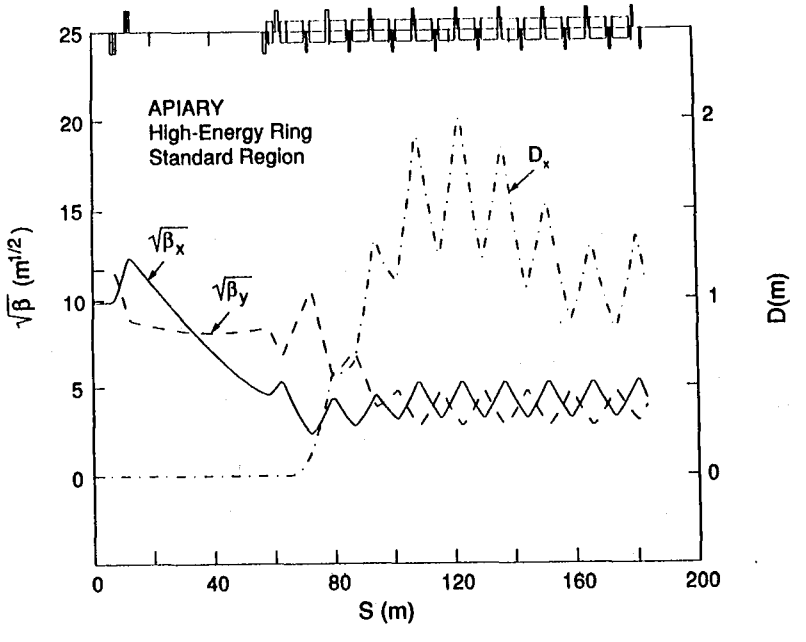

Fig. 3.1–11
The optics for the remaining long straight sections of the high-energy ring.

Complete optics functions for half of the full superperiod are shown in Fig. 3.1–12. There is slight beating of the dispersion function, but overall the matching is good.

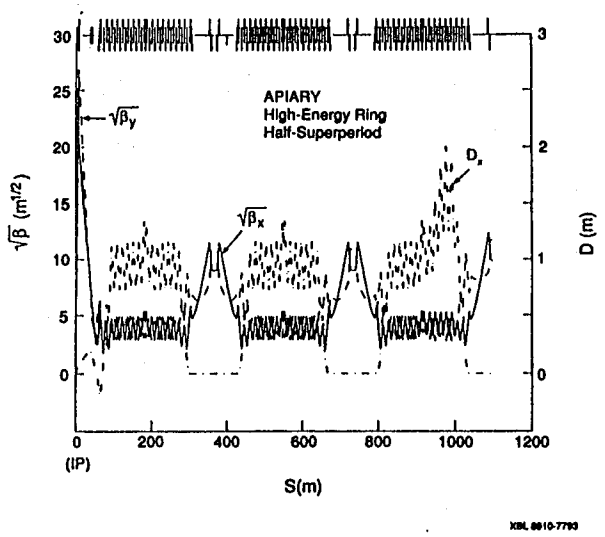

Fig. 3.1–12
Optics functions for half of the superperiod in the high-energy ring.

Natural chromaticities for the optics shown here are $\xi_x = -57$ and $\xi_y = -53$; these are somewhat below the typical values for the PEP collider optics, and correction does not present any problem. One must take care, however, that the local chromaticity associated with the strong quadrupole triplet in the IR does not get out of hand. It is important to minimize the distance of the triplet from the IP insofar as possible.

As with the low-energy ring, a number of issues will need to be pursued during the optimization phase:

- Optimizing the beta functions, etc., at the rf locations is needed in order to minimize transverse impedance contributions from the rf hardware
- Alternative schemes to create round beams in the high-energy ring must be explored

The first issue, optimizing the beta functions, is probably straightforward, but will require additional quadrupoles in the rf straight sections. The second issue, making round beams, is less clear-cut, as discussed below.

Achieving Round Beams

In the low-energy lattice, our calculations predict that the vertical emittance will be dominated by the contribution from the vertical bending magnets that separate the beams. Because these bends are strong and create substantial vertical dispersion, our estimates show that the vertical emittance is slightly larger than the horizontal emittance, without any significant contribution from the wigglers. In fact, we find that the horizontal emittance of the low-energy ring is also dominated by the contribution from the same region of the lattice—the vertical bending magnets.

To see why this might be so, we refer back to Fig. 3.1–4, which shows that, because of the lack of quadrupoles, the horizontal dispersion in the vertical bending magnets is only slightly less than the dispersion in the vertical plane. When synchrotron radiation is emitted in this portion of the lattice, there is an increase in both the vertical and the horizontal emittance values. It may well be advisable to add quadrupoles in this region to permit more emittance control, but there seems little doubt that round beams are well within our grasp for the low-energy ring. The wigglers at present are in a dispersion-free region, so they contribute to the damping time without impacting the emittance. In this circumstance, there may be no particular advantage to having wigglers in both planes.

Not surprisingly, the situation in the high-energy ring is more difficult. We have demonstrated that we can produce a more or less round beam by placing vertical wigglers in a region that has about 0.5 m of vertical dispersion. The drawback, however, is that the strength of the wigglers increases the synchrotron radiation emission in the high-energy ring considerably—about a factor of three. This, in turn, would require that the synchrotron radiation in the low-energy ring increase proportionately to maintain equal damping decrements. It may be more efficient to utilize a scheme similar to the vertical separation bump that works quite effectively in the low-energy ring, but this has not been investigated yet.

Given these difficulties in making a round beam in the high-energy ring, it would seem worthwhile to also explore alternative approaches to production of round beams. The use of skew quadrupoles, for example, must be studied in some detail to better understand the pros and cons of this option *vis-à-vis* the beam-beam interaction. As a first step in this effort, we have examined the effects of rotating the Q3R quadrupoles on each side of the IP. We find that rotating them in the opposite sense by 6.1 mrad suffices to bring the emittance ratio to $\varepsilon_y/\varepsilon_x \approx 1$. Thus it will be possible to create a round beam relatively easily with skew quadrupoles. Two further issues—whether this technique causes a loss of dynamic aperture or leads to beam-beam interaction problems—are now under investigation.

Relaxed Startup Conditions

The initial luminosity of the APIARY collider will be 3×10^{33} $cm^{-2}\ s^{-1}$, as opposed to the ultimate design goal of 1×10^{34} $cm^{-2}\ s^{-1}$. There are several options available to accomplish this "relaxed" startup:

- Increase β^* values
- Decrease I (with or without increasing bunch separation)

The first possibility would ease the requirements for the superconducting IR quadrupoles and the chromaticity correction scheme, but does not seem to be otherwise beneficial. Decreasing the beam current is probably the simplest and most beneficial thing to consider. This reduces the power requirements for the rf system, lowers the heat load on the vacuum-chamber walls, reduces the gas desorption (thus decreasing the gas pressure in the ring and improving the beam lifetime) and reduces the coupled-bunch instability growth rates (thus decreasing the power requirements of the feedback system quadratically).

If the reduction in beam current were accomplished via reducing the number of bunches and increasing the bunch spacing, rather than simply by reducing the beam current per bunch, it might initially permit the elimination of one of the horizontal separation magnets, which could be beneficial in minimizing the synchrotron radiation background in the detector. This approach would also reduce the bandwidth requirement for the multibunch feedback system, although this aspect is not thought to be a problem.

3.2. Beam-Beam Simulation Results

The results of our beam-beam simulation studies for the APIARY collider are summarized in Figs. 3.2–1 and 3.2–2. Compared with the lattice parameters described in Section 3.1, we have chosen slightly different betatron tunes that avoid the excitation of coherent dipole motion, as explained in Section 2.2. The particular values used in the simulations are:

$\nu_{x,+} = 16.905$ $\qquad$ $\nu_{y,+} = 15.71$

$\nu_{x,-} = 21.34$ $\qquad$ $\nu_{y,-} = 18.205$

All the energy transparency criteria established in Section 2.2 except the fourth one are satisfied for the APIARY lattices. That is, we do not have identical values in each ring for the quantity $(\sigma_\ell Q_s/\beta^*)$, which is required in order to have the same betatron phase modulation due to synchrotron motion. Using the actual lattice parameters, the value of $\sigma_\ell Q_s/\beta^*$ in the low-energy ring is about four times that in the high-energy ring.

Fig. 3.2–1a shows the rms beam sizes predicted from the simulations as a function of the nominal beam-beam tune shift parameter, ξ_0. It can be seen that the low-energy beam blows up more than does the high-energy beam; this is thought to result from the mismatch in the betatron phase modulation. The dynamic beam-beam parameters, ξ_+ and ξ_-, are plotted in Fig. 3.2–1b as a function of ξ_0. The vertical ξ value has dropped to one-third of the nominal value at $\xi_0 = 0.05$. Figure 3.2–2 shows the corresponding luminosity, which reaches 53% of the design value of 1×10^{34} cm^{-2} s^{-1} at $\xi_0 = 0.05$.

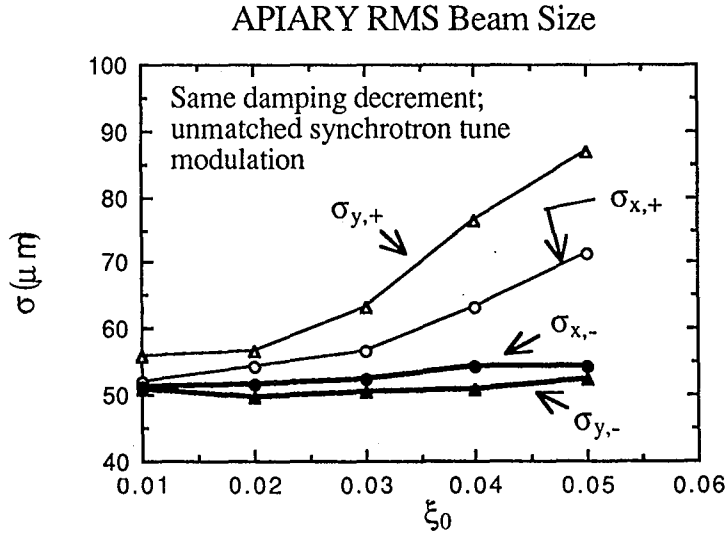

Fig. 3.2–1a
RMS beam sizes vs. ξ_0.

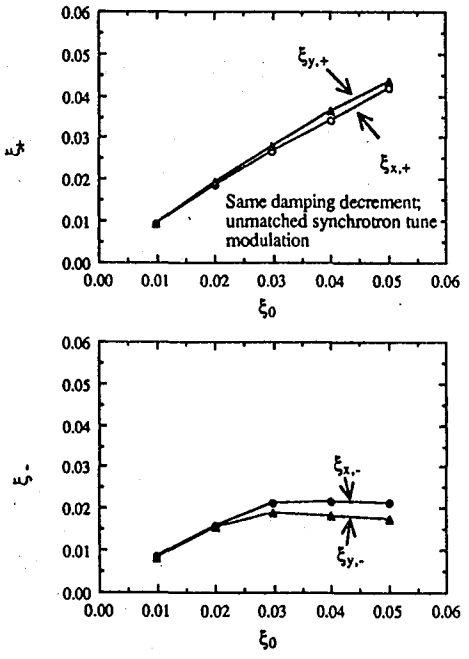

Fig. 3.2–1b
ξ_+ and ξ_- vs. ξ_0.

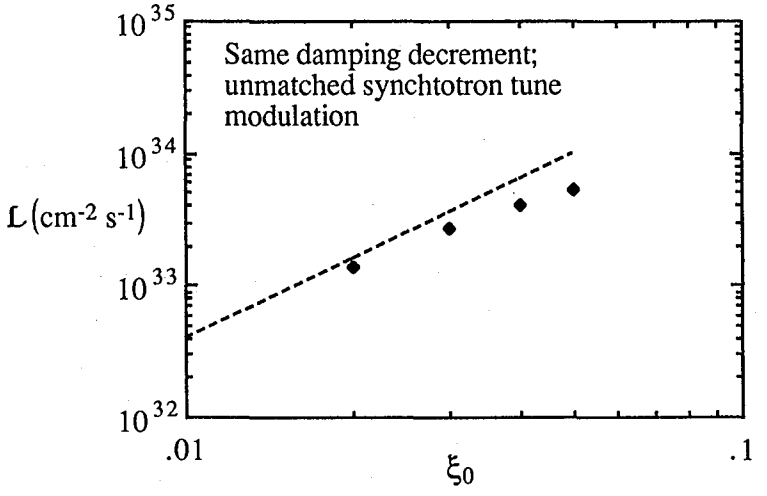

Fig. 3.2–2
Luminosity vs. ξ_0.

To verify our hypothesis about the influence of the mismatch in betatron phase modulation, we also examined how the luminosity would behave if the fourth criterion were satisfied. We can accomplish this by artificially adjusting either the momentum compaction factor or the energy spread. Fig. 3.2–3a shows the behavior of the rms beam sizes when the energy spread of the low-energy ring is decreased to equalize the quantity $\sigma_\ell Q_s/\beta^*$ in both rings. Now, the two beams behave almost identically. Figure 3.2–3b shows that the dynamic beam-beam parameter increases to $\xi = 0.038$ at $\xi_0 = 0.05$.

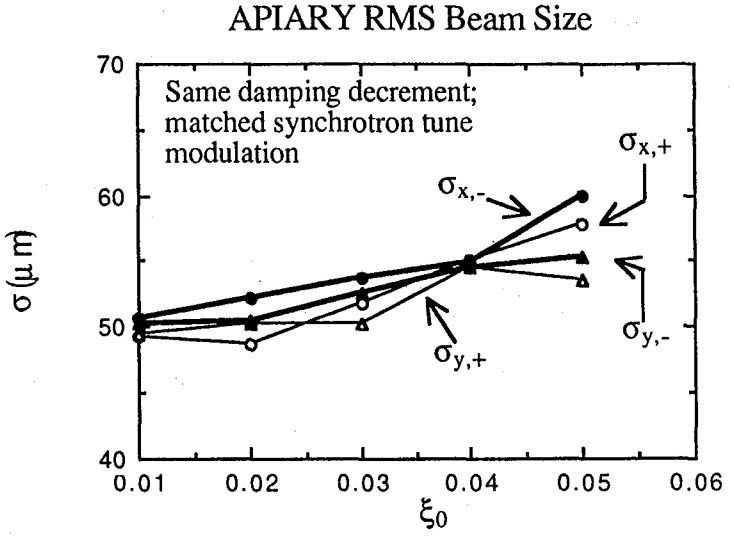

Fig. 3.2–3a
RMS beam sizes vs. ξ_0.

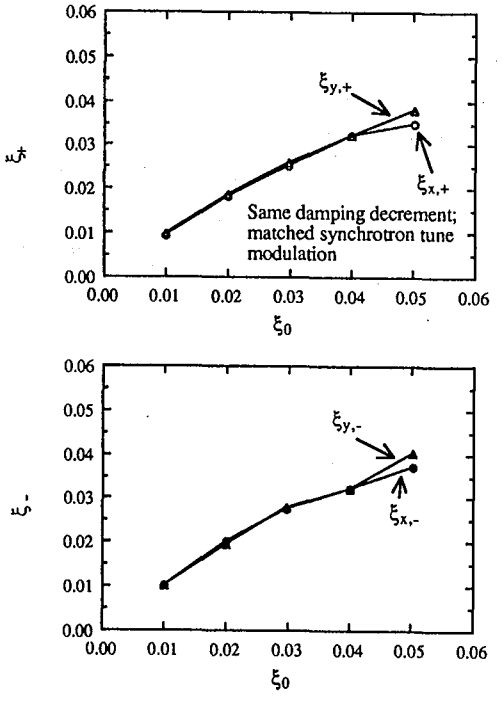

Fig. 3.2–3b
ξ_+ and ξ_- vs. ξ_0.

As expected, the luminosity, shown in Fig. 3.2–4, then reaches 0.75 x 10^{34} cm^{-2} s^{-1} at the design beam current, i.e., 75% of the target value.

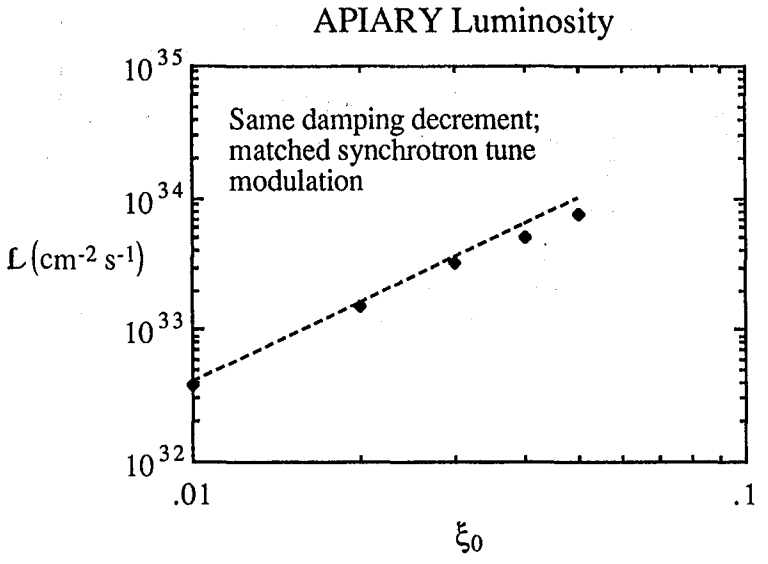

Fig. 3.2–4
Luminosity vs. ξ_0.

To elucidate the role of the damping decrement, we merely switched off the enhanced damping from wigglers in the low-energy ring. The resultant luminosity, is below the design value when the damping decrements in the two rings are not comparable. The loss of luminosity results from a blowup of the low-energy beam in the horizontal plane. For a mismatch of a factor of nine in the damping decrements, for example, the luminosity drops to 4 x 10^{33} $cm^{-2}s^{-1}$.

3.3. Intensity-Dependent Collective Effects

In this section, we examine issues related to the large beam currents required to provide a high-luminosity asymmetric collider—that is, the *collective effects* relevant to the APIARY design. The focus here is on single-ring issues, before the beams are brought into collision. The topics considered are:

- Single-bunch thresholds
- Emittance growth from intrabeam scattering (IBS)
- Beam lifetimes (from Touschek scattering, gas scattering, and quantum excitation)
- Multibunch instabilities

The effects of multibunch instabilities are quite severe, and will likely be one of the limitations to the performance of the APIARY collider. In this case, contrary to standard wisdom, it is the high-energy ring that potentially presents the most difficulties, since this ring has more of the rf hardware that drives the multibunch instabilities. The results reported here were all obtained with the LBL accelerator physics code ZAP.[18]

High-Energy Ring

The high-energy-ring calculations are based on the lattice described in Section 3.1. The ring has a circumference of 2200 m and an rf frequency of 353.2 MHz, leading to a harmonic number of h = 2592. The required bunch separation for reaching the design luminosity of 1×10^{34} cm^{-2} s^{-1} corresponds to 864 equally spaced bunches in the ring; i.e., every third rf bucket is filled.

High-Energy Ring Single-Bunch Thresholds

Longitudinal Microwave Instability. To estimate the growth from the longitudinal microwave instability, we must assume a value for the broadband impedance of the ring. For the APIARY high-energy ring, this value—usually dominated by the rf in a high-energy storage ring—is expected to be lower than the value of $|Z/n| = 3\ \Omega$ obtained from measurements at PEP.[19,20]

The equivalent broadband contribution to the impedance seen by the beam can be estimated, for a given rf system, following the approach of Reference 18. Basically, we estimate the frequency shift that would be induced in a long beam bunch by the aggregate of the many cavity HOMs, and equate it to the strength of a Q = 1 broadband resonator that would produce the same effect. That is, we take

$$\left|\frac{Z_{\parallel}}{n}\right|_{BB,rf} = \sum_{HOMs} \left|\frac{Z_{\parallel}}{n}\right|_j = \sum_j \left(\frac{R_s\,\omega_0}{Q\,\omega_R}\right)_j \qquad (3.3\text{–}1)$$

where R_s, ω_R, and Q are the shunt impedance, resonant angular frequency, and quality factor, respectively, of the j^{th} HOM, and ω_0 is the particle revolution (angular) frequency. With this approach, we find that the present PEP rf system contributes an equivalent broadband component of $|Z/n| \approx 0.026\ \Omega$/cell. Although the design of the smoother room-temperature rf cavity described in Section 3.4 is helpful in minimizing the shunt impedance, the same prescription applied to this case yields an equivalent broadband contribution of $|Z/n| \approx 0.019\ \Omega$, about a 25% improvement.

A more significant gain can be made by producing the required voltage and providing the required power to the beam (to replenish the losses to synchrotron radiation) with many fewer rf cells than the 120 used now at PEP. In the design described in Section 3.4, the voltage is provided by only 20 rf cells. This decrease in the number of cells would by itself reduce, by about a factor of six, the broadband impedance in the ring that stems from the rf system (estimated to be about two-thirds of the total). The decrease in the impedance of individual cells provides another 50% improvement, so we expect to decrease the rf contribution to the broadband impedance by nearly one order of magnitude. If the rf hardware were to totally dominate all contributions to impedance, the overall impedance of the ring might be expected to decrease by this factor. Clearly, however, the broadband impedance from the other components in the beam path (valves, bellows, BPMs, etc.) must contribute to the total seen by the beam, and there will be additional hardware in the APIARY ring (e.g., more powerful feedback kickers) that will have an effect.

With this in mind, we have adopted for now a total broadband impedance of $|Z/n| = 1.5\ \Omega$ for the high-energy ring—a factor of two better than PEP. Even this fairly conservative assumption does not lead to any difficulties in the parameter regime in which the APIARY high-energy ring is designed to operate.

To maintain bunches that are short compared with the smaller β^* value of 2 cm in the low-energy ring, we adopt an rf voltage in the high-energy ring of 25 MV. As shown in Fig. 3.3–1, this voltage gives an rms bunch length of $\sigma_\ell \approx 1$ cm at the required single-bunch current of 3.5 mA. The expected bunch lengthening, and widening, beyond threshold are shown in Fig. 3.3–2, based on the threshold formula given in Eq. (3.3-2):

$$I_b = \frac{\sqrt{2\pi}\,|\eta|\,(E/e)\,\sigma_p^2\,\sigma_\ell}{R\left|\frac{Z}{n}\right|_{eff}} \qquad (3.3\text{–}2)$$

where η is the phase-slip factor, σ_p is the rms relative momentum spread, and R is the machine radius. We remain well below the threshold at the required single-bunch current.

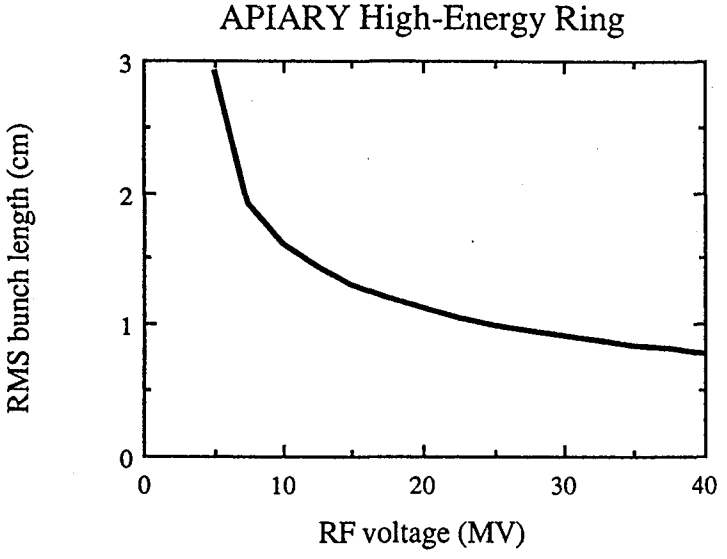

Fig. 3.3-1
Predicted bunch lengthening from the longitudinal microwave instability for the APIARY high-energy ring with a single-bunch current of 3.5 mA. A low-frequency broadband impedance of $|Z/n| = 1.5\ \Omega$ was taken, and an impedance roll-off according to SPEAR Scaling was assumed.

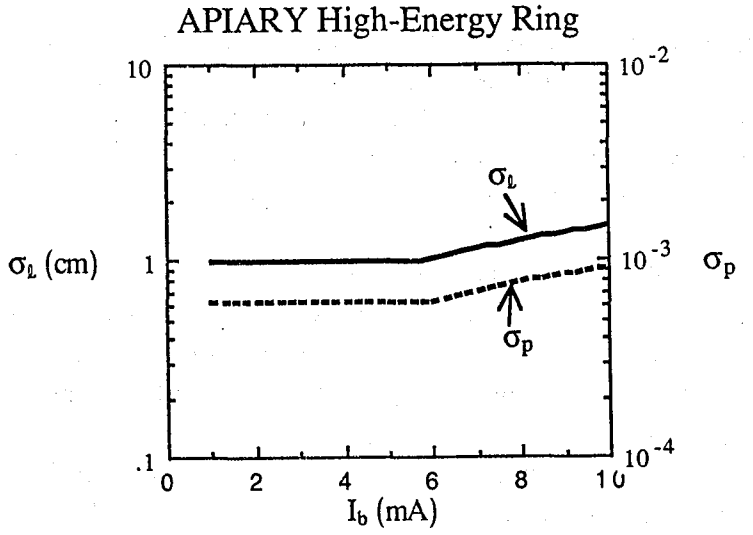

3.3-2
Predicted bunch lengthening and widening for the APIARY high-energy ring as a function of single-bunch beam current.

The curves in Fig. 3.3–2 are based on the so-called SPEAR Scaling ansatz,[21] which is a phenomenological representation of the fact that beam bunches that are short compared with the dimensions of typical surrounding structures do not sample the broadband impedance very effectively. The expected reduction in impedance given by this model is

$$\left|\frac{Z}{n}\right|_{eff} = \left|\frac{Z}{n}\right|_0 \left(\frac{\sigma_\ell}{b}\right)^{1.68} \qquad (3.3\text{–}3)$$

where b is the beam pipe radius.

Transverse Mode-Coupling Instability. Because the ring is large, we must also consider the transverse mode-coupling instability, which is known[20] to limit the single-bunch current in PEP. This instability arises when the imaginary part of the transverse impedance $Z_\perp$ couples the frequency of the m = 0 and m = -1 synchrotron sidebands. For long bunches, the threshold is expected to scale as

$$I_b = \frac{4\,(E/e)\,\nu_s}{\langle \mathrm{Im}\,(Z_\perp)\,\beta_\perp \rangle\, R} \frac{4\sqrt{\pi}}{3}\,\sigma_\ell \qquad (3.3\text{–}4)$$

where ν_s is the synchrotron tune, $\beta_\perp$ is the beta function at the location of the impedance, and R is the average ring radius. Although the transverse impedance is expected to decrease for

very short bunches,[21] we are operating in a regime where the mode-coupling threshold is more or less independent of bunch length. For the impedance presently expected for the high-energy ring, a simple scaling from measured PEP data based on Eq. (3.3–4) suggests that the transverse mode-coupling threshold should be somewhat greater for APIARY than for PEP, even though APIARY will have a lower beam energy. The scaled threshold value, 14 mA/bunch, is well beyond the required single-bunch current of 3.5 mA and should pose no problem.

Since the rf cavities are major contributors to the transverse impedance, it is clear from Eq. (3.3–4) that it is best to "hide" them in a low-beta region of the ring. This should be more easily accomplished in the APIARY high-energy ring than in PEP, because the total length of rf structure will be considerably shorter. Furthermore, the large aperture rf cavities envisioned for the ring will have an improved transverse impedance compared with the present PEP cavities. Thus, the gain in transverse threshold may be even higher than the assumed reduction in longitudinal impedance would suggest.

High-Energy Ring Intrabeam Scattering

Although we are considering a fairly high energy beam, the requirements for relatively short bunches and relatively high peak currents make emittance growth from intrabeam scattering a possible concern. IBS occurs because, in the bunch rest frame, not all particles are moving in the same direction, so they can collide. In general, the temperatures in the transverse phase planes (x and y) are higher than in the longitudinal plane. This results in small-angle multiple scattering occurring mainly in such a way as to transfer momentum from the transverse to the longitudinal plane. However, in dispersive regions of the lattice (regions where the position of a particle depends on its energy deviation) the resultant momentum change is equivalent to exciting a betatron oscillation, and thus gives rise to an increase in horizontal emittance. Our estimates for the APIARY high-energy ring indicate that no growth is expected in this energy range, so we will not consider this subject further.

High-Energy Ring Beam Lifetime

For a high-energy electron beam, there are three main processes that lead to beam loss: Touschek scattering, gas scattering, and quantum excitation. For the APIARY design, the first of these effects is not important, but the second one is, and the third one has the potential to be so.

Touschek Scattering. The Touschek scattering mechanism is also a single-bunch effect that is related to the IBS mechanism described above. The main difference is that we are concerned now with large-angle, single scattering events that change the scattered particle's momentum sufficiently to make it fall outside the momentum acceptance of the accelerator.

The limit on the tolerable momentum deviation from the design value can come from several sources. There is a longitudinal limit from the potential well ("rf bucket") provided by the rf system. Particles deviating in momentum from the nominal value by more than this amount do not undergo stable synchrotron oscillations and are lost. There can also be a transverse limit on momentum acceptance, arising from the excitation of a betatron oscillation when the Touschek scattering event takes place in a dispersive region of the lattice. For large momentum deviations ($\delta p/p \approx$ several percent), the resultant betatron oscillation can either hit the vacuum chamber wall elsewhere in the lattice (physical aperture limit) or exceed the dynamic aperture of the machine. (The term "dynamic aperture" refers to the largest betatron amplitudes that can remain stable, after the various nonlinear magnetic fields experienced by a particle as it circulates have been taken into account.) Because the lifetime for Touschek scattering increases approximately as $(\Delta p/p)^3$, where $(\Delta p/p)$ is the limiting momentum acceptance value, there is the potential for a strong degradation if the acceptance is too low.

The rf voltage in the high-energy ring, selected to be 25 MV in order to ensure short beam bunches, actually provides an excessively large acceptance ($\Delta p/p = 1.5\%$) compared with the estimated limitation from the physical aperture ($\Delta p/p = 0.7\%$). This is not beneficial to the lifetime, since it results in a higher bunch density and thus a higher collision probability; this is the price we must pay to obtain short bunches. Fortunately, the

Touschek lifetime is not a concern in this parameter regime. At 9 GeV, a Touschek lifetime of about 500 hours is predicted for the high-energy ring.

Gas Scattering. Gas scattering involves collisions with residual gas nuclei present in the vacuum chamber. Such collisions can be either elastic or inelastic (Bremsstrahlung). In the former case, particle loss results from the excitation of a betatron oscillation that exceeds the physical or dynamic aperture of the ring; in the latter case, the loss results from a momentum change that exceeds the momentum acceptance of the ring (see discussion above).

In the case of the APIARY high-energy ring, we will ultimately have to accommodate up to 3 A of circulating beam to reach our luminosity goal. This high beam current will give a large amount of desorbed gas load, and substantial pumping speed is needed to maintain a background gas pressure better than 10 nTorr in the ring. Given that most present colliders operate in the pressure range of about 10 nTorr, we will base our lifetime estimates on this value (N_2 equivalent). It is important to note, however, that achieving such a pressure will require an innovative design for the vacuum chamber, as discussed in Section 3.6.

For the high-energy ring, the estimated half-life from gas scattering—dominated by the Bremsstrahlung process—is two hours at a pressure of 10 nTorr. This beam loss process is much more severe in its effects than the Touschek scattering process; therefore we have placed great emphasis on a vacuum system design capable of maintaining a good pressure in the presence of a large gas load from synchrotron-radiation desorption. If the present PEP vacuum system were to be employed for the APIARY high-energy ring at full current, for example, we would expect a pressure in the ring of several *hundred* nTorr, which would lead to a beam lifetime of only minutes.

Quantum Lifetime. It is worth remembering that one must also keep a watchful eye on the quantum lifetime in a high-energy ring. This loss mechanism results from particles being scraped from the tails of the Gaussian distribution that results from the statistical nature of the synchrotron radiation emission process. The lifetime from this effect goes as:[22]

$$\tau_q = \tau_x \frac{e^{\xi^2/2}}{\xi^2} \qquad (3.3\text{–}5)$$

where ξ is the available aperture in units of the rms beam size, σ_x. For an acceptance of $\xi = 6$, the resultant quantum lifetime is about 15 hours, but for $\xi = 5$ the lifetime would be only about 5 minutes. To account for misalignments that can reduce the available aperture, a typical rule of thumb is to allow for an aperture of at least $\xi = 10$ in both planes.

In a high-luminosity collider the required β^* value is only a few centimeters, which can result in very large beta function values ($\beta \approx 700$ m in our case) in the IR quadrupole triplets, and thus in very large rms beam sizes ($\sigma_x \approx 5$ mm) there. For the high-energy ring, a quadrupole aperture radius of about 5 cm is needed at the superconducting quadrupole triplet.

Presuming that the parameters are suitably chosen to avoid difficulties with quantum lifetime, we can see from the above discussion that the (single-beam) lifetime of the high-energy ring will be dominated by gas scattering, which, as noted, makes the vacuum system a critical issue. To put our predictions in perspective, we note that the luminosity lifetime in a high-luminosity collider will also be limited by the beam-beam scattering at the interaction point. Porter[23] has estimated the cross section of this process for a typical B-factory collider design and finds a luminosity lifetime of about two hours. Combining this with the estimates for single-beam loss mechanisms above suggests that the overall luminosity lifetime will be on the order of 1 hour, which implies the need for a dedicated and very powerful injection system to maintain an acceptable value for the average luminosity.

High-Energy Ring Coupled-Bunch Instabilities

In a storage ring, wakefields in high-Q resonant structures can cause different beam bunches to interact. In general, such high-Q resonances result from the higher-order modes of the rf cavities. For certain values of relative phase between bunches, the coupled-bunch motion can grow and become unstable, leading to beam loss. In addition to the relative phase between bunches, the instabilities are characterized by their motion in longitudinal (synchrotron) phase space, as illustrated schematically in Fig. 3.3–3. Longitudinally, the a = 0 mode (which corresponds to no motion) cannot be unstable, so the lowest longitudinal instabilities are characterized by the a = 1 (dipole) synchrotron motion. In the *transverse* case, the a = 0 motion can also become unstable (referred to as "rigid-dipole" motion).

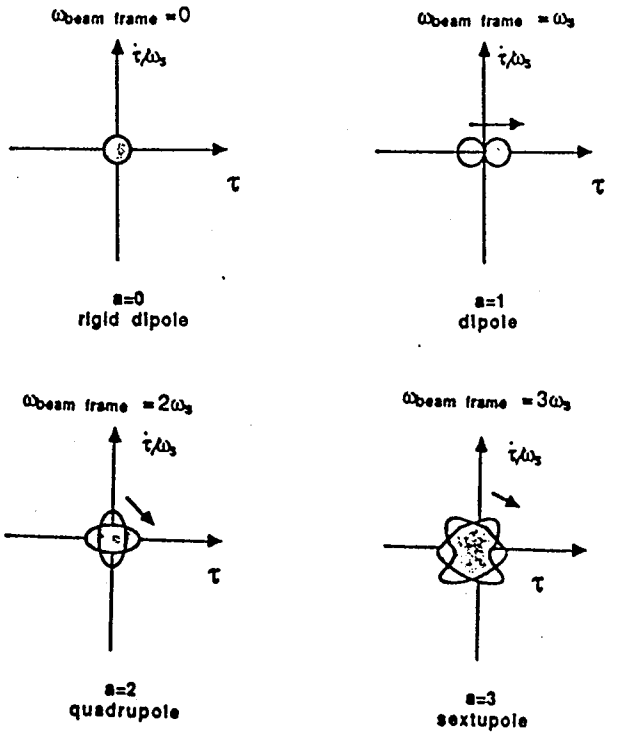

Fig. 3.3-3
Schematic diagram of the lowest few coupled-bunch synchrotron modes. For longitudinal instability, only modes $a \geq 1$ are possible; transversely, the $a = 0$ mode can also be unstable. The most troublesome cases for APIARY are $a = 1,2$ longitudinally and $a = 0,1$ transversely.

In the case of a high-luminosity B-factory design, we typically require a large number of rf cells, both to produce the voltage needed to provide the short bunches and to replace the beam power lost to synchrotron radiation at each turn. Combined with the required very high average beam currents, the substantial rf system can produce extremely rapid growth of coupled-bunch instabilities. In all the cases studied here, the most severe

growth comes from the lowest synchrotron modes, that is, a = 1 and a = 2 longitudinally, and a = 0 and a = 1 transversely. Higher synchrotron modes are predicted either to be Landau-damped or to be growing slowly enough for radiation damping to be effective.

We have estimated the growth rates for both longitudinal and transverse instabilities for typical APIARY parameters, that is, 864 bunches having a total current of 3 A. Given the uncertainties in determining the actual higher-order modes for any particular rf system that we study, it is most sensible to interpret the results shown here "logarithmically." That is, we are interested in seeing whether the fastest growth rates are 1 ms, 0.1 ms, etc., and we should not ascribe too much significance to growth rates that differ by a factor of two.

To give a feeling for the range of possibilities, three different cases were studied:

Case A: PEP RF, Q/5; 80 cells (with only 1 A beam current)

Case B: Single-cell, room-temperature (RT) cavities (see Section 3.4); 20 cells

Case C: As in B, but with HOM's de-Qed by a factor of 100; 20 cells

For case A, we take the higher-order modes of the existing PEP rf system,[24] which consists of 24 five-cell cavities, i.e., 120 cells. Because this system is capable of providing 39 MV, as opposed to the 25 MV we require for the APIARY high-energy ring, the number of cells used in the calculations was reduced from 120 to 80 cells; we note, however, that the scenario assumed here envisions that all the existing klystrons would still be employed to provide the requisite power. The de-Qing represented by Case A is intended simply to mock up the effect of the mechanical differences between PEP rf cavities by representing groupings of the slightly displaced resonant frequencies in terms of single resonators with a somewhat broader frequency span. For these calculations, we assumed a beam current of only 1 A in the ring. The scenario being envisioned here involves beginning operation of APIARY at a reduced luminosity level, in which case it might be possible to get by with the present rf system temporarily.

In Case B, we examine the possible benefits of a newly designed rf cavity that has a shape similar to that of a superconducting cavity; that is, the walls have a very smooth contour and there is a large diameter beam port to minimize trapped HOMs. One consequence of this design is that the cavity shunt impedance is rather low, so power costs will increase somewhat. However, in the limit of being in a heavily beam-loaded regime, the lower shunt impedance is not a major issue.

Case C represents what might happen if the higher-order rf modes of the single-cell system were heavily de-Qed by external means, such as HOM couplers. (We note that achieving an equivalent level of Q reduction in the PEP five-cell cavities would not be an easy task, to say the least. However, such a drastic reduction in Q should be practical in the case of specially designed single-cell, room-temperature rf cells.) In addition, Case C is intended to show the potential benefits that accrue when a superconducting rf system is employed. By this we mean that the rf cavity described in Section 3.4 could serve in either a room-temperature or a superconducting system.

It is not entirely clear how to compare the two interpretations of the Case C results on an equal footing. The gradient achieved in a superconducting cavity should be higher than that in an equivalent room-temperature cavity, so it might be that fewer cells would be needed to provide a given voltage. On the other hand, the use of relatively few superconducting cells to produce the required voltage means that the large beam power that must be supplied has to be delivered through relatively few individual cavity windows. Such high-power cavity windows have not been demonstrated operationally in a superconducting environment.

In a similar vein, the required removal of the HOM power from the superconducting environment may be more difficult than the equivalent task in the room-temperature case. For now, we have taken the window-power constraint to dominate, that is, we assume that the power provided to the superconducting cavity (per window) would only be half that for an equivalent room-temperature cavity. With this assumption, the number of rf cavity cells would be the same in either scenario, so the Case C

results can be interpreted as representing either 20 cells of de-Qed room-temperature or superconducting rf. We have confirmed, by comparison with existing data,[25] that the HOMs used in our calculations are roughly consistent with the kinds of values actually obtained from superconducting rf cells.

Predictions of longitudinal growth times (for the fastest growing mode) for each of the three rf scenarios considered are summarized in Table 3.3–1. For the standard PEP rf system (Case A), we see that both the a = 1 (dipole) and a = 2 (quadrupole) modes grow very rapidly compared with the radiation damping time. The predicted dipole-mode growth times are so short that they are less than the synchrotron period itself, making the model used to estimate the growth rates suspect. Nonetheless, the calculated values serve as a severe warning. The more optimized cavity shape, but without de-Qing (Case B), does much better, giving a = 1 growth times of about 0.1 ms (but for I = 3 A rather than I =1 A as in Case A). Substantial de-Qing or the use of superconducting RF (Case C) does help slow down the growth considerably, to times longer than 1 ms. Note that the feedback system power required to counteract these instabilities will scale as the square of the growth rate, so a change of a factor of ten is extremely significant.

Table 3.3-1
Longitudinal coupled-bunch growth times for APIARY high-energy ring (9 GeV; τ_E = 18.5 ms)

(A) PEP, Q/5[a)]	
$\tau_{a=1}$	0.02 ms
$\tau_{a=2}$	0.4 ms
(B) Room temperature[b)]	
$\tau_{a=1}$	0.2 ms
$\tau_{a=2}$	6.4 ms
(C) RT/SC, Q/100[b)]	
$\tau_{a=1}$	4 ms
$\tau_{a=2}$	235 ms

a) Estimated for I = 1 A; growth times at I = 3 A would decrease by a factor of three from those shown.
b) Estimated for I = 3 A.

Transverse results, summarized in Table 3.3–2, are similar to those for the longitudinal case. Here too, we find that the lowest two synchrotron modes, a = 0 and a = 1, grow faster than the radiation damping rate. We again note the benefits of substantial de-Qing or superconducting rf (Case C) in slowing down the growth rates to more manageable levels.

(A) PEP, Q/5[a)]	
$\tau_{a=0}$	0.04 ms
$\tau_{a=1}$	0.9 ms
(B) Room temperature[b)]	
$\tau_{a=0}$	0.3 ms
$\tau_{a=1}$	7 ms
(C) RT/SC, Q/100[b)]	
$\tau_{a=0}$	0.5 ms
$\tau_{a=1}$	11 ms

Table 3.3-2
Transverse coupled-bunch growth times for the APIARY high-energy ring (9 GeV; τ_x = 36.8 ms)

a) Estimated for I = 1 A; growth times at I = 3 A would decrease by a factor of three from those shown.

b) Estimated for I = 3 A.

Investigations done previously have indicated that the behavior shown in Tables 3.3–1 and 3.3–2 is insensitive to energy in this regime, so increasing the energy asymmetry by raising the energy of the high-energy ring to 12 or 14 GeV would not be especially helpful. It is also found that the coupled-bunch growth rates for the case of a high-luminosity collider scale mainly with total current, and do not change significantly if the bunch pattern changes (e.g., choosing half as many bunches, with twice the single-bunch current). This latter study—carried out using a time-domain multibunch instability code written by K. Thompson at SLAC—qualitatively confirms the growth time predictions made here with ZAP, and shows that, for example, leaving a gap in the bunch train (to clear ions) does not affect the growth rates significantly.

Low-Energy Ring

Major parameters of the low-energy ring considered here (see Section 3.1) were summarized in Table 3.1–1. The ring is assumed to operate at the same rf frequency (353.2 MHz) as PEP, which leads to a harmonic number of 864. Reaching the desired beam current requires 288 bunches with 10.4 mA/bunch. To maintain short beam bunches in this ring (see Fig. 3.3–4), the rf system must provide at least 10 MV. This requires 30 cells of standard PEP rf, or 10 cells of the new rf system described in Section 3.4.

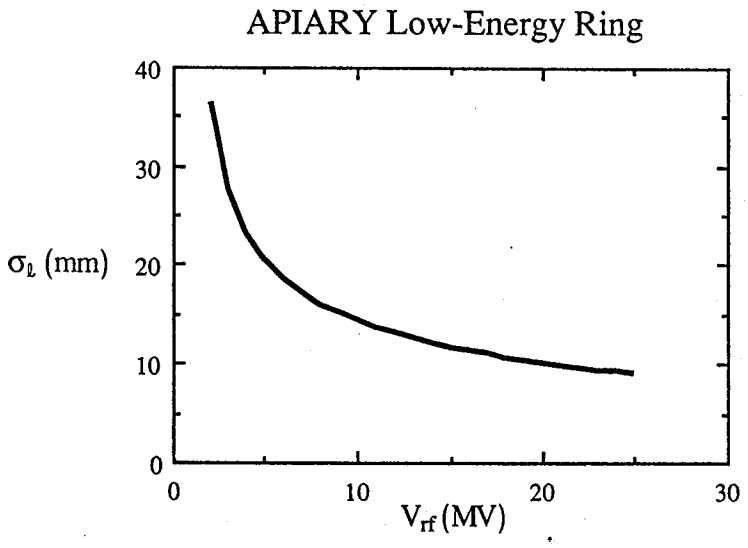

Fig. 3.3-4
Predicted natural bunch length for the APIARY low-energy ring as a function of rf voltage.

Low-Energy Ring Thresholds

Taking into account the expected[21] impedance roll-off for short beam bunches, the longitudinal microwave instability threshold for the low-energy ring is shown in Fig. 3.3–5. For this ring, each rf cell is estimated, by means of Eq. (3.3–1), to contribute about 0.06 Ω of (low-frequency) broadband impedance, and an additional 1 Ω allowance is made for the vacuum chamber contribution. Together, these two sources contribute about 1.6 Ω of broadband impedance. To account for other impedance sources, such as feedback kickers, we have (somewhat arbitrarily) increased the broadband impedance used in the calculations shown here to 3 Ω. As is clear from Fig. 3.3–5, this impedance value does not lead to any problems.

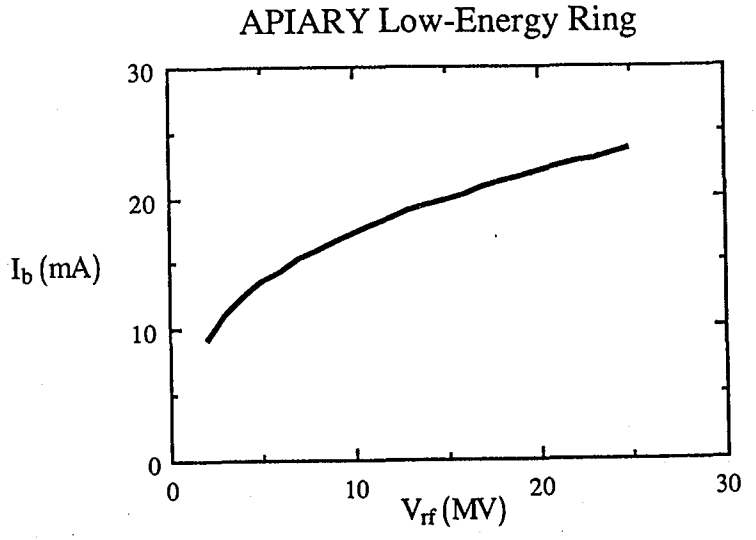

Fig. 3.3-5
Predicted threshold for longitudinal microwave instability for the APIARY low-energy ring. The threshold is above the required single-bunch current of 10.4 mA throughout most of this voltage range.

It is also worth noting here that we have estimated the natural momentum spread of the low-energy beam to be 1×10^{-3}. This relatively large value is associated with the significant amounts of "extra" synchrotron radiation (generated in the wigglers and vertical separation magnets) needed to achieve the equal damping decrement and round beam conditions discussed in Section 2.2. On the one hand, the increase in momentum spread has the undesirable effect of increasing the natural bunch length of the ring to 1.4 cm at $V_{rf} = 10$ MV but, on the other hand, it has the beneficial effect of stabilizing the bunches against growth from the longitudinal microwave instability, as can be seen from inspection of Eq. (3.3–4).

Transverse thresholds were predicted to be well beyond the range of interest, and so are of no concern.

Low-Energy Ring Intrabeam Scattering

In this case, the lower beam energy enhances the IBS growth rates, and the single-bunch current is much higher than for the high-energy beam, but these aspects are compensated by the larger transverse emittance values and by the more rapid radiation damping rate. Thus, we again predict no emittance growth from intrabeam scattering.

Low-Energy Ring Beam Lifetime

Touschek Scattering. As for the high-energy ring, the physical momentum acceptance limit, $\Delta p/p \approx 0.6\%$, dominates that of the rf bucket ($\Delta p/p \approx 1.7\%$). Although the lower energy causes the Touschek lifetime to decrease compared with that in the high-energy ring, the lifetime at 3.1 GeV—nearly 200 hours—is still not of concern.

Gas Scattering. At a gas pressure of 10 nTorr (N_2 equivalent), the lifetime is predicted to be dominated by the inelastic scattering process. Similar to what was found for the high-energy ring, the overall beam half-life is about 2 hours. Because the lifetime depends mainly on the background gas pressure in the low-energy ring, special care must be taken in the design of the vacuum chamber; this topic is discussed in Section 3.6.

Quantum Lifetime. The beta functions in the low-energy ring are generally rather small, but there is nonetheless one area where quantum lifetime could be an issue—in the IR superconducting quadrupole doublet. These magnets require the highest possible gradient and, both because the beta functions are increasing rapidly with distance from the IP and because azimuthal space is restricted, they cannot simply be lengthened. The design specifications for both quadrupoles call for an available beam aperture of only $\xi = 10$. This is sufficient, but leaves little margin for beam misalignments. In practice, it is already necessary for other reasons to have good control of the orbit in this region, so this aspect does not imply a new constraint, but it should be noted that care will be required in the alignment of these quadrupoles to avoid beam loss.

Low-Energy Ring Coupled-Bunch Instabilities

For the low-energy ring we studied the same three rf scenarios described earlier, with the number of rf cells reduced compared with the high-energy case to account for the lower voltage requirement. The general caveat mentioned earlier about not overinterpreting the results applies equally here.

Longitudinal growth times, summarized in Table 3.3–3, are more or less comparable to those for the high-energy ring. We see a less-strong preference here for substantial de-Qing or for the superconducting rf scenario, inasmuch as the results for Case B and Case C are roughly comparable, but the choice of a PEP-like rf system still looks unattractive. The results of Cases B or C are not unlike those predicted for the Advanced Light Source, now under construction at LBL. Feedback is needed, but the requirements should be manageable.

(A) PEP, Q/5[a)]	
$\tau_{a=1}$	0.02 ms
$\tau_{a=2}$	0.05 ms
(B) Room temperature[b)]	
$\tau_{a=1}$	1 ms
$\tau_{a=2}$	19 ms
(C) RT/SC, Q/100[b)]	
$\tau_{a=1}$	1 ms
$\tau_{a=2}$	30 ms

Table 3.3-3
Longitudinal coupled-bunch growth times for the APIARY low-energy ring (3.1 GeV; τ_E = 6.2 ms)

a) Estimated for I = 1 A; growth times at I = 3 A would decrease by a factor of three from those shown.

b) Estimated for I = 3 A.

Similar statements apply to the transverse growth times, which are summarized in Table 3.3–4. The preference for a new rf cavity design is apparent. Because of the faster (absolute) damping times in the low-energy ring, growth of the higher synchrotron modes ($a \geq 2$) is not a problem.

Table 3.3-4
Transverse coupled-bunch growth times for the APIARY low-energy ring (3.1 GeV; τ_E = 12.3 ms)

(A) PEP, Q/5[a)]	
$\tau_{a=1}$	0.02 ms
$\tau_{a=2}$	0.05 ms
(B) Room temperature[b)]	
$\tau_{a=1}$	1 ms
$\tau_{a=2}$	19 ms
(C) RT/SC, Q/100[b)]	
$\tau_{a=1}$	1 ms
$\tau_{a=2}$	30 ms

a) Estimated for I = 1 A; growth times at I = 3 A would decrease by a factor of three from those shown.

b) Estimated for I = 3 A.

Summary of Findings

We have seen here that the performance of both the high- and low-energy rings is likely to be limited mainly by coupled-bunch instabilities. Especially for the high-energy ring, we see a preference for the use of either highly de-Qed or superconducting rf cells. These choices tend to reduce the longitudinal impedance by permitting the voltage to be produced with many fewer cells and by permitting the cavity to be more "monochromatic." Furthermore, such cavity designs serve to lower the transverse impedance by having a relatively large bore size and by permitting the siting of the rf cells in a low-beta region of the ring.

Taken together, these features lead to a strong reduction in coupled-bunch instabilities and a strong increase in the transverse single-bunch threshold. Even after all of this, the ability of APIARY to achieve its full luminosity goal will depend largely on the capability of the feedback system (described in Section 3.5).

Total beam current limitations in both rings will depend upon the ability of the vacuum system to maintain an acceptable pressure, below 10 nTorr, in the presence of 3 A of circulating beam. We note here that there is an additional vacuum complication if a smaller circumference low-energy ring is employed, as discussed in Section 3.6. Single-bunch limitations appear to arise only from the allowable beam-beam tune shift, that is, neither bunch lengthening and widening due to the longitudinal microwave instability (which places a limit on the allowable broadband impedance), nor current limitations arising from the transverse mode-coupling instability are predicted to be constraints in the multibunch scenario considered here.

3.4. RF Systems

The rf systems for the APIARY collider rings must be capable of stably storing hundreds of bunches of electrons or positrons, each with a current of several mA. As discussed earlier, the most severe limitation on stable performance arises from coupled multibunch instabilities, which are driven by narrow, resonant higher-order modes (HOMs) of the rf cavities. For the usual room-temperature reentrant cavities, growth times under these beam conditions are predicted to be fractions of a millisecond; counteracting such growth would require extraordinarily powerful feedback systems.

Despite this difficulty, it seems clear that the multibunch mode of operation is essential for a high-luminosity B factory—there is no reason at present to imagine that tenfold to hundredfold improvements in luminosity will result from increases in the beam-beam tune-shift limit. In fact, it appears preferable to have many bunches with less current per bunch, as discussed earlier. There are three reasons for this view:

1. Single-bunch instabilities are decreased. Indeed, the maximum single-bunch currents will be limited by the transverse mode-coupling instability, which is driven mainly by the transverse impedance due to numerous rf cavities at high-beta locations in the ring.

2. Beam power losses to higher-order modes are reduced considerably, due to the lessened harmonic content of more closely spaced bunches.

3. Multibunch coupled motion is driven predominantly by average current, and is predicted to be so strong in B-factory colliders that it would be relatively insensitive to the temporal pattern of the bunches.

It is clear that the present PEP rf system is inappropriate for a B-factory collider. PEP has 24 five-cell reentrant rf cavities, for a total of 120 cells. The rf cavities occupy about 100 m in the ring and, on the average, they sample a rather high beta-function value—about 30 m. The bore size of these room-temperature cavities is typically small, which gives a high transverse impedance. The combination of high beta functions at the cavity locations and high transverse impedance is already known to limit the beam current.[19,20] (Note that, as discussed earlier,

more than two-thirds of the impedance in PEP stems from the substantial rf system.)

For the APIARY collider, these factors argue strongly for replacing the PEP rf system with compact, lower-impedance rf cavities. The new rf system must have the following features:

- Lowest possible number of cavities that can achieve the desired voltage (i.e., many fewer cells than PEP now has)
- Minimal higher-order impedance
- Large bore size to reduce transverse impedance
- Compact length so the rf can be localized in low-beta regions of the rings
- High gradients (up to 3–5 MV/m)

Fortunately, these requirements can be met with either of two approaches: superconducting rf cavities or specially designed, low-impedance conventional cavities.

In either approach, *single-cell rf cavities with the same shape as the superconducting cavities of LEP should be used;* this choice reduces HOM impedance and lends itself to taking full advantage of the HOM loading and coupling techniques already developed[25,26] at CERN for LEP and at DESY for HERA. The frequency used for the LEP rf system, 352 MHz, is essentially the same as that already used in PEP, so a cavity shape appropriate for the APIARY rings has already been developed and tested at CERN.

RF Scenarios

The room-temperature approach would use copper cavities, each driven by a single, commercially available 1-MW klystron. Using a high input power minimizes the number of cavities needed, but would require development of a cavity input window capable of transmitting 1 MW of rf power without breakdown. Such windows are now used for output coupling in klystrons; with some R&D they can be made to work for input power coupling in cavities as well. We do not anticipate problems with meeting the cooling requirements of the copper cavities, since the cavity shape is ellipsoidal (in fact, almost spherical) and is therefore relatively easy to cool.

In the superconducting approach, each klystron would drive two cavities, so the power per window would be reduced to 500 kW. This reduction in input power compared with the room-temperature scenario is possible because superconducting rf cavities have far lower wall losses than room-temperature cavities. Thus, we expect that—at any given level of power coupled through a window—the superconducting approach will have the advantage of requiring fewer cavities.

On the other hand, a superconducting rf system requires refrigeration and makes use of generally more complex technology, so it would probably be the more costly approach. Obviously, if R&D efforts lead to a high-power window design capable of handling 1 MW in a cryogenic environment, the use of superconducting rf becomes even more attractive.

With either rf scenario, the proposed cavities have an active length of 0.33 m. However, their overall geometry is complicated because each cavity requires input and loading couplers; we assume that at least 1 m of azimuthal space in the ring will be required per cavity.

Parameters of conventional and superconducting rf cavities for the 9- and 3.1-GeV APIARY rings are compared in Table 3.4–1 on the next page.

Table 3.4–1
Comparison of room-temperature and superconducting rf-system parameters for the APIARY storage rings.

High-Energy Ring

	Room Temp.	Supercon.
Accelerating voltage [MV]	25	25
Cavity shunt impedance* [MΩ]	2.77	277 000
Number of cavities	20	20
Gap voltage per cavity [MV]	1.25	1.25
Field gradient [MV/m]	3.75	3.75
Wall loss per cavity* [kW]	280	0.003
Wall loss, total for ring* [kW]	5640	0.056
Number of 1-MW klystrons*	20	10
Total klystron power* [MW]	20	10
Available power for beam and waveguide losses* [MW]	14.36	10

Low-Energy Ring

	Room Temp.	Supercon.
Accelerating voltage [MV]	10	10
Cavity shunt impedance* [MΩ]	2.77	277 000
Number of cavities	10	10
Gap voltage per cavity [MV]	1	1
Field gradient [MV/m]	3.0	3.0
Wall loss per cavity* [kW]	180	0.002
Wall loss, total for ring* [kW]	1810	0.018
Number of 1-MW klystrons*	10	5
Total klystron power* [MW]	10	5
Available power for beam and waveguide losses* [MW]	8.2	5.0

*) Denotes significant differences between room-temperature and superconducting scenarios.

Cavity Shape and Parameters

The shape for one quadrant of the rf cavity we are considering is shown in Fig. 3.4–1. This shape was used for computing the properties of the cavity fundamental mode (TM_{010}) with the frequency-domain electromagnetic code URMEL. The exact frequency used in the computations was 352.0525 MHz, corresponding to a wavelength of 0.852 m; this differs slightly from the nominal PEP frequency of 353.2 MHz. Predicted parameters of the cavity are summarized in Table 3.4–2.

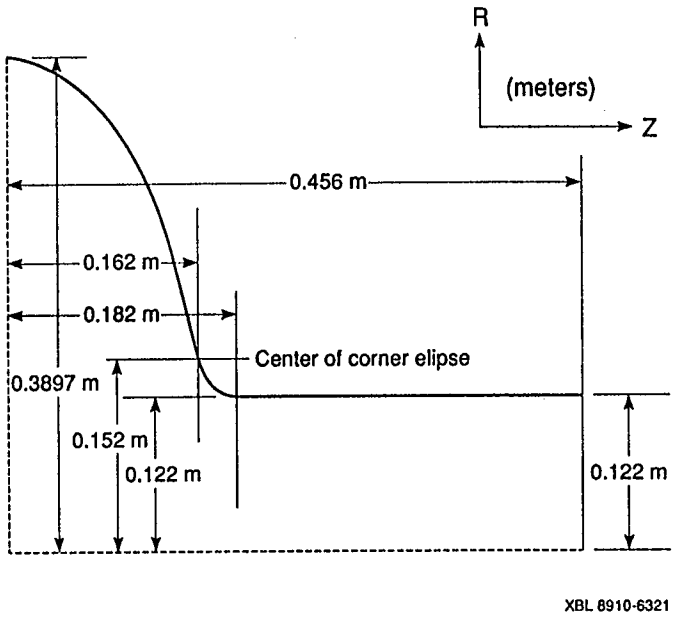

Fig. 3.4–1
Shape of a single quadrant of the rf cavity used at LEP which we have selected for APIARY.

Table 3.4–2
Predicted properties of APIARY rf cavity.

Parameter	Value
TM-mode beam-tube cutoff frequency, f_c [MHz]	940.5134
Ratio of fundamental to cutoff frequency, f/f_c	0.374
Unloaded Q at fundamental	45 218
(R/Q) at fundamental [Ω]	61.41
Single-particle loss parameter for the fundamental mode,[a] k_l (= $V^2/4U$) [V/pC]	0.0628

[a] V is the peak voltage and U is the stored energy.

Figs. 3.4–2 through 3.4–4 below show the electric-field patterns (direction and relative strength) of the fundamental and of two higher-order longitudinal modes, including that at the pipe cutoff frequency, i.e., $f/f_c = 1$.

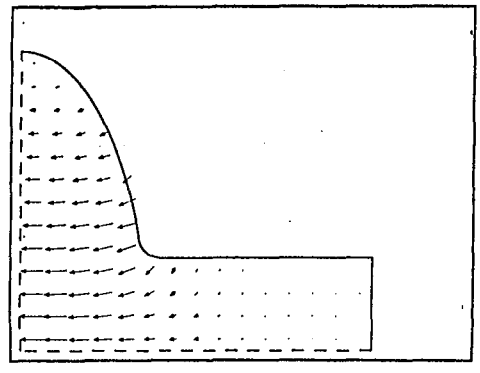

Fig. 3.4–2
Electric-field pattern at 352.11 MHz.

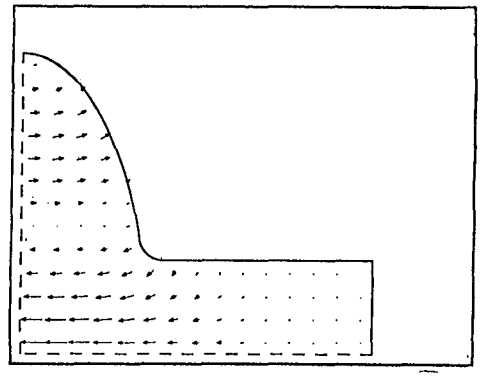

Fig. 3.4–3
Electric-field pattern at 726.33 MHz.

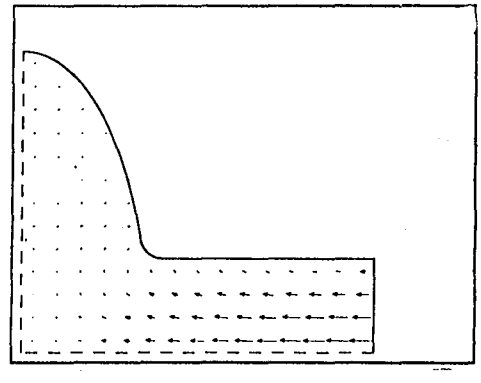

Fig. 3.4–4
Electric-field pattern at 963.37 MHz, the pipe cutoff frequency.

General Remarks on the Superconducting RF System

The total power P required for any rf system can be written as: *

$$P = \left(\frac{P_{SR} + P_{HOM}}{2}\right)\left[1 + \sqrt{1 + \frac{2u^2}{NR_s\left(1 - \frac{P_{HOM} + P_{Diss}}{P_{window}}\right)}}\right] \quad (3.4\text{–}1)$$

where

u is the field gradient [MV/m]
N is the number of cavity cells
R_s is the shunt impedance per cell [Ω]
P_{HOM} is the higher-order-mode power loss per cell [W]
P_{Diss} is the power dissipation per cell [W]
P_{window} is the power fed through each rf window [W]
P_{SR} is the synchrotron-radiation power [W]

From Eq. (3.4–1) we see that, for a given P, P_{SR}, and P_{HOM}, the number of cells goes down as the power per window goes up. At the Blois Workshop[27] it was concluded that superconducting rf would become attractive only if it is possible to transmit more than 400 kW through a window. (Other requirements identified at the workshop include a fundamental Q of 2×10^9, a loaded Q ≈ 50–100 for the higher-order modes, and a gradient of 5–9 MV/m.) Otherwise, room-temperature cavities that are shaped like superconducting ones (to allow efficient HOM loading) would be equally attractive.

The prospect of achieving these performance levels in superconducting rf cavities holds great promise. The required gradient and fundamental Q have already been achieved. At DESY, broadband de-Qing of HOMs has been advanced to the level of $Q_L \approx 200$–500 with specially designed HOM couplers.[25]

* (Discussion with F. Willeke of DESY on this point is gratefully acknowledged)

Considerable progress has also been made in high power transmission through windows. In the TRISTAN ring at KEK, levels of 85-100 kW per window have been reached during low-current beam tests in the accelerator. The 500-MHz superconducting cavities in Petra at DESY have achieved 350 kW per window for 18 ms and 250 kW per window for 3 hours, both in laboratory tests at room temperature. The 352-MHz CERN cavities for the superconducting LEP upgrade, whose design we would use, are rated at 120 kW per window and have been tested in the SPS ring under actual beam conditions; furthermore, they have achieved 380 kW in room-temperature laboratory tests at DESY. Finally, at Cornell, power levels in excess of 500 kW have been reached in laboratory tests under ideal conditions.

There do not seem to be any fundamental limits that would prevent us from achieving the goal of producing high-power, high-quality, single-cell superconducting rf cavities of the type needed for B-factories, although considerable R&D and detailed technical design remain to be done. In particular, special attention must be paid to three issues:

- Thermal isolation of the power window from the cryogenics
- Coupling the power into the cavities
- Coupling out high levels of HOM power loss through the cryogenic, superconducting environment into room-temperature loads

Perhaps the most important barrier to the use of superconducting rf systems is psychological. At present, there is no operational experience with using such systems to support beam currents on the order of amperes in a stable fashion. (We note, however, that the LEP-style cavities installed in the SPS ring survived a test involving circulation of proton-beam currents as high as 300 mA without damage.) Questions of quenching, thermal decoupling, and high beam loading weigh heavily. Fortunately, significant R&D is in progress at various laboratories. Furthermore, it is comforting to know that a specially designed room-temperature rf system would go a long way towards meeting the B-factory requirements in the meantime, given some improvements in rf-window capabilities.

The effects on the beam of higher-order modes of both the room-temperature and superconducting cavities were discussed in Section 3.3. To briefly summarize, we find that even with these well-designed cavities, growth of coupled multibunch motion—albeit at a reduced rate with growth times of 1 ms—can be expected. A feedback system will be essential, so it will be necessary to design one at the outset. The salient issues for the feedback system are the level of power required and the hardware complications introduced. In addition, one must consider whether the feedback hardware (detectors and kickers) defeats its own purpose by adding too much impedance to the ring.

3.5. Feedback Systems

If no improvements were made in rf system design, the APIARY storage rings would presumably employ standard, room-temperature, reentrant rf cavities. Because of the relatively high shunt impedances and high quality factors (Q) of the higher-order modes of such cavities, this choice would lead to significant growth rates for coupled-bunch instabilities—both longitudinal and transverse—and the feedback system would have to face the task of controlling coupled-bunch motion on a time scale of 0.1 ms or less, as estimated earlier. However, with the improved rf system (either superconducting or modified room-temperature) proposed here, the feedback system need only control coupled-bunch motion with an e-folding growth time of about 1 ms.

In this section we will focus on the feedback system needs for the APIARY high-energy ring, as these are the more demanding. This is so because there is considerably more installed rf needed in the high-energy ring to achieve the requisite 1-cm rms bunch length, and because of the greater rigidity of the beam. The low-energy ring will have a feedback system of relatively modest power, with characteristics qualitatively similar to those described below.

Modes of higher order than the quadrupole synchrotron mode longitudinally, or the dipole synchrotron mode transversely, should be effectively suppressed by synchrotron-radiation damping. Thus, we need only consider dipole (a = 1) and quadrupole (a = 2) synchrotron motions for longitudinal feedback, and only monopole (a = 0) and dipole (a = 1) synchrotron motions for transverse feedback.

The feedback-system bandwidth W required to affect the coupled-bunch motion of B symmetrically spaced bunches in the ring is

$$W = \frac{1}{2} B f_0 \quad , \qquad (3.5\text{–}1)$$

where f_0 is the bunch revolution frequency. To achieve the ultimate luminosity goal of 1×10^{34} $cm^{-2}\,s^{-1}$, every third rf bucket in PEP must be filled, for a total of 864 bunches. From Eq. (3.5–1), the bandwidth required would be about 60 MHz, which is moderate by modern standards.

For a growth time τ (the inverse of the growth rate g) of 1 ms, the fractional feedback correction energy δE required per turn to correct an error ΔE is

$$\left(\frac{\delta E}{\Delta E}\right)_{turn} = \frac{g}{f_0} = (\tau f_0)^{-1} = 7.33 \times 10^{-3} = \frac{1}{136} \, , \qquad (3.5\text{–}2)$$

and, as explained in Appendix C, the required feedback voltage per turn at the kicker, δV_k, is given by :

$$\delta V_k = 2\left(\frac{g}{f_0}\right)\frac{\Delta E}{e} = 2\varepsilon\left(\frac{g}{f_0}\right)\left(\frac{E_0}{e}\right) \quad , \qquad (3.5\text{–}3)$$

where ε (given by $\varepsilon = \Delta E/E_0$) is the estimated maximum relative energy error to be damped. In the fully injected "collider mode," we assume

$$\varepsilon = \sigma_{\Delta E/E,\ bunch} \approx 8 \times 10^{-4} \qquad (3.5\text{–}4)$$

at $E_0 = 9$ GeV; that is, we detect and correct errors equivalent to the rms energy spread in each bunch. About 106 kV of longitudinal feedback correction voltage is then required.

As this is a rather high voltage, we need a kicker with the highest possible shunt impedance to reduce the required power. The required kicker power is given by [28]

$$P_k = \frac{1}{2}\frac{(\delta V_k)^2}{R_\parallel T^2} \quad , \qquad (3.5\text{–}5)$$

where $R_\parallel T^2$ is the kicker shunt impedance modified by the transit-time factor, T. If the kicker power is limited to a reasonable value of 50 kW, the required total shunt impedance of the kicker is 112 kΩ.

A feasible feedback scenario employing a specific type of kicker that meets these requirements of bandwidth, power, and shunt impedance is described below.

Design Scenario

We have considered various types of kickers[28] and pickups, e.g., capacitive plates, resonant cavities, the stripline family of devices, and traveling-wave structures. Stripline quarter-wavelength ("λ/4") series loops appear to be the most attractive. A resonant cavity could provide very high shunt impedance, which minimizes power requirements, but at the cost of bandwidth. Even at a high frequency like 1 GHz, the Q of a cavity would have to be lowered significantly in order to achieve the necessary bandwidth. To obtain a bandwidth of $\Delta f = 60$ MHz, the Q (given by $f/\Delta f$) would have to be about 17, which would be rather difficult to obtain. Moreover, resonant cavities would add relatively more impedance in the beam's path (typically double what striplines would add).[29] However, it is feasible, as discussed at the end of this section, to employ a series of separately powered tuned cavities, each with a bandwidth of about 10 MHz and together spanning 60 MHz.

Stripline electrodes are directional couplers and have terminals at both ends. Their signals may therefore be added by simple series connection; such an array is shown in Fig. 3.5-1, taken from Reference 28. The sinusoidal signals, progressing downstream, add in phase if the closely spaced loops are λ/4 long at midband and if the connecting transmission lines (each of impedance $Z_L \approx 100\ \Omega$) are λ/2 long. Assuming no mismatch in signal and

particle velocities, the response of N such loops is N times enhanced over that of a single loop, and the bandwidth narrows linearly as the transit time becomes longer. The frequency bandwidth $\Delta\omega$ within the half-power range is,[28] for $N \geq 2$, approximately $0.9(\omega/N)$. By using the series array of striplines described here, it is easy to exercise flexibility in exchanging bandwidth for gain and, through proper matching, to avoid wasting power on unused bandwidth.

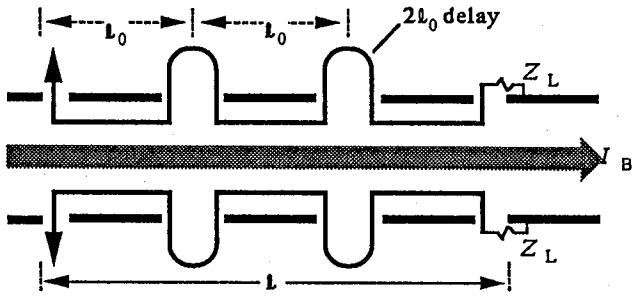

Fig. 3.5–1
Array of series-connected stripline electrodes.

The product of bandwidth and peak power gain (i.e., shunt impedance) is proportional to the pickup length ℓ and is given by[28]

$$R_{\parallel}T^2\Delta\omega \approx \frac{3.6}{\pi} Z_L c\,(k_0 g_{\parallel})^2 \ell = \frac{1.5}{\pi^2}\left(Z_0 c k_0^2\,\ell\right) , \qquad (3.5\text{–}6)$$

where $g_{\parallel}{}^2 = 1/2$ is a reasonably attainable geometric factor; Z_0 is the free-space impedance (= 377 Ω); and $k_0 = \omega_0/c$, with ω_0 being the central angular frequency of the kicker.

We envision a series loop stripline pair at a central frequency of 1 GHz. (Although higher frequencies give higher shunt impedance, practical problems with assembling the device in the vacuum chamber are encountered for central frequencies beyond about 1 GHz; we take this as a practical upper limit for the design frequency of the feedback system.) The 1-GHz, $\lambda/4$ striplines are 7.5 cm long. For the required bandwidth of 60 MHz, we would need 15 such loops connected in series. In practice, however, reflections and so forth would cause significant power attenuation across such a long series of loops. A summary of performance figures for 5-, 10-, and 15-loop arrays is presented in Table 3.5–1.

	Attenuation[a] (%)	$R_{\|\|}T^2$ (kΩ)	Bandwidth (MHz)	Length (cm)
5 loops	20	2.5	180	37.5
10 loops	50	10.0	90	75.0
15 loops	80	22.5	60	112.5

[a] Estimated input power attenuation due to reflections, etc.

To have an effective kicker power of 50 kW (which would require 112 kΩ of total shunt impedance) we could utilize either 45 five-loop arrays (total length 17 m) or 12 ten-loop arrays (total length 9 m). Taking attenuation into account, the power fed per meter of structure would be 3.7 kW (or 1.4 kW per array) for the five-loop arrays, and about 11 kW (or 8.3 kW per array) for the ten-loop arrays. Considering the complexity of the cooling manifold needed for these high-power kickers, the five-loop array scenario appears to be the best choice. Note that any of these arrays would be feasible to build, but all would require extreme care in minimizing reflections, matching impedance, etc.

The kickers and pickups will also respond to the driving beam current, and will generate wakefields that will act back on the beam. Typically, the broadband impedance from these devices is peaked at the central frequency (1 GHz here) with a bandwidth determined by the device length (e.g., 180 MHz for the five-loop array); there are also higher harmonics (2 GHz, 3 GHz, etc.) present, but with ever-decreasing strength. The peak value of the longitudinal impedance $R_{\|}T^2$ at the fundamental frequency is typically a quarter of the shunt impedance.[28] The central frequency of 1 GHz corresponds to a revolution-frequency harmonic of $n \approx 7338$ for PEP.

The total longitudinal resistive broadband impedance at the peak of the kicker fundamental is then

$$\frac{Z_{\|}}{n} = \frac{1}{4}\frac{R_{\|}T^2}{n} \approx 4\,\Omega \qquad (3.5\text{–}7)$$

for $R_{\|}T^2 = 112$ kΩ. Considering the contribution from the pickups to be about 25% of this (because there will be fewer pickups than kickers), the total resistive longitudinal impedance

is $(Z_{\|}/n)_T \approx 5\ \Omega$. The low-frequency reactive impedance will be reduced from this figure by the Q value of the structure ($Q \approx 5.5$) to about 1 Ω. Contributions from the higher harmonics will fall off rapidly with frequency; with careful design these can be suppressed to low levels.

The bandwidth of the impedance generated by the feedback structure described here is broad enough to avoid inducing instability in the coupled-bunch motion it is supposed to cure, that is, its wakefields have sufficient time to damp between successive bunch passages. On the other hand, the impedance bandwidth is not large enough to affect single-bunch (internal) motion significantly.

For the purpose of estimating the effects on a single bunch, such as bunch lengthening, we must calculate an "effective broadband impedance." This involves a convolution of the frequency-dependent impedance with the power spectrum of the bunch, $h_a(\omega)$, as described in Reference 18:

$$\left[\frac{Z_{\|}}{n}\right]^a_{eff} = \sum_{n=-\infty}^{\infty} \left[\frac{Z_{\|}(\omega_{n,a})}{(\omega_{n,a}/\omega_0)}\right] h_a(\omega_{n,a}) \qquad (3.5\text{–}8)$$

where $\omega_{n,a} = n\omega_0 + a\omega_s$, with a being the synchrotron mode number. Explicit computation of this sum yields a rather low value of this effective impedance (on the order of 0.4 Ω). Thus, the feedback system is not expected to exacerbate any beam instabilities.

Wideband multibunch feedback can be implemented in many ways:

- Fast bunch-by-bunch feedback that influences single bunches directly; this requires only simple filtering and can be visualized simply in the time domain
- Mode-by-mode damping; this is accomplished by performing careful modal analysis in the frequency domain and selecting and affecting specific modes
- All-mode damping; this may be necessary when dealing with large numbers of bunches, but it requires many electronics channels with complicated notch filtering and special frequency-dependent gain and phase characteristics

For our situation, which involves very many multibunch azimuthal modes but only a few synchrotron modes (dipole and quadrupole), the fast and direct method of bunch-by-bunch feedback is preferred, being conceptually and electronically straightforward. The following steps must be carried out:

- Beam signals are detected over a suitably large bandwidth ($\geq$ 60 MHz)
- Detected phase and slope of the zero-crossing are processed with fast phase-shifters, delays, and voltage modulators
- The modified signals are fed through a power amplifier and applied directly to the kicker.

With today's high-frequency digital signal processing, this method is entirely feasible. A block diagram of the feedback loop is shown in Fig. 3.5–2.

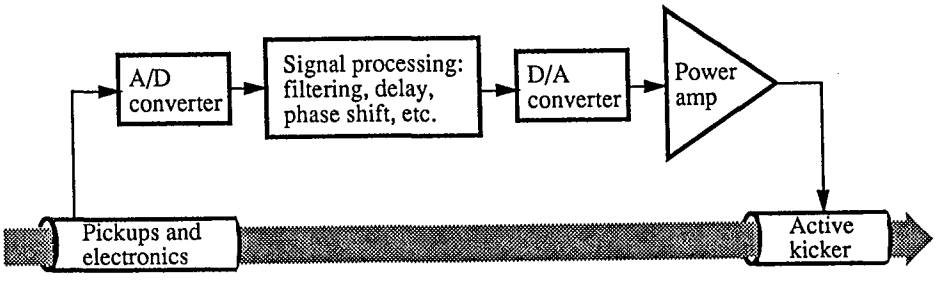

Fig. 3.5–2
Diagram of feedback loop.

We recognize that broadband power amplifiers centered around 1 GHz with a bandwidth of 60 MHz and 50–100 kW of power may not be available. Therefore, we envision a series of six stagger-tuned television-type klystrons (having bandwidths up to 11 MHz and power output up to 40 kW), with different center frequencies, and spanning a bandwidth of 60 MHz around a center frequency of, say, 800 MHz. Sufficient power is available from the klystrons to make up for the somewhat reduced shunt impedance of the kickers at 800 MHz compared with the 1 GHz center frequency discussed earlier. Six channels would be needed, each containing an appropriate bandpass filter followed by a suitably tuned klystron and another bandpass filter, before all the channel signals are combined through a signal combiner and finally fed to the broadband kicker. This system is illustrated schematically in Fig. 3.5–3.

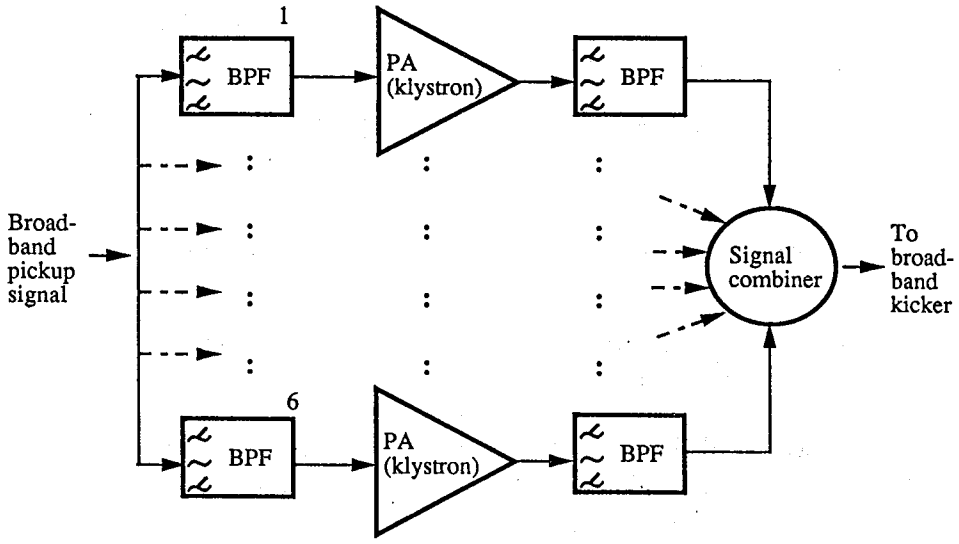

Fig. 3.5–3
Stagger-tuned series of six klystrons and associated circuitry feeding the broadband kicker.

Since each of the channels is narrowband, there is no disadvantage to using, instead of a broadband kicker, six narrowband resonant cavities, each with $Q \approx 80$ and frequencies that are different for each cavity but spanning a total bandwidth of 60 MHz around a high frequency of 800 MHz. With this choice, illustrated in Fig. 3.5–4, we have six separate channels feeding six sets of separate kickers, avoiding the complications of signal combining. Cavities of this description should be achievable. Their shunt impedance[28] is given approximately by Eq. (3.5–6), with the factor 1.5 replaced by 2.

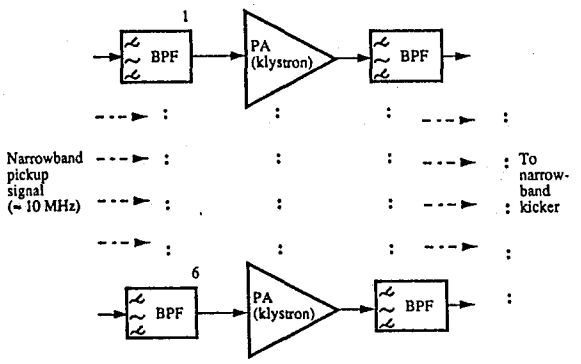

Fig. 3.5–4
By using six separate channels feeding six separate sets of kickers, we can avoid the problems of signal combining.

At injection, larger coherent oscillation amplitudes stemming from injection errors must be handled, along with the inevitable small oscillations of the stored beam that result from injection kicker mismatches. (Injection kickers have been known to induce significant beam-core jitter and this effect dominates many rings at injection). However, the injected current per pulse is typically 1 mA, more than two orders of magnitude below the stored current. The feedback power levels required to damp the freshly injected beams would also be smaller, due to the lower growth rates. It is feasible to think of two separate feedback systems—one for high-power damping of the core of the high-current beam, another for lower-power handling of the tail of the beam at injection. Given an injection profile of beam current and errors as a function of time, one can combine, tailor, and match the feedback systems to achieve the required damping scenario.

Feedback to control injected particles with large errors may require special pickups and kickers that are sensitive only to the amplitudes found in the tail of the beam. Examples could

include structures that are broadband and are simply nonlinear along the radial direction.

For multibunch growth times of 0.1 ms, the situation becomes qualitatively different, and addressing it may well be impractical. Even for a total kicker shunt impedance of 1 MΩ, a total effective kicker power of 500 kW would be required. This would require, in turn, fifty 1.125-m-long, 15-loop, series-connected striplines covering 57 m of circumferential length. The bandwidth would be ideally matched to 60 MHz but, with 80% attenuation, one would have to feed about 45 kW of power per meter of active feedback structure. Supplying the power is merely a matter of cost, but the high power per meter of structure is a nontrivial technical issue. In this high-power application, traveling-wave structures hold considerable promise,[28] but they need more developmental work. Technological sophistication would be required, and a major R&D effort related to traveling-wave structures would be crucial in this context.

3.6. Synchrotron Radiation and Vacuum

When an electron beam circulates in a storage ring, the vacuum-chamber walls are subjected to synchrotron radiation. This radiation incident on the walls produces very high thermal flux densities due to the narrowness of its spatial distribution, which means that the chamber wall must be cooled. Normally, this is accomplished by water cooling the external surface of the chamber. An additional benefit associated with the cooling is that it maintains the chamber wall at a relatively low temperature, thus decreasing the gas load resulting from thermal desorption.

There are two design issues related to the copious production of synchrotron radiation in a high-intensity storage ring:

- Heating of the vacuum chamber walls due to the high thermal flux density
- Radiation-induced gas desorption (both photodesorption and thermal desorption)

In this section we will estimate these effects and see what impact they have upon collider performance. As we shall see, the difficulties associated with the high beam currents in the APIARY storage rings are all amenable to standard engineering solutions. Note that we use "electrons" in this section in the generic sense of referring either to electrons or to positrons.

Wall Heating

In the APIARY design (at its full luminosity), we are dealing with a beam current in each ring more than a factor of 10 higher than is typical for a high-energy storage ring, so the heat load is quite high. As will be obvious from the discussion below, the difficult parameter to deal with is not the power *per se*, but rather the linear thermal flux density. For this reason, it turns out that—contrary to intuition—a small-circumference ring is a more difficult problem to deal with. In fact, if a very small low-energy ring design were selected, the heating problem would be considerably more severe than in the high-energy PEP ring, despite the fact that the beam energy, and thus the synchrotron radiation power itself, is lower than in the high-energy ring. For this reason, our main focus is on the low-energy ring. In the design example analyzed here, the ring has a circumference $C = 733.3$ m, or one-third that of PEP.

To estimate the heat load, we start from the well-known expression for the synchrotron radiation power (in watts), given by:

$$P_{SR} = \frac{88.5\, E^4\, I}{\rho} \qquad (3.6\text{–}1)$$

where E is the total energy (in GeV), I is the total beam current (in mA), and ρ is the bend radius of the dipoles (in m). For the low-energy ring, we take a typical value of $\rho = 25$ m. Then, the linear power density (in W/cm) along the radiated circumferential path length is given by

$$P_L = \frac{0.01 \cdot P_{SR}}{2\pi\rho} = \frac{0.885\, E^4\, I}{2\pi\rho^2} \quad . \qquad (3.6\text{–}2)$$

For a 3.1-GeV, 3000-mA beam, as would correspond to the low-energy ring at a luminosity of $\mathcal{L} = 1 \times 10^{34}$ cm^{-2}s^{-1}, we obtain $P_L = 63$ W/cm.

The vertical angular spread (in radians) of the synchrotron radiation fan is given approximately by

$$\theta \approx \frac{m_0 c^2}{E} = \frac{1}{\gamma} \quad , \qquad (3.6\text{–}3)$$

which, for a 3.1-GeV electron beam, is $\theta = 0.17$ mrad. Although not strictly true, we will assume here that the power is uniformly distributed over this angular extent, in which case we calculate the height of the vertical band illuminated by the synchrotron radiation fan to be

$$h = 2\left[\sigma_y^2 + d^2 \cdot \left(\sigma_{y'}^2 + \theta^2\right)\right]^{1/2} \qquad (3.6\text{–}4)$$

where σ_y is the rms beam height, $\sigma_{y'}$ is the rms angular spread, and d is the tangential distance from the beam orbit to the chamber wall, as shown in Fig. 3.6-1.

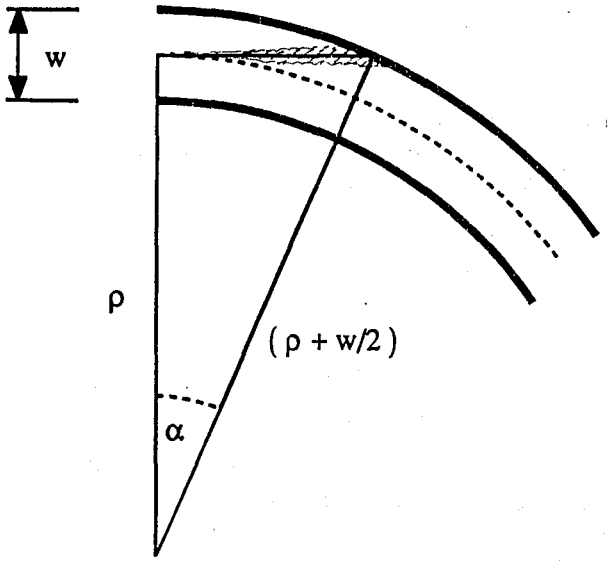

Fig. 3.6–1
Geometry of the synchrotron-radiation fan hitting the vacuum-chamber wall (not to scale).

The value for d can be easily calculated from the geometry shown in Fig. 3.6–1, where w/2 is the transverse distance from the beam orbit to the outer wall of the vacuum chamber:

$$d = \sqrt{\left(\rho + \frac{w}{2}\right)^2 - \rho^2} \quad . \qquad (3.6\text{–}5)$$

For a standard vacuum chamber half-width of 6 cm and a 25 m bending radius, we would obtain d = 1.7 m, with an angle of incidence given by $\alpha = d/\rho = 69$ mrad. A specially designed dual-chamber vacuum system such as we envision could have an effective half-width much larger than 6 cm, which would increase the photon beam height considerably.

For the low-energy ring, we take the equivalent half-width value to be 26 cm, so that d = 3.6 m and $\alpha = 145$ mrad. (Note that, in the case of the high-energy ring, there is an interference problem with the coil of the PEP dipoles, and the dual-chamber vacuum system must extend even further out than indicated here for the low-energy ring. Therefore we take a half-width of 41 cm for the high-energy ring, which increases d to 11.6 m.) To be conservative, we estimate the radiation power density ignoring the contribution from the finite beam size, that is, we take $\sigma_y = \sigma_{y'} = 0$ in Eq. (3.6–4). With this approach, we find the height of the illuminated strip to be $h = 2\theta d = 1.19$ mm, and the thermal flux density becomes $P_A = P_L/h = 530$ W/cm^2. This

value is only half of the value that has long been used at SLAC as an acceptable design value for beam stoppers, collimators, scrapers, etc., and both SPEAR and PEP operate without problems at this power density level. If a more realistic beam height were assumed, e.g., for a typical beta-function value of 5 m in the dipoles, we would get h = 2.2 mm from Eq. (3.6–4) and the thermal flux density would drop to P_A = 290 W/cm^2. Nonetheless, in the estimates of heat loads below we take the conservative and more pessimistic view that the beam size is negligible.

It is important to note that our flux density estimate applies to the case of a photon beam incident on the vacuum chamber wall at a shallow angle (α = 145 mrad in the example above). In the worst-case of an object *normal* to the incident flux, such as a flange or radiation mask, the density would increase in the ratio sin (π/2)/sin (α) = 1/0.145 $\approx$ 7, giving P_L = 435 W/cm or P_A = 3.7 kW/cm^2. These values are clearly unacceptable, so inclined masks in two dimensions, etc., will be required to reduce the thermal loads to reasonable values.

Having calculated the thermal flux, we can now estimate the temperature drop ΔT across the vacuum chamber wall. We use the model illustrated in Fig. 3.6–2, where the thermal flux is taken to vary in a 45° cone from the initial source of height h through a wall of thickness W.

Fig. 3.6–2
Thermal-flux model.

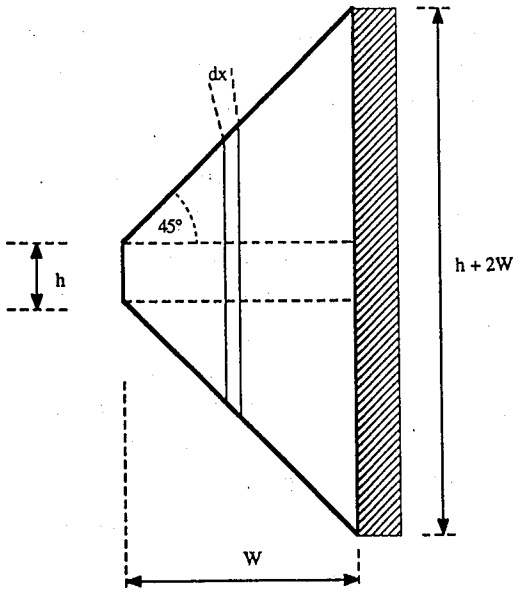

The change in temperature in this case is given by

$$\Delta T = \frac{P_L}{K}\int_0^w \frac{dx}{(h+2x)} = \frac{P_L}{2K} ln\left(\frac{h+2W}{h}\right) \qquad (3.6\text{–}6)$$

where K is the thermal conductivity of aluminum. (A typical value for an Al alloy is 1.7 W/cm-°C). For a 1 cm wall thickness and h = 1.19 mm we get $\Delta T = 53°C$.

Next, we estimate the required water cooling requirements. The temperature difference between the water and the vacuum chamber wall is given by

$$\Delta T_W = \frac{LP_L}{h_W L\,(h+2\,W)} \qquad (3.6\text{–}7)$$

where $h_W = 0.8$ W/cm^2-°C is the heat transfer coefficient for water at a reasonable flow velocity of 6 ft/s, and $L\cdot(h + 2W) = 2.119\cdot L$ cm^2 is the area being cooled. For our case, we find $\Delta T_W = 37°$ C, so the total temperature difference between the inner wall of the chamber and the cooling water is 90° C. Given an inlet water temperature of 22° C, the inner wall temperature would be 112° C. For a 5-m chamber, the total heat to be removed is $L\,P_L = 500\cdot 63$ W = 31.5 kW. The required flow rate, Q (gal/min), to remove this heat is given by

$$Q = \frac{3.8\times 10^{-3}\,L\cdot P_L}{\Delta T} \qquad (3.6\text{–}8)$$

so, for an allowable water temperature rise of 10° C, we find Q = 12 gal/min = 2765 in^3/min. To achieve the specified flow velocity of 6 ft/s = 4320 in/min, the required area of the cooling passage is given by

$$A = \frac{2765\ \text{in}^3/\text{min}}{4320\ \text{in/min}} \approx 0.6\ \text{in}^2 \qquad (3.6\text{–}9)$$

Thus, a cooling passage of dimensions 1 in × 0.6 in would suffice.

Based on these considerations, the chamber inner wall temperature will be in the neighborhood of 110° C, which should not lead to difficulties. It is worth noting that the initial operation of the collider at reduced luminosity, and thus reduced beam current, would also mitigate the heat loads considerably.

Table 3.6–1 summarizes both the ultimate and relaxed luminosity cases for the high- and low-energy rings, compared with values from PEP and SPEAR. We see that the wall temperature for the full-luminosity case in the low-energy ring is much higher than the typical SPEAR value, but is rather similar to the original design specification for the PEP chamber. Similarly, we see that the dual-chamber vacuum system keeps the wall temperature for the high-energy ring comparable to the original PEP design specification, despite a fifteenfold increase in beam current.

Table 3.6–1a
Comparison of radiation loads and heat fluxes in SPEAR and the APIARY low-energy ring

PARAMETER	SPEAR	APIARY Low Energy High Current	APIARY Low Energy Low Current
Magnetic radius [m]	12.713	24.905	24.905
Bend magnet field [T]	0.3937	0.4153	0.4153
Energy [GeV]	1.50	3.10	3.10
Current [mA]	200.00	3000.00	1000.00
Power [kW]	7	985	328
Chamber wall linear flux [W cm^{-1}]	0.88	62.97	20.99
Beam divergence θ [mrad]	0.34	0.16	0.16
Tangential distance d (m)	1.13	3.61	3.61
Angle of incidence α [mrad]	88.78	144.87	144.87
Beam height [mm]	1.369	1.190	1.190
Linear flux on masks at 90° [W cm^{-1}]	9.96	436.20	145.40
Wall heat load [kW cm^{-2}]	0.01	0.53	0.20
Heat load on masks at 90° [kW cm^{-2}]	0.07	3.67	1.39
Wall thickness [cm]	0.7	1.00	1.00
ΔT across wall [°C]	0.49	41.22	14.31
ΔT, chamber to water [°C]	0.72	37.15	12.47
ΔT, total, inner wall to water [°C]	1.20	78.37	26.77
Inlet water temperature [°C]	22.00	22.00	22.00
Water temperature rise [°C]	0.15	10.88	3.63
Average wall temperature [°C]	23.28	105.90	50.58

Table 3.6–1b
Comparison of radiation loads and heat fluxes in PEP and the APIARY high-energy ring.

PARAMETER	PEP	APIARY High Energy High Current	APIARY High Energy Low Current
Magnetic radius [m]	165.000	165.000	165.000
Bend magnet field [T]	0.3033	0.1820	0.1820
Energy [GeV]	15.00	9.00	9.00
Current [mA]	200.00	3000.00	1000.00
Power [kW]	5436	10567	3522
Chamber wall linear flux [W cm^{-1}]	52.43	101.92	33.97
Beam divergence θ [mrad]	0.03	0.06	0.06
Tangential distance d (m)	4.06	11.64	11.64
Angle of incidence α [mrad]	24.62	70.54	70.54
Beam height [mm]	1.152	3.256	3.256
Linear flux on masks at 90° [W cm^{-1}]	2129.79	1446.12	482.04
Wall heat load [kW cm^{-2}]	0.46	0.31	0.10
Heat load on masks at 90° [kW cm^{-2}]	18.49	4.44	1.48
Wall thickness [cm]	0.7	1.00	1.00
ΔT across wall [°C]	37.53	55.66	18.55
ΔT, chamber to water [°C]	43.25	54.78	18.26
ΔT, total, inner wall to water [°C]	80.78	110.45	36.82
Inlet water temperature [°C]	22.00	22.00	22.00
Water temperature rise [°C]	9.06	17.61	5.87
Average wall temperature [°C]	107.31	141.25	61.75

Gas Desorption

Gas desorption in an electron storage ring arises from two causes:

- Thermal outgassing
- Synchrotron-radiation-induced photodesorption

The first mechanism is common to all vacuum systems, and occurs in the absence of synchrotron radiation. In essentially all electron storage rings, the thermal outgassing component of the pressure is negligible compared with that from the photodesorption, and contributes mainly to the base pressure of the ring in the absence of a circulating beam. The gas load from synchrotron radiation, on the other hand, determines the actual running pressure of the ring.

In the case of the APIARY design, the two rings will each have a circulating beam current of approximately 3 A to reach the ultimate luminosity goal of 1×10^{34} $cm^{-2}s^{-1}$. This beam current is at least an order of magnitude beyond the typical value for today's colliders, and as such presents an appreciable challenge to the vacuum system designer.

To estimate the desorption rate, we follow the approach of Gröbner et al.[30] After taking the spectrum of the synchrotron radiation photons into account, we can express the photon flux in the spectral interval (0,x) in the form

$$\dot{N}(x) = \frac{\sqrt{3}\, r_e}{e\hbar c} F(x)\, E\, I \qquad (3.6\text{–}10)$$

where

$$x = \frac{\varepsilon}{\varepsilon_{crit}} = \frac{\varepsilon}{\left(\frac{3}{2\hbar c}\right)\left(\frac{\gamma^3}{\rho}\right)} \qquad (3.6\text{–}11)$$

with ε the photon energy, ε_{crit} the critical energy in the dipoles, and F(x) the integral over the modified Bessel function

$$F(x) = \int_0^x \int_u^\infty K_{5/3}(y)\, dy\, du \quad . \qquad (3.6\text{–}12)$$

For large values of x, F(x) $\rightarrow$ 5.53. After rearranging and inserting appropriate values for the constants, we obtain for the total flux

$$\dot{N} = 8.08 \times 10^{17}\ E{\cdot}I \quad [\text{photons/s}] \qquad (3.6\text{–}13)$$

where E is in GeV and I is in mA. Desorbed gas molecules are produced in proportion to the photon flux, with the proportionality constant, η_F, giving the number of molecules produced per incident photon, that is,

$$\dot{N}_{Mol} = 8.08 \times 10^{17}\ E{\cdot}I{\cdot}\eta_F \quad [\text{molecules/s}] \qquad (3.6\text{–}14)$$

There has been a great deal of discussion in the literature about the appropriate value for η_F; typical values range from about 2×10^{-7} to 5×10^{-6}. For this document, we take a conservative choice of $\eta_F = 1.5 \times 10^{-5}$, which was used in the PEP and SPEAR designs. Using the Ideal Gas Law, we can relate the number of molecules to a gas load with a conversion factor of 3×10^{-20} Torr-liters/molecule. This gives the effective gas load from the photodesorption as

$$Q_{gas} = 2.42 \times 10^{-2}\ E{\cdot}I{\cdot}\eta_F \quad [\text{Torr·liters/s}] \qquad (3.6\text{–}15)$$

or, for our assumed desorption coefficient of $\eta_F = 1.5 \times 10^{-5}$,

$$Q_{gas} = 3.64 \times 10^{-8}\ E{\cdot}I \quad [\text{Torr·liters/s}] \ . \qquad (3.6\text{–}16)$$

In Table 3.6–2, we use Eq. (3.6–16) to estimate the gas loads produced in the various storage rings under consideration. Maintaining a pressure of 10 nTorr in the low-energy ring requires a total pumping speed of about 350 000 l/s. To put this into perspective, it is about the same pumping capacity, per meter of ring circumference, as is being installed on the ALS ring at LBL.[31] If it turns out that a lower η_F value can be justified, the pumping requirements can be reduced accordingly. Similarly, the high-energy ring requires about three times the pumping speed of the low-energy ring and is three times as long, so its requirement is also compatible with the ALS specifications.

Table 3.6–2a
Comparison of vacuum loads and pumping speed requirements in SPEAR and the APIARY low-energy ring.

PARAMETER	SPEAR	APIARY Low Energy High Current	APIARY Low Energy Low Current
Magnetic radius [m]	12.713	24.905	24.905
Bend magnet field [T]	0.3937	0.4153	0.4153
Energy [GeV]	1.5	3.1	3.1
Current [mA]	200	3000	1000
Power [kW]	7	985	328
Gas load [Torr-l s^{-1} mA^{-1}]	3.63×10^{-8}	7.50×10^{-8}	7.50×10^{-8}
Total photon gas load [Torr-l s^{-1}]	1.09×10^{-4}	3.38×10^{-3}	1.13×10^{-3}
Assumed desorption coefficient (η_F)	1.50×10^{-5}	1.50×10^{-5}	1.50×10^{-5}
Photon gas load [Torr-l s^{-1} m^{-1}]	1.36×10^{-6}	2.16×10^{-5}	7.19×10^{-6}
Base pressure required [Torr]	1.00×10^{-8}	1.00×10^{-8}	1.00×10^{-8}
Distributed pumping [l m^{-1} s^{-1}]	136	2157	719
Total distributed pumping [l s^{-1}]	10 890	337 590	112 530
Coefficient of thermal desorption [Torr-l cm^{-2}]	1.5×10^{-11}	1.0×10^{-11}	1.0×10^{-11}
Calculated wall temperature [°C]	23.28	105.80	50.59
Thermal desorption [Torr-l @ °C cm^{-2}]	2.33×10^{-11}	5.72×10^{-11}	2.04×10^{-11}
Total perimeter of ring [m]	190	733	733
Calculated thermal load [Torr-l m^{-1}]	6.98×10^{-8}	1.72×10^{-7}	6.12×10^{-5}
Total calculated thermal load [Torr-l]	1.33×10^{-5}	1.26×10^{-4}	4.48×10^{-5}
Total gas load [Torr-l]	1.22×10^{-4}	3.50×10^{-3}	1.17×10^{-3}
Total pumping [l sec^{-1}]	12 217	350 169	117 014

Table 3.6–2b
Comparison of vacuum loads and pumping speed requirements in PEP and the APIARY high-energy ring

PARAMETER	PEP	APIARY High Energy High Current	APIARY High Energy Low Current
Magnetic Radius [m]	165	165	165
Bend Magnet Field [T]	0.3033	0.1820	0.1820
Energy [GeV]	15	9	9
Current [mA]	200	3000	1000
Power [kW]	5436	10 567	3522
Gas load [Torr-l s^{-1} mA^{-1}]	3.63×10^{-7}	2.18×10^{-7}	2.18×10^{-7}
Total photon gas load [Torr-l s^{-1}]	1.09×10^{-3}	9.80×10^{-3}	3.27×10^{-3}
Assumed desorption coefficient (η_E)	1.50×10^{-5}	1.50×10^{-5}	1.50×10^{-5}
Photon gas load [Torr-l s^{-1} m^{-1}]	1.05×10^{-6}	9.45×10^{-6}	3.15×10^{-6}
Base pressure required [Torr]	1.00×10^{-8}	1.00×10^{-8}	1.00×10^{-8}
Distributed pumping [l m^{-1} s^{-1}]	105	945	315
Total distributed pumping [l s^{-1}]	108 900	980 100	326 700
Coefficient of thermal desorption [Torr-l cm^{-2}]	1.5×10^{-11}	1.0×10^{-11}	1.0×10^{-11}
Calculated wall temperature [°C]	107.31	141.25	61.75
Thermal desorption [Torr-l @ °C cm^{-2}]	1.07×10^{-10}	9.42×10^{-11}	2.78×10^{-11}
Total perimeter of ring [m]	2200	2200	2200
Calculated thermal load [Torr-l m^{-1}]	3.22×10^{-7}	2.83×10^{-7}	8.35×10^{-8}
Total calculated thermal load [Torr-l]	7.08×10^{-4}	6.22×10^{-4}	1.84×10^{-4}
Total gas load [Torr-l]	1.80×10^{-3}	1.04×10^{-2}	3.45×10^{-3}
Total Pumping [l sec^{-1}]	179 724	1 042 250	345 070

Required Modifications to the PEP Ring

The present PEP vacuum system suffers from being incompatible with the high currents required for a high-luminosity B-factory. It has been proposed, therefore, to reorient the PEP C-magnet dipoles such that the open side of each magnet is towards the outside of the tunnel. The benefit of such a modification is that it permits the use of a dual-chamber vacuum system, as illustrated schematically in Fig. 3.6–3.

Unfortunately, much of the synchrotron radiation desorption will take place not in the dipole chambers, but in the straight sections joining the dipoles (where a standard beam pipe is used for the quadrupole and sextupole magnets). An estimate of the thermal loading in this area, following the approach outlined earlier in this section, indicates that the values will be within the original design specifications for the PEP chamber and should be manageable. However, the pressure with a 3-A beam current will be roughly ten times the present PEP pressure, which would be unacceptable for the beam lifetime.

In the short term, when the APIARY collider is operating at a reduced luminosity, it might suffice to simply provide additional local pumping. However, the vacuum system is likely to be conductance limited in this region, so the beneficial effects of additional pumping will be limited. Thus, it is likely that a dual vacuum chamber arrangement will be required in the quadrupole straight sections as well as in the dipoles. If so, the quadrupoles and sextupoles would need to be redesigned as C-magnets and completely replaced. Given that the beam energy required for the APIARY high-energy ring is well below the PEP design value of 15 GeV, it may be possible to reduce the length of the quadrupole magnets. On the other hand, the new focusing arrangements produce relatively high chromaticity values, so it might well be desirable to increase the length of the sextupoles. Acceptable designs for C-quadrupoles and C-sextupoles are already available from the ALS,[31] so feasibility is not an issue, but larger bore sizes would be required in this application.

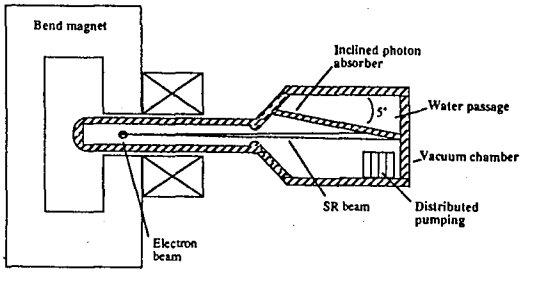

Fig. 3.6–3
Schematic of dual-chamber vacuum system

Installation of the Low-Energy Ring in the PEP Tunnel

During its initial design phase, room was made available in the PEP tunnel to accommodate an additional (proton) ring that was to have been located on top of the electron ring. Fig. 3.6–4 shows a cross section of the PEP tunnel as this was envisioned. Although the second ring was never built, it raises the interesting possibility of adding the APIARY low-energy ring in this location. If the new ring were prepared in advance, such that it could be installed during the same shutdown needed for reorienting the PEP dipoles and upgrading the PEP vacuum system, the incremental installation time would be minor. We estimate the required length of the shutdown to be about two years; the additional penalty for installation of a second ring simultaneously is thought to be only about six months.

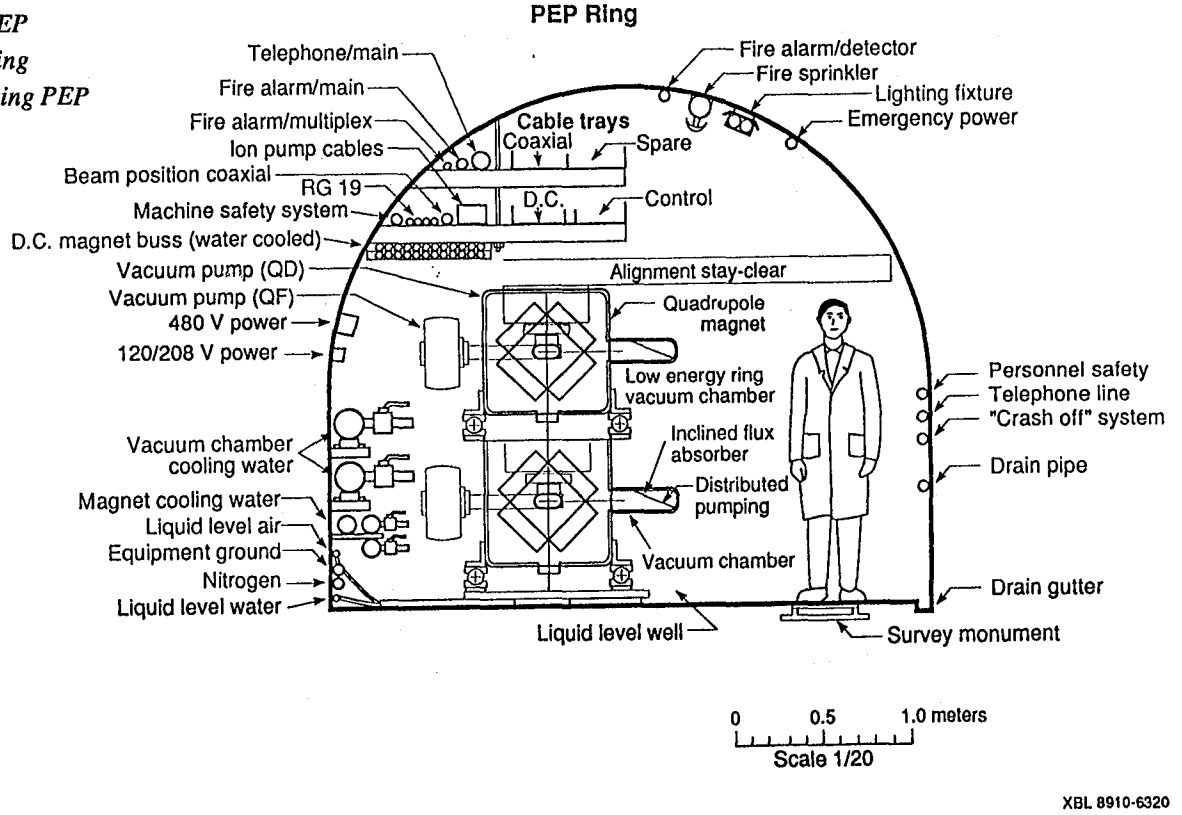

Fig. 3.6–4
Cross section of the PEP tunnel with a second ring installed atop the existing PEP ring.

Work is presently under way to explore a lattice design for such a ring. However, it is already clear that the damping time at 3.1 GeV for such a large ring would not be sufficient to avoid difficulties with the beam-beam interaction, so a lattice with wigglers to adjust the emittance and damping times would be

mandatory. We believe that such a wiggler-dominated low-energy ring will be required in any case, so this is not a disadvantage. For such a large ring, the required dipole field is rather low, which should permit the magnet and lattice designers a great deal of flexibility to optimize the ring design. In addition, the potential savings in conventional facilities are attractive.

Radiation from Wigglers

We showed in Section 2.2 the desirability of maintaining equal damping decrements in the high- and low-energy rings to minimize the effects of the energy asymmetry on the beam-beam interaction. To accomplish this, we envision the use of wigglers to create additional energy loss. The damping decrement for a storage ring can be written as

$$\lambda = \frac{T_0}{\tau_x} = \frac{U_0}{2E} \qquad (3.6\text{–}17)$$

from which it is clear that, for equal damping decrements, the required synchrotron radiation energy loss per turn for the high- and low-energy APIARY rings must simply scale proportionately to the beam energy in the ring. In the high-energy lattice (ρ = 165 m; E = 9 GeV), the energy loss is dominated by the normal bends, so we can obtain the energy loss from

$$U_0 = 0.0885 \frac{E^4}{\rho} \qquad (3.6\text{–}18)$$

which gives U_0 = 3.52 MeV/turn. For equal damping decrements then, we need an energy loss in the low-energy ring of

$$U_{0,+} = U_{0,-} \frac{E_+}{E_-} = 3.52 \left(\frac{3.1}{9.0}\right) = 1.21 \text{ MeV/turn} \qquad (3.6\text{–}19)$$

In the low-energy ring, we have a bend radius of ρ = 24.9 m, so, from Eq. (3.6–18), we have U_0 = 0.33 MeV/turn, i.e., only about one-quarter of the requisite amount. (To create the matched damping decrement from the bending magnets alone would require a bend radius of 6.75 m, which is impractical in terms of thermal power density.) In addition to this contribution, we must consider the synchrotron radiation

emission in the very strong vertical bends used to separate the two beams beyond the IP. For a total vertical bending length of L_V = 20 m, the energy loss from the two sets of vertical separation magnets in the IR can be estimated by scaling Eq. (3.6–18):

$$U_{0,V} = 0.0885 \frac{E^4}{\rho} \frac{L_V}{2\pi\rho} = 0.29 \text{ MeV/turn} \qquad (3.6\text{–}20)$$

(Note that this loss corresponds to more than 400 kW in each set of dipoles, so special vacuum chambers will be needed here as well as for the horizontal dipoles.) Thus, the lattice itself is contributing a total energy loss of 0.62 MeV/turn from the bending and separation magnets. To reach equal damping decrements, then, we must produce an additional energy loss of 0.59 MeV/turn from elsewhere. In the present lattice, we accommodate this need by including wiggler magnets in some of the straight sections.

At present, we envision two horizontal and two vertical wigglers, each with 5 periods of λ_W = 1 m, in each of four utility straight sections located symmetrically around the ring. The total length of wigglers is thus 80 m; for now, we assume equal lengths of horizontal and vertical wigglers, but this ratio will be refined during the conceptual design phase. For a wiggler field that varies sinusoidally along the beam trajectory, the total radiated power in MeV/turn is given by:

$$U_{0,W} = 6.33 \times 10^{-4} E^2 B_0^2 L_W \qquad (3.6\text{–}21)$$

where E is in GeV, B_0 is the peak field in T, and L_W is the wiggler length in m. With the requirements above, a wiggler field of B_0 = 1.1 T would be needed to provide the additional 0.59 MeV/turn to equalize the damping decrements.

As mentioned above, the wigglers will be located in four straight sections around the ring. At the full design current of 3 A, each will produce about 450 kW of synchrotron radiation power. This power must be dealt with externally to the ring vacuum chamber in specially designed photon beam dumps.

To see what the power density will be, we estimate the angular spread in the wiggler bend plane to be given by:

$$\delta_w = \frac{K}{\gamma} = 9.34 \times 10^{-3} \frac{B_0 \lambda_W}{\gamma} = 17 \text{ mrad} \qquad (3.6\text{–}22)$$

and in the non-bend plane to be

$$\psi = \left(\frac{\varepsilon_y}{\beta_y} + \frac{1}{\gamma^2} \right)^{1/2} = 0.22 \text{ mrad} \qquad (3.6\text{–}23)$$

At a distance 40 m downstream from the source point, the illuminated area is

$$A = D^2 \delta_W \psi = 236 \text{ cm}^2 \qquad (3.6\text{–}24)$$

and we have a thermal power density of $P_A = 450/236 = 1.9$ kW/cm^2. This is somewhat higher than would be comfortable to handle, but if the absorber is inclined at 20° to the incident photon beam the power density drops to 650 W/cm^2, which we feel is acceptable.

3.7. Synchrotron Radiation Masking and Beam-Pipe Cooling

Radiation Masking

Synchrotron radiation from the beam going through bending magnets and quadrupoles near the IP can be a possible source of background in the detector. To estimate this for the APIARY design, variants of the program QSRAD were used to trace beam-particle trajectories through the magnetic optics near the IP and tally the number of photons hitting various surfaces near the detector. The program EGS was then used to estimate the probability of scattering, or backscattering, into the detector region. For these simulations, nominal beam bunches of 1.59×10^{11} particles were assumed for both beams. The beam spatial distribution was taken to consist of a Gaussian profile with the nominal rms size, along with a tail having 7.2% of the primary beam intensity (1.15×10^{10} particles) in a Gaussian of 2.7 times the nominal rms value. Both components of the distribution were truncated at the 10σ level. (This model for the beam profile is based on experimental data from MAC at PEP.) The studies were done for two sources: radiation from the IR quadrupoles and radiation from the IR bending magnets.

Quadrupole Radiation

The geometry of the magnetic elements and masks located near the IP is shown in Fig. 3.7-1. The faces of the inner bending magnets are at ±20 cm, with an aperture that exceeds the beam-stay-clear dimension, taken here as 12σ for the nominal beam size.

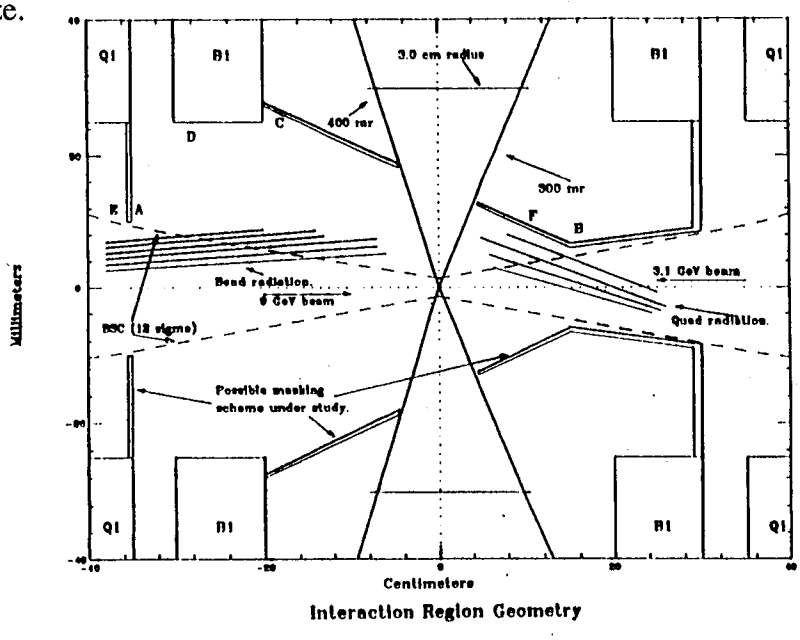

Fig. 3.7–1
Geometry of the magnetic optics near the interaction point. Tentative locations of masks are indicated.

We find that synchrotron radiation from the 9 GeV beam going through the innermost quadrupole doublet (QD1 and QF2) does not contribute to the detector backgrounds. The radiation from this source is confined to a cylinder with a 6-mm radius throughout the interaction region (±20 cm). Some radiation from the next set of quadrupoles (QD4, QF5, QD6) does reach the detector, but with relatively low intensity.

By contrast, we find that synchrotron radiation from the 3.1-GeV beam in the quadrupoles does pose some difficulties. If there were no masks inside of 20 cm from the IP, direct radiation could hit the detector beam pipe with a photon flux of about 10^7 photons per crossing. To shield the small detector beam pipe (3-cm radius, spanning ±10 cm from the IP) from this direct radiation, a mask having a 6-mm aperture radius is positioned where the 3.1 GeV beam enters the IP region (see Fig. 3.7-1). Direct radiation from the 3.1 GeV beam that hits the edge of the mask and the face of the mask on the downstream side of the IP can scatter, or backscatter, into the detector region.

Table 3.7-1
Preliminary estimates of background from quadrupole synchroton radiation (photons per crossing)

Scattering Surface[a]	Photons (> 4 keV) hitting surface	Solid angle to detector beam pipe (msr)	Second-surface reflection fraction	Photons incident on beam pipe
A	2.0×10^9	0.17	0.003	3
B	2.9×10^7	240	0.003	7
B direct	2.9×10^7	0.44	--	1
C direct	7.3×10^5	3.7	--	8
D direct	2.5×10^7	0.73	--	55[b)]
E	1.8×10^9	0.17	0.003	0.02

a) See Fig. 3.7-1.
b) This value can be reduced by using a sawtooth mask surface, which lowers the effective mask surface area by a factor of 10-100 and thus lowers the photon rate by the same amount.

Table 3.7–1 summarizes our results for the photon flux hitting the detector beam pipe. It is assumed that this pipe is composed of 500 μm of beryllium coated inside with 25 μm of silver; only 10% of the incident flux will be transmitted through such a pipe. To put the values in Table 3.7-1 in perspective, we note that 1 photon/cm^2 per crossing corresponds to roughly 1 Mrad/yr in silicon. This amount of exposure in a radiation-hardened device is considered to be tolerable. Thus, with the geometry presently envisioned, an acceptable rate would be about 5000 photons per crossing incident on the inside of the beam pipe, which is well beyond what we expect. More refined numbers require consideration of the details of the photon energy spectrum. Because these results are not yet based on an optimized IR design (from the viewpoint of radiation masking), it is expected that significant improvements will result from iterations between the IR optics and masking designs.

Dipole Radiation

Synchrotron radiation from the 9-GeV beam in B2 must be masked to prevent its hitting the beam pipe directly. This is done with a 10-mm mask at 35 cm, located on the inboard end of Q1 and a second mask (not shown in Fig. 3.7-1) at 70 cm. However, significant numbers of photons hit rescattering mask surface F in Fig. 3.7-1 and these have the potential to reenter the detector. Optimization of the beam separation bending magnets from the viewpoint of minimizing background has not yet been carried out, but is expected to ameliorate this source of background.

The results quoted here are presently very preliminary. Clearly, much work remains to be done to reduce the photon rate in the detector, and to provide adequate cooling for the masks.

Beam-Pipe Cooling

In a high-luminosity collider, the finite resistivity of the beam pipe will result in power of the order of 1 kW being dumped in the region of the detector, where the beam pipe must be of small diameter to allow precise vertex detection. The change in diameter of the vacuum chamber to reach beam-pipe radii of 3 cm in the interaction region will also result in higher-order-mode losses of comparable or greater size. These losses are absorbed

as heat by the beam pipe, so it is necessary to provide active cooling in the interaction region. This cooling system must not introduce a large amount of material in the path of the particles, as multiple Coulomb scattering in the beam pipe would then compromise the precision of vertex detection.

We have considered a variety of designs to cool the beam pipe. While we do not yet have a fully engineered solution, several approaches appear to provide sufficient capacity while meeting the constraint of a small amount of material. In collaboration with the Jet Propulsion Laboratory of Caltech, we have investigated a variety of design concepts, all based on coolant flowing in an annular region surrounding the beam pipe:

- Helium gas at atmospheric pressure
- Helium gas at five atmospheres
- Helium gas acting as a carrier for a water mist
- Transpiration cooling, in which a capillary layer of water, maintained on the outer wall of the vacuum pipe, is surrounded by a flow of dry helium gas
- Water

In addition, a heat pipe design has been studied. It appears that a simple system, based either on five-atmosphere helium or on water, will meet our needs. In all these studies, we have imposed the following boundary conditions:

- The temperature gradient along the 50-75 cm length of beam pipe is less than 10° C with a heat load of 2 kW
- The temperature difference between the inner and outer walls of the annulus is less than 20° C
- The total amount of material (excluding plating to absorb x-ray photons) shall not exceed the equivalent of 1 mm of beryllium

Extruded beryllium is commercially available in the appropriate diameters and length with 0.5-mm-thick walls. We are investigating whether thinner wall material can be obtained.

Although the effort to produce an engineered design is ongoing, it appears that adequate cooling of the beam pipe in a high-luminosity storage ring is a quite tractable problem.

3.8. Beamstrahlung

The radiation loss due to "beamstrahlung" (Bremsstrahlung caused by the mutual electrical and magnetic effects of two beams) can be characterized by the beamstrahlung parameter δ, which gives the fractional energy radiated by a single particle in the beam. For the APIARY collider, this energy is entirely in the classical regime,[32] since the upsilon parameter Υ, even for the 9-GeV beam, is much less than unity:

$$\Upsilon \equiv \frac{2\hbar\omega_c}{3\gamma m_0 c^2} = \frac{5}{6}\,\frac{\gamma r_e^2 N_B}{\alpha\sigma_\ell\sigma_y(1+r)} = 2.6\times 10^{-6} << 1 \qquad (3.8\text{–}1)$$

where α is the fine-structure constant and r is the aspect ratio. The beamstrahlung will be in the range of 10–100 keV, with a critical photon energy E_{crit} of 35 keV. The beamstrahlung parameter in this classical regime is given by[32]

$$\delta \approx F_1\,\frac{r_e^3 N_B^2 \gamma_0}{\sigma_x\sigma_y\sigma_\ell}\,\frac{4r}{(1+r)^2} \qquad (3.8\text{–}2)$$

where

F_1 = 0.22 is a form factor independent (to within a few percent) of the aspect ratio r,

γ_0 is the relativistic gamma factor of the radiating particle,

N_B is the number of particles in the opposing bunch, and

σ_x, σ_y, and σ_ℓ are the dimensions of the opposing bunch.

In our design, the average beam currents are the same, so N_B is the same for both rings. The value for the beamstrahlung parameter δ of the 9-GeV beam would then be about 6.39×10^{-8}, leading to a total beamstrahlung power of

$$P_{beamstr.} = \delta I\left(\frac{E}{e}\right) \approx 1.72\ \text{kW}$$

for round beams.

As expected, beamstrahlung is much less severe in the low-energy ring. The low-energy beam would have about one-third the δ of the high-energy beam and about one-ninth as much beamstrahlung power loss, regardless of the circumference.

The beam-disruption parameter D is given by[32]

$$D = \frac{r_e N_B \sigma_\ell}{\gamma \sigma_x \sigma_y}\left[\frac{2r}{1+r}\right] . \qquad (3.8\text{–}3)$$

Its value is about 0.3; in other words, beam disruption is modest and most of the beamstrahlung would be emitted ahead of the beams, fanning out only a few milliradians. A fraction of this radiation may hit the apertures of the superconducting quadrupoles, so their design would have to allow for this source of heating.

3.9. Injection System

APIARY will require high-energy, low-emittance sources of positrons and electrons suitable for filling the storage rings rapidly. Ideally, the filling time should be much shorter than the luminosity lifetime of the rings (which is set by the size of the low-energy ring). For the purpose of estimating the characteristics of the injection system, the maximum time for a complete fill of the positron ring is taken to be about 100 s. Because of the expected short luminosity lifetime, it is clear that a dedicated—and powerful—injection system is required. This linac could, subject to other demands, be the existing linac and damping ring complex used for SLC, or it could be a totally new system. Here we describe the design of a new linac system that basically duplicates the capability of the existing SLC injection system.

In the design of an injection system several choices must be made:

- Using linac injection at the full energy of each storage ring vs. using an intermediate booster synchrotron
- Using conventional linac technology vs. using high-gradient linacs plus GW-power rf sources (being developed for linear colliders) for accelerating electrons and positrons to high energy
- Using a conventional (non-superconducting) damping ring for cooling the positron beam vs. using a compact damping ring with superconducting dipoles

Given the challenges in the collider itself, and the need for very efficient and reliable injection to maintain a high average luminosity, it seems prudent at this stage to opt for proven technology wherever possible; this principle will generally guide our decisions.

Outlined below is a design concept for a fast injector using the proven technology routinely used at SLAC. This approach minimizes technical risk and forms a basis for comparison with other schemes using "advanced technology." The injection scheme uses full-energy injection from a linac with an intermediate accumulator ring to increase the capture efficiency in the high-energy linac and positron ring. Because ion effects on the stored electron beam are expected to decrease with increasing electron energy, the positrons are loaded into the

3.1-GeV ring and the electrons into the 9-GeV ring. Here, we focus mainly on the positron injection scenario, as that will be the performance limitation of the injection system.

The components of a system that will provide full-energy injection into the collider rings are illustrated in schematic fashion in Fig. 3.9–1.

Fig. 3.9–1
Components of a full-energy injection system for the APIARY collider rings (not to scale).

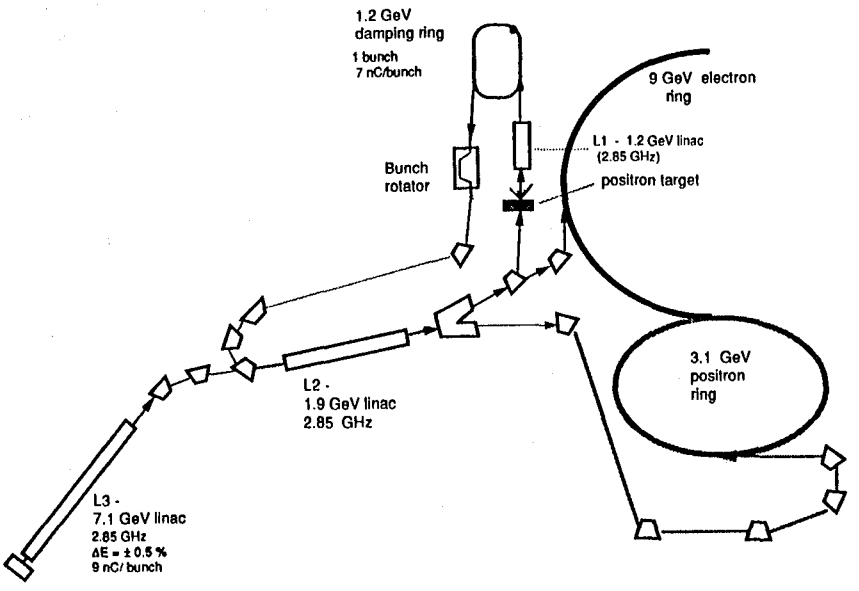

High-Energy Linacs

An electron beam of moderate brightness is produced with a standard SLC gridded electron gun and is subsequently accelerated to an energy of 9 GeV in a pair of conventional SLAC disk-loaded structures, L3 and L2 in Fig. 3.9–1, whose main characteristics are summarized in Table 3.9–1. The 1.9-GeV linac, L2, serves both to accelerate the positron bunches up to 3.1 GeV and to increase the energy of the electron bunches to 9 GeV. The beam exiting this linac passes through a passive dipole beam-splitter that directs the electrons to a pulsed dipole that switches the beam to the positron target or to the high-energy storage ring; accelerated positrons are sent directly to the appropriate storage ring.

Beam parameters	
Energy [GeV]	7.1
Repetition rate [Hz]	180
Particles per bunch	5.8×10^{10}
Number of bunches	5
γ_0	13 895
Emittance [m-rad]	7.2×10^{-9}
Accelerator parameters	
RF frequency [GHz]	2.856
Active length [m]	401.8
Gradient [MeV/m]	17.7
Fill length [m]	3.05
Fill time [ns]	849.1
Number of sections	132
Cavities/section	87
Structure efficiency	0.59
Total power [MW]	4180

Table 3.9–1
Operational characteristics of S-band linac

As Fig. 3.9–2 shows, the complete loading scenario for the 3.1-GeV positron ring, using single pulses from the linac, takes 110 seconds.

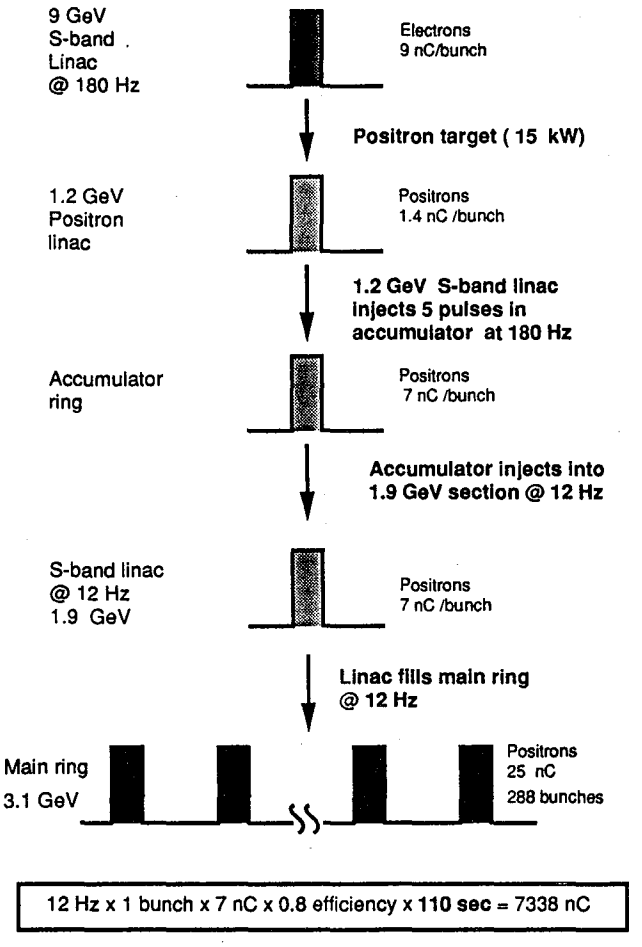

Fig. 3.9–2
Single-pulse operation during injection with an S-band linac.

Because the frequencies of the PEP rf system and the SLAC linac structure are not harmonically related, the simplest procedure is to operate the linacs in a mode in which a single bunch (with a charge of 8–10 nC) is accelerated with an energy variation of less than ±0.5%. The single-bunch loading in this operation is 2.3%. Power to the accelerating structure could be supplied by Type 5045 klystrons directly or it could be injected via SLED cavities to give higher peak power. The former choice would permit a long train of high-current bunches, whereas the latter minimizes the cost per MeV for single-bunch operation. Assuming the use of modulators identical to those now in use at SLAC, the repetition rate of the linac would be limited to 180 Hz. For now, we favor the SLED approach, since the rf frequencies of the linac and storage ring do not lend themselves well to true multibunch filling.

Positron Target

The filling time of the positron ring is ultimately limited by the design of the positron target. Here, the design of the positron production target follows that of the SLC positron source. The target itself is a water-cooled, high-Z (tungsten-rhenium) slab followed by a pulsed, high-field (5 T) solenoid to capture the positrons for injection into an S-band linac (L1 in Fig. 3.9–1). The linac, operating at 2.856 GHz, accelerates the positrons up to 1.2 GeV for injection into the damping/accumulator ring. As for the SLC system, the first 50 MeV of linac is operated at high gradient ($\approx$ 40 MV/m) and employs solenoidal focusing.

The beam load on the target during the filling period of the 3.1-GeV positron ring is approximately 15 kW—less than the full design value for the SLC source. Based on previous practice, it is possible to capture $\approx$ 0.05 positrons per electron per GeV in the acceptance of a low-energy linac. During subsequent handling of the positron beam, additional losses will reduce the effective positron yield by a further factor of three. Thus, the rate of producing usable positrons from the high-Z target is expected to be 16 nC/s per kW of incident electron beam. Present positron production targets have been designed to handle a beam power of 30-50 kW.

Given our aim of a conservative design for the injection system, we assume that a practical production target capable of handling 50 kW of beam power is possible using moving components. Nonetheless, a design for this power level is likely to be more costly than the 15–30-kW design that represents present SLAC experience. Even if the low-energy ring were enlarged so it would fit into the PEP tunnel, the power required at the positron target to maintain a suitably short filling time could be kept below 50 kW.

Accumulator Ring

Our choice for a fast accumulator/damping ring is similar to the 1.2-GeV SLC positron damping ring (see Table 3.9–2), which has conventional iron dipoles that operate at very high field (2 T). It is known that the broadband impedance, $|Z/n|$, of the SLC damping ring is suitable for accumulating about 5 nC of positrons without substantial bunch lengthening; a carefully designed vacuum chamber could produce even lower impedance and thus permit even higher currents. The normalized acceptance of the ring is well matched to the emittance of the beam from the positron linac, L1. As presently configured, such a ring can operate at 120 Hz and could be modified to run at 180 Hz. After 5 damping times ($\tau_e \approx 2.5$ ms), the accumulator ring is emptied into a pulse compressor, i.e., a bunch rotation section that we take to be a duplicate of the SLC bunch rotator. The bunched beam then feeds the linac, L2; the overall cycle rate for the process is 12–15 Hz.

Parameter	Value
Energy, E [GeV]	1.21
Radius, R [m]	5.61
Beam pipe aperture, a [mm]	12
Dipole fraction, F_m	0.36
Dipole field, B_{dipole} [T]	2.0
Normalized longitudinal emittance, ε_ℓ [mm]	200
Momentum spread, σ_p/p	7.54×10^{-4}
Bunch length ,σ_ℓ [mm]	5.8
V_{rf} [kV]	700
Energy loss/turn ,U_{loss} [kV]	92
Damping time, τ [ms]	2.45
Acceptance, ε_n [m-rad]	1×10^{-2}
Impedance required, $\|Z/n\|$ [Ω]	0.44
Horizontal tune, ν_x	7.29

Table 3.9–2
SLC damping ring characteristics.

Alternative Scenarios

If the aperture of the positron ring were sufficiently large, it might be unnecessary to use an intermediate accumulator. Indeed, if the filling rate of the positron ring must be increased (as in the case of a low-energy ring that resides in the PEP tunnel), then it is preferable to avoid the repetition rate bottleneck imposed by the damping ring and inject the storage ring directly from the linacs. Consequently, the positron ring must have sufficient aperture to allow direct linac injection of a considerably higher-emittance beam.

A modified layout (Fig. 3.9–3) shows the injection scenario without an intermediate ring. In this case, the first linac operates with SLED cavities at 6.4 GeV, whereas the second (2.6 GeV), linac operates without SLED in a long-pulse mode so that the positron pulses can be accelerated during the same linac rf fill as the electrons that produced them. In the absence of a damping ring, the transfer line from the 500-MeV positron linac L1 to the linac L2 must be designed to be isochronous as well as achromatic. By the time the positron beam reaches 500 MeV, the bunch will have an energy spread of ±2% and a normalized emittance of 10^{-2} m-rad—a value twenty times larger than the equilibrium normalized emittance of the beam in the 3.1 GeV positron ring.

Fig. 3.9–3
Injection scenario without an intermediate ring.

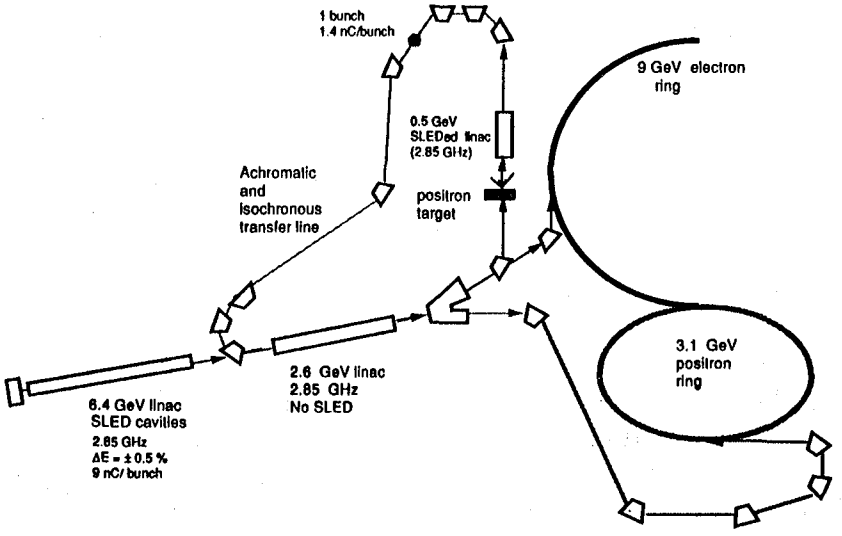

Using the scheme of Fig. 3.9–4, the positron ring can be filled in about 70 seconds. If the positron ring were increased in size to 2200 m (thus increasing the number of positrons required to fill it), this scheme could be used to fill the low-energy ring in 220 seconds; the filling time would decrease to 110 seconds if the modulators that feed the klystrons were redesigned to allow operation at 360 Hz.

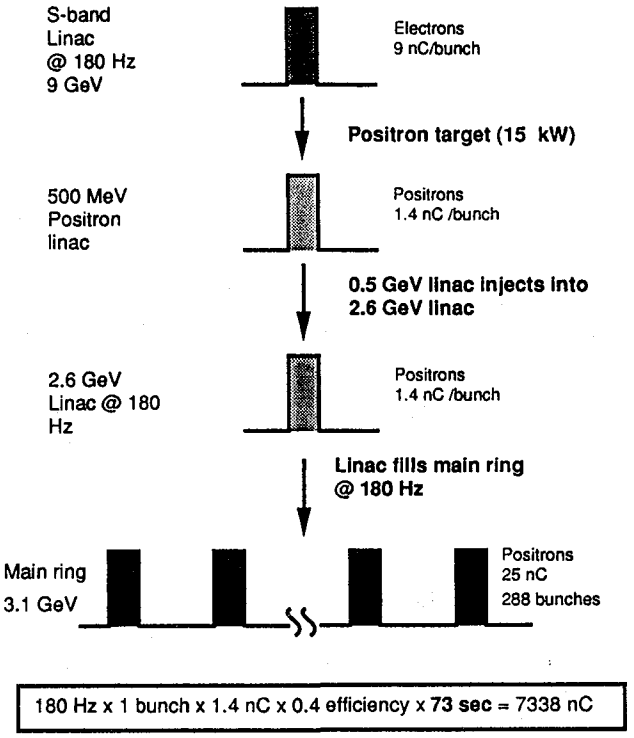

Fig. 3.9–4
Fill time without an intermediate ring.

Near the superconducting quadrupoles that surround the interaction region and through the small beam pipe region where the detector is located, the ratio R_a of the physical aperture of the positron storage ring to the rms beam size is about 10. As the emittance of the directly injected positron pulse will be roughly 20 times the natural equilibrium emittance of the 3.1-GeV ring (ε_X = 123 nm-rad), the injected beam size will be about four times larger than the equilibrium value. Thus, the aperture will be only twice the size of the injected pulse. Although the quantum lifetime of the bunch for R_a= 5 would be much longer than the damping time, at R_a= 2 a substantial fraction of the originally injected pulse would not survive the damping process.

It is not clear whether the loss of particles and the consequent spray of radiation (which will be greatest where R_a is smallest) will compromise the operational integrity of the superconducting quadrupoles and/or the detector. The possibility of increased beam loss near the detector also decreases the likelihood that the injection system will be able to "top off" the ring while the detector is operating.

Use of the SLC Linac

One can easily formulate an injection scenario for the PEP-based B factory using the main SLC linac, gun, positron source, and positron damping ring. (This possibility would only be practical if the B factory were given complete control of the system as the primary user.) A 100-s filling time is well within the capability of the existing hardware operating at 60 Hz. To serve this purpose, the SLC linac would require modifications to permit positron extraction at 3.1 GeV and electron extraction at 9 GeV.

Summary

From this initial analysis we conclude that existing technology can readily provide rapid filling of the APIARY positron ring in a period of about 100 seconds. In particular, the positron source can be readily scaled to high production rates while remaining well within the state of the art. Requirements for the system described here could be relaxed considerably if it were possible to top off the storage ring when the beam intensity falls below, say, 80% of the nominal value. Indeed, the most pressing technical challenge for injection may well be the design of a detector that can continue to operate while the storage rings are being topped off.

Although the system described here is suitable for a full-energy injection system for APIARY, a final evaluation of the cost and risks of the most conservative approach, using an accumulator, *vis-à-vis* the alternative of eliminating the intermediate damping ring, will require a cost-optimized, fully consistent physics design of all major components, including the lattices of both of the storage rings and the damping rings, and the optics for transfer beam lines will have to be matched to the characteristics of the rings.

3.10. Special-Purpose Hardware

To implement the APIARY collider outlined in this report, it will be necessary to design and fabricate some special-purpose, state-of-the-art devices. Foremost among these will be the feedback system, discussed in Section 3.5, and the superconducting quadrupoles, which we will discuss here. Although we have not yet invested any serious design effort into these magnets, we have investigated the magnet parameter specifications to get a feeling for their degree of difficulty to achieve. As we will see below, the triplet required for the high-energy ring is expected to be relatively straightforward, whereas the doublet required for the low-energy ring is more of a challenge. In both cases, the parameter that seems most difficult to work with is not the gradient, but rather the longitudinal separation distance between magnets.

High-Energy Ring

As described in Section 3.1, the IR of the high-energy lattice contains a pair of superconducting quadrupole triplets, located about 6 m on either side of the IP. Because of the relatively long distance of the quadrupoles from the IP, the beam size is increasing rapidly there, and the required focusing strength is therefore substantial. In the present optics, the following parameters have been taken for these magnets.

- Maximum gradient: 72 T/m (corresponding to 5 T at r = 69.4 mm)
- Magnetic lengths:

  74.4 mm (QD4)
  192.0 mm (QF5)
  121.0 mm (QD6)

- Separation between magnets: 250 mm

The gradient requirement was originally obtained by constraining the field at the edge of the aperture to be 5 T, along with a second constraint that the quadrupole aperture remain at least 10 times the rms beam size at its location (to avoid beam loss associated with the degradation of the quantum lifetime, as

discussed in Section 3.3). Although these parameters are not trivial, we note that they are quite similar to parameters of the low-beta quadrupoles now being constructed[33] for the Amy detector at TRISTAN. The Amy quadrupoles will have a gradient of 70 T/m, a "good field" aperture radius of 40 mm, a coil inner radius of 70 mm, and a magnetic length of 1.17 m.

In the APIARY high-energy-ring quadrupoles, the coil radius corresponding to the 69.4 mm aperture radius would be about 75 mm. Thus, the gradient and coil spacing that are required for our purposes are clearly compatible with existing technology. Indeed, the quadrupoles can be designed to meet the specifications listed above at a temperature of 4.5 K. Then, if necessary or desirable, the achievable gradient could be increased by reducing the operating temperature to 2 K. Alternatively, the capability of operating at lower temperatures could be considered as a performance safety margin at this stage.

One of the difficult aspects of the design of the triplet for the high-energy ring concerns the separation between magnets. At the present time, the available separation between the magnetic elements to accommodate the coil geometry is 25 cm. While this is probably sufficient, it would greatly simplify the engineering design of the magnets if a larger separation were permissible. If it were necessary to somewhat increase the spacing between magnets, the operating gradients could probably be increased accordingly to maintain the same integrated focusing strengths; this change should be relatively invisible to the lattice optics.

Low-Energy Ring

In the low-energy ring, the optics call for a superconducting quadrupole doublet, the closest member of which is only about 42 cm from the IP. Desired parameters for the magnets are summarized in Table 3.10-1.

	QD1	QF2
Gradient [T/m]	345	207
Normalized strength, k [m^{-2}]	-34.5	20.7
Field at edge of aperture [T]	5.18	5.18
Aperture radius [mm]	15	26
Magnetic length [cm]	14.5	16
Separation between elements [cm]	5	

Table 3.10–1
Preliminary specifications for the APIARY low-energy-ring superconducting quadrupole doublet

To examine the feasibility of these parameters, we studied this example design:

Coil inner diameter: 36 mm

Coil outer diameter: 83 mm

Coil configuration: 6 layers

Cable: 11 strands × 0.648 mm (0.0255 in.) diameter;
Nb-46%-Ti in Cu matrix;
Cu:NbTi ratio 1.3

Cable operating temperature: 2 K

Those cable parameters correspond to the standard SSC outer-strand specifications. Taking a simple coil shape of 30° per octant for an approximate calculation, we obtain the operating parameters summarized in Table 3.10–2.

	No saturation	Saturation
B_{max} [T]	9.1	8.7
G_{max} [T/m]	425	415
Overall current density [A/mm^2]	560	635
I_{ss} [A]	2985	3385
Operating current density [A/mm^2]	460	528
Operating current, I_o [A]	2452	2814
Operating gradient [T/m]	345	345

Table 3.10–2
Operating conditions for APIARY low-energy ring superconducting quadrupoles.

For this design, then, the apparent operating margin—defined as the ratio of the short-sample current, I_{ss}, to the operating current—is 3385/2814 = 1.20. In practice, of course, the margin will be reduced somewhat because of cable degradation, etc. Nonetheless, it appears that an operating gradient of 345 T/m is a reasonable and achievable goal.

We believe, however, that for a standard design the minimum space required between the two quadrupole magnets is roughly 8 cm (assuming that both coils share the same cryostat and that the ends can be suitably turned up). A detailed study will be required to determine a design for the magnet ends that simultaneously satisfies the needs for:

- Maximum field limit at the conductor
- Adequate mechanical support
- Acceptable field harmonics
- Minimum length

It is worth noting that the larger-bore member of the doublet (26-mm aperture radius) has the same field at the coil, but a lower current density. Therefore, its operating gradient could be somewhat higher if need be. Making this quadrupole stronger and somewhat shorter would be beneficial in alleviating the problems associated with the small separation between magnets. Another means to alleviate the separation problem would be to explore alternative focusing possibilities, such as ways to achieve the integrated focusing and defocusing effects of the quadrupole doublet in a single, continuous superconducting element. This approach is currently under study.

4. Major R&D Areas

Reaching the ultimate design luminosity of 10^{34} cm^{-2} s^{-1} will depend critically on successful R&D in a few major areas. These fall into two categories: technology issues and beam dynamics issues.

4.1. Technology R&D Issues

IR Focusing Optics. The required low-beta IR optics demands strong-focusing superconducting quadrupoles of special design in the low-energy ring. (Superconducting quadrupoles are also employed in the high-energy ring, but their parameters are rather similar to those of an existing design[33] at TRISTAN.) The quadrupole parameters call for a compact system with high pole-tip field (about 5 T). Permanent-magnet quadrupoles are often an attractive option, but are inadequate for this purpose. The individual focusing and defocusing quadrupoles in the IR are short, have small apertures, and are closely spaced, so the actual fields will be dominated by end effects. Design of such magnets will involve detailed three-dimensional field calculations. Afterwards, a careful analysis of the effects that the nonlinear fields produce on the particle orbits must be carried out.

Finally, it will be necessary to build a prototype and test it both in the laboratory and, to examine its behavior in a high-radiation environment, under beam storage conditions in PEP. As mentioned earlier, a simple and attractive solution may be the design of a superconducting doublet or triplet with continuous focusing in which the coils twist around azimuthally along the beam's path. The integrated focusing effect on the beam would be the same and such a design seems feasible.

RF System. The low-impedance rf system, which could be either room-temperature or superconducting, is another major area of R&D. Extensive electromagnetic field calculations and low and high power tests in an rf test stand would be required. Special emphasis must be placed on the design and testing of high-power rf windows, fundamental power couplers and HOM loading couplers. If power through the rf window were to turn out to be a significant problem, one might envision an

R&D program on *windowless* transmission of rf power through high-quality, high-vacuum waveguides (differentially pumped to isolate the cavity from the klystrons) straight into the cavity. The choice between a specially designed room-temperature rf system and one based on superconducting cavities can only be made provisionally during the conceptual design stage; a final decision would most likely follow only from the results of these R&D studies.

For the superconducting rf scenario, there are a number of other issues that will have to be addressed:

- Behavior of the system in the high synchrotron radiation environment in both rings
- Stability of the rf system under a situation of essentially 100% beam loading
- Cost and complications of cryogenics, etc.

The first step in any of these studies would involve a careful engineering design, fabrication and testing of a single-cell rf unit at 353 MHz, with both power and HOM couplers, and windows. Two such studies would have to be performed—one each for the room-temperature and superconducting versions.

Feedback System. Careful designs of high-sensitivity, broadband pickups and kickers for the feedback systems would have to be made. A low-power feedback system is already in the works at PEP. This system utilizes an existing 800 MHz cavity, de-Qed to damp 18 bunches.[34] Following design and fabrication, a high-power feedback system could be tested in PEP in the following configurations:

- 7 GeV with 2.3 A
- 11 GeV with 0.32 A

Both these configurations would lead to a synchrotron radiation power of 3 MW, which is compatible with the present specifications for the PEP rf system installed power and also with the vacuum-chamber radiation-handling capability. The vacuum chamber need not be replaced for these tests, although that step will be required for the ultimate operation at a luminosity of 1×10^{34} cm^{-2} s^{-1}.

Crab Cavity. If a finite-crossing-angle scenario were adopted for the final collider design, significant R&D would be required on the design and construction of a "crab cavity," which is necessary to eliminate the possibility of synchrobetatron resonances. Following a specific design, a small-angle and also a large-angle crab cavity would be built, and each tested both for its effectiveness and to measure whether the specified tolerances on amplitude and phase fluctuations have been achieved.

Vacuum chamber. Significant effort has to be spent on the design of high-quality vacuum chambers capable of handling large doses of synchrotron radiation power and of maintaining good vacuum in the presence of large beam currents. Special attention must be paid to improved cooling schemes and to the design of radiation outlet ports (e.g., for the very-high-power radiation from wigglers) that produce minimum electromagnetic disturbance (impedance) in the path of the beam.

IR Design. The design of the small beam pipe at the IP (required for vertex detection) must be carefully studied, as must the issues of radiation masking and cooling—both in the immediate IP region and in the magnets that bracket it. Extreme care and some degree of conservatism need to be exercised in the final design of these components.

4.2. Beam Dynamics R&D Issues

The main beam dynamics issue would revolve around the physics of the "beam-beam limit" (as it enters into the luminosity) for asymmetric colliders. The role of damping decrements and the question of round *vs.* flat beams are the most important issues to be considered. R&D can proceed mainly via detailed computer simulations, but controlled beam dynamics experiments in PEP will also play a crucial role. The computer simulations should include such features as:

- The realistic thick-lens effect of finite-sized bunches
- The non-Gaussian nature of the beams
- The possible coherent beam-beam modes, both high-frequency internal bunch modes and low-frequency bunch-to-bunch modes

It should be emphasized that our understanding of the beam-beam effect, as outlined in this report, is adequate for us to venture into a conceptual design of the collider. Indeed, it is likely that further detailed understanding will not come until after the collider is in operation. One exception to this, however, concerns the issue of round beams. *It will be crucial to devote PEP beam time to beam dynamics experiments to study the feasibility of creating round beams in the high-energy APIARY ring.*

Round beams in PEP could be achieved either by inserting a number of wigglers in artificially created vertically dispersive regions, or by adjusting the normal quadrupoles and possibly adding skew quadrupoles to the lattice, thus altering the coupling to give a round beam at the IP. Emittance coupling via a coupling resonance can also be pursued, although the introduction of such a systematic resonance structure would seem to be unfavorable from a beam-beam point of view. Experiments at different beam energies in PEP would also elucidate the role of the damping decrement in achieving a high beam-beam tune-shift limit.

Other beam dynamics efforts must focus on experimental investigations of multibunch instabilities and their cures, on the transverse mode-coupling instability, and on gymnastics with the PEP optics in general.

5. A Construction and Upgrade Program for a PEP-Based B-Factory

With an ultimate luminosity goal of 10^{34} cm^{-2} s^{-1} in mind, we envision a stepwise, strategic scenario of design, R&D, and construction that will lead to an initial implementation of a collider with 1×10^{33} cm^{-2} s^{-1} luminosity followed relatively quickly by improvements that give a luminosity of 3×10^{33} cm^{-2} s^{-1}. We would initially try relaxing the requirements in those areas where we are pushing the technology the furthest. Continuing R&D efforts, in parallel with construction of this initially relaxed machine and during its subsequent operation, would then allow for a final upgrade to a luminosity of 10^{34} cm^{-2} s^{-1} by replacing or upgrading specific hardware components in the machine; flexibility to accommodate these changes will have been built into the design. We outline here an example of one possible upgrade strategy.

The low-beta IR optics configuration is very strongly coupled to the design luminosity, and is not easily and smoothly tunable without significant changes. For this reason, we propose designing and implementing the IR optics optimized for 10^{34} cm^{-2} s^{-1} luminosity at the outset. The most important parameter that would define a "relaxed" startup ($\mathcal{L} = 1\text{-}3 \times 10^{33}$ cm^{-2} s^{-1}) would be the beam current; initially it would be only 1/10-1/3 of the ultimate goal. Reducing the beam current would cause a proportional reduction in all the effects that stem from synchrotron radiation and beam intensity—the root causes of the problems in cooling, vacuum, and rf systems that have pressed the technology the hardest.

Let us envision how we could achieve a luminosity of up to 3×10^{33} cm^{-2} s^{-1} without such technological improvements. The rings would each have to store about 1 A of current. This reduction in beam current would be accomplished by keeping the same current per bunch but reducing the *number* of bunches by a factor of three. The bandwidth required for the feedback system is then reduced from 60 MHz to 20 MHz.

The scenario envisioned for reaching the relaxed startup configuration depends to some extent on whether or not the low-energy ring is to be located in the PEP tunnel.

In the more likely scenario in which the low-energy ring is installed in the PEP tunnel, it would be necessary to make major modifications to the PEP hardware from the outset. For example, all of the present magnet stands would need to be lowered to accommodate the new ring (which we would place atop of the existing PEP ring, as shown in Fig. 3.6-4). In this case, it would be most efficient to make many of the longer-term modifications to PEP simultaneously.

To handle the ultimate beam current of 3 A, it will be necessary to reorient the PEP dipoles such that the open side of the C points towards the outside of the ring. A new dual-chamber vacuum system, specially designed to handle the heat load and gas-desorption vacuum load, would be installed at this time. Our present estimates indicate that the vacuum chamber in the straight sections between dipoles must also be specially constructed. This would involve replacing all the existing quadrupole and sextupole magnets in these regions with newly fabricated C-magnet designs.

A new RF system would also be installed during this major installation shutdown, although it would not be absolutely necessary to initially install all of the RF required for the full design luminosity. Alternatively, a room-temperature RF system could be installed at this time, to be replaced subsequently by a superconducting system if experience warranted it. Similarly, the feedback system installed initially could be a more modest system to handle only the 1-A beam current case. If the components were all available in advance, the installation of the new ring and the upgrade of PEP would proceed in parallel and could be completed in about 3 years.

If the low-energy ring were in a separate enclosure, it might be possible to initially keep PEP more or less as-is. The vacuum chamber would remain in place although more pumping would be needed. New rf and feedback systems and IR optics (including superconducting quadrupole doublets) would also be installed. In this relaxed mode, one could confidently use the low-energy ring with a modified room-temperature RF system, as described in this report, without any luminosity penalty. The vacuum chamber and vacuum system of the low-energy ring would have to be designed, however, with the ultimate high luminosity in mind.

With either scenario, an upgrade to a luminosity of 10^{34} cm^{-2} s^{-1} would require no changes in the 3.1 GeV ring.

Following the feasibility study presented in this report, one could immediately launch a conceptual design effort. Such an effort would, after considering the pros and cons, arrive at a definitive decision on head-on collision *vs.* crossing "crabwise" at an angle. The study would also consider the technical feasibility of constructing the low-energy ring in the PEP tunnel (which was built to accommodate an additional proton ring that was never installed). Such a scenario would be attractive from the cost, convenience and technology points of view. The choice between modified room-temperature RF and superconducting RF in PEP probably could not be made at the conceptual design stage and would have to await further R&D, but by the time of startup in the relaxed mode, one would know which option to choose. All during the construction phase, the effort on design and construction of a detector would proceed so it could be installed as soon as relaxed operation begans.

A possible program schedule for R&D and construction activities is shown in Fig. 5–1 for the preferred scenario in which the two rings coexist in the PEP tunnel.

Fig. 5–1
A Possible Schedule of Program for a PEP - based B-Factory R&D and Construction

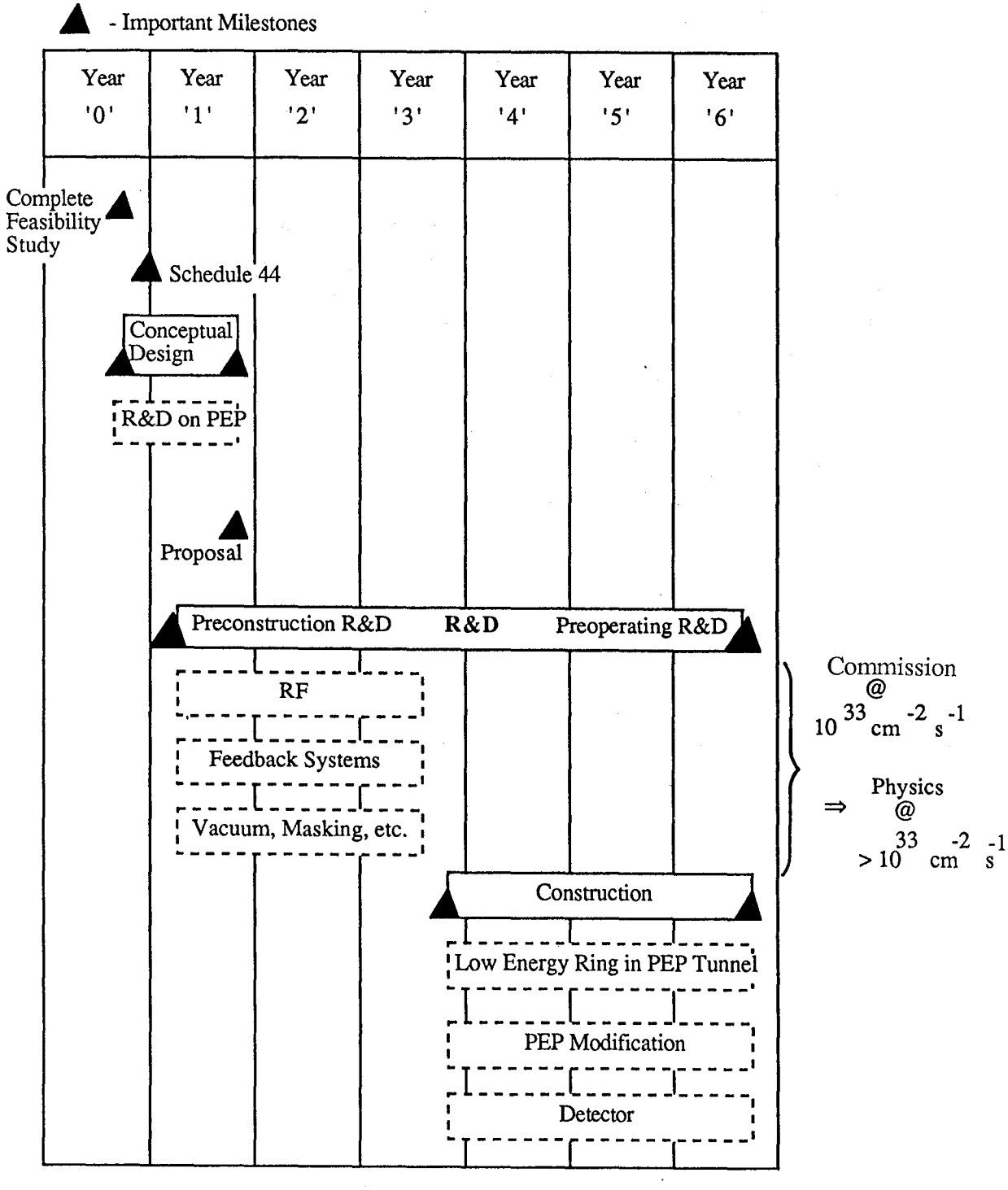

6. Conclusions and Outlook

In this report we have provided a feasible design scenario for an asymmetric B factory based on PEP at SLAC. The foundations of our approach are to utilize state-of-the-art storage ring technology, careful engineering, and a design philosophy that stresses flexibility. The concept outlined here permits the immediate design and subsequent construction of a collider capable of an initial luminosity of 1×10^{33} cm^{-2} s^{-1}, without requiring any undeveloped technologies. Thereafter we envisage a rapid evolution to a luminosity of 3×10^{33} cm^{-2} s^{-1}. Furthermore, the design has sufficient latitude for the collider to reach its ultimate luminosity goal of 1×10^{34} cm^{-2} s^{-1} with further development efforts.

The issues associated with the very high beam intensities required to achieve a luminosity of 1×10^{34} cm^{-2} s^{-1}, such as synchrotron radiation heating and photodesorption, and designs of the rf and feedback systems, have been given a considerable amount of detailed attention.

Radiation-induced heating and gas desorption, which together place severe demands on the design of the vacuum system, are challenging, but are amenable to sophisticated engineering solutions.

For now, we believe that the rf system could be either a specially designed room-temperature version or a superconducting design. The room-temperature design is simple and could be implemented immediately with some improvements in the power transmission capability of rf windows. A proof-of-principle cavity design for the superconducting cavity already exists, although some R&D would be required to validate it in a high-current application such as we are considering. Substantial engineering effort and attention to detail will be required in the design of the rf system in order to damp the higher-order modes down to a level where the growth times of coupled multibunch instabilities are no faster than 1 ms.

Assuming we are successful in damping the rf cavity modes to a sufficient level, the required feedback system, although demanding in terms of power, is quite feasible. We have explored a specific parametric design for the feedback system, and have shown that it can be implemented. These two aspects—rf and feedback—will unquestionably require the utmost care in the construction of a B factory.

If—as we intend—the low-energy ring is sited in the PEP tunnel, it would be prudent to implement the required modifications to the PEP ring right at the outset, as the low-energy ring is being built and installed. For a design employing a separate low-energy ring, the PEP vacuum chamber may not have to be replaced immediately to achieve a relaxed start-up at a luminosity of 1×10^{33} cm^{-2} s^{-1}. However, it would be necessary to replace the rf system and to implement a high-power feedback system in PEP.

The required superconducting quadrupole triplet in the high-energy ring can already be designed following similar ones built for TRISTAN, and the superconducting doublet for the low energy ring is considered to be achievable as far as gradients are concerned. In the case of the low-energy doublet, however, the mechanical problem of close spacing between the quadrupoles would require detailed engineering. An alternative approach here might be to try to alleviate the spatial problems by means of a special, continuously focusing design.

The injection system requirements could be easily met by the present SLC injector complex. If that is not available, a newly built, similarly designed conventional system would be adequate.

Given encouragement, support, and a dedicated team, we have every reason to have a good hope of success in completing such a challenging and potentially rewarding enterprise, which would be a major tool in a sustained B-physics program at SLAC.

References:

1. The Physics Program of a High-Luminosity Asymmetric B-Factory, SLAC-353, LBL PUB-5245, CALT-68-1588, October 2, 1989.

2. K. Berkelman, invited talk presented at the La Thuile Symposium, February 29-March 5, 1988.

3. F. Abe et al., "Proposal for Study of B-Physics by a Detector with Particle Identification and High Resolution Calorimetry at Tristan Accumulator Ring", KEK-Report 1988.

4. A. N. Dubrovin, A. N. Skrinsky, G. N. Tumaiki and A. A. Zholents, "Conceptual Design of a Ring Beauty Factory", EPAC Accelerator Conference, Rome, June 1988, vol. 1. p. 467.

5. "Proposal for an Electron Positron Collider for Heavy Flavor Particle Physics and Synchrotron Radiation," PR-88-09, July 1988, report from Paul Scherrer Institute, CH-5234 Villigen, Switzerland.

6. H. Nesemann, W. Schmidt-Parzefall and F. Willeke, "The Use of Petra as a B-Factory", EPAC Accelerator Conference, Rome, June 1988, vol. 1, p. 439.

7. D. Hitlin, "Requirements: High Luminosity Asymmetric B-Factory", Proc. Workshop On High Luminosity Asymmetric Storage Rings for B Physics, CALT-68-1552.

8. A. A. Garren et al., "An Asymmetric B-meson Factory at PEP", Proc. Particle Accelerator Conference, March 1989, Chicago; LBL-26982.

9. R. H. Siemann, "Simulations of Electron-Positron Storage Rings", CBN-89-4, May 1984. Invited paper at the Third Advanced ICFA Beam Dynamics Workshop on "Beam-Beam Effects in Circular Colliders", May 29-June 3, 1989, Novosibirsk, USSR.

10. S. Chattopadhyay et al., "On Damping Rings with Zero Momentum Compaction and Other Issues", Proc. ICFA Workshop on Low Emittance Beams, BNL, Upton, NY, March 20-28, 1987, BNL-52090.

11. C. Pellegrini, talk at the Workshop on B-Factories and Related Physics Issues, Blois, France, June 26-July 1, 1989.

12. K. Yokoya, private transmittal of Beam-Beam Simulation Code, written by himself, to our colleagues at LBL.

13. R. H. Siemann, "The Accelerator Physics Challenges of B-Factories", CLNS 89/938, August, 1989, Plenary talk at the XIV Int'l. Conf. High Energy Accelerators, Tsukuba, Japan, August 22-26, 1989.

14. H. Wiedemann, "Beam-Beam Effect and Luminosity in SPEAR", Proc. Beam-Beam Interaction Seminar, SLAC-PUB-2624, (1980).

15. S. Myers, Nonlinear Dynamics Aspects of Particle Accelerators (Berlin: Springer-Verlag, 1986, edited by J. M. Jowett, S. Turner and M. Month), p.176.

16. S. Chattopadhyay, "Physics and Design Issues of Asymmetric Storage Ring Colliders as B-Factories", invited Talk at XIV International Conference on High Energy Accelerators, August 22-26, 1989, Tsukuba, Japan. To be published in the proceedings.

17. M. A. Furman, "A Symplectic Coherent Beam-Beam Model", Proc. Third Advanced ICFA Beam Dynamics Workshop, May 29-June 3, 1989, Novosibirsk, USSR.

18. M. S. Zisman, S. Chattopadhyay, and J. Bisognano. 1986. ZAP User's Manual. Lawrence Berkeley Laboratory Report No. LBL-21270 (unpublished).

19. L. Z. Rivkin. 1987. Collective Effects in PEP. In Proc. of Workshop on PEP as a Synchrotron Radiation Source: 139-156. M. S. Zisman, 1987, *ibid.*:157-184.

20. M. S. Zisman, M. Borland, J. Galayda, A. Jackson, S. Kramer, & H. Winick. 1988. Study of Collective Effects for the PEP Low-Emittance Optics. Lawrence Berkeley Laboratory Report No. LBL-25582 and Stanford Synchrotron Radiation Laboratory Report No. ACD-Note 59 (unpublished). S. Kramer, L. M. Borland, J. Galayda. A. Jackson, H. Winick, & M. S. Zisman. 1989. Study of Collective Effects in a Low-Emittance PEP Lattice. In Proc. of 1989 Particle Accelerator Conference, Chicago, IL.

21. M. S. Zisman. 1988. Influence of Collective Effects on the Performance of High-Brightness Synchrotron Radiation Sources. In Proc. of JAERI-Riken Symposium on Accelerator Technology for the High-Brilliance synchrotron Radiation Sources, Tokyo, Japan: 311-346.

22. M. Sands. 1970. The Physics of Electron Storage Rings—An Introduction. Stanford Linear Accelerator Center Report No. SLAC-121. National Technical Information Service, Springfield, Virginia.

23. F. Porter. 1988. An Initial Parameter List for An Asymmetric e^+e^- Storage Ring B-Factory. California Institute of Technology Informal Note FCP-881130 (unpublished).

24. J. D. Jackson, Ed. 1986. Superconducting Super Collider Conceptual Design Report. SSC-SR-2020:168.

25. E. Haebel and J. Sekutowicz, "Higher Order Mode Coupler Studies at DESY", DESY M-86-06, July 1986.

26. D. Boussard et al., "Further Results From The Test of a 352 MHz Superconducting Cavity in the CERN SPS", CERN/EF/RF 88-3, 12 October, 1988.

27. D. Rubin, Talk on RF at the Workshop on B-Factories and Related Physics Issues, Blois, France, June 26-July 1, 1989.

28. G. Lambertson, "Electromagnetic Detectors", LBL-26075, 1989. Also presented at the Joint U.S.-CERN School on Particle Accelerators, Isola di Capri, Italy, Oct. 20-26, 1988.

29. G. Lambertson, private communication.

30. O. Gröbner et al., "Studies of Photon Induced Gas Desorption Using Synchrotron Radiation". Vacuum, vol. 33, p.397, 1983.

31. "1-2 GeV Synchrotron Radiation Source", Conceptual Design Report, July 1986, LBL publication, PUB-5172 Rev.

32. P. B. Wilson, "Future e+e- Linear Colliders and Beam-Beam Effects", SLAC-PUB-3985, May, 1986. Invited talk at the Stanford Linear Accelerator Conference, California, June 2-6, 1986.

33. K. Tsuchiya et al., "Superconducting Quadrupole Magnets for the Tristan Low-beta Insertion", 11th International Conference on Magnet Technology, Tsukuba, Japan, Sept. 25-29, 1989.

34. Internal note of PEP Feedback Group, "A Feedback System for PEP to Suppress Multibunch Instabilities", SSRL/SLAC, Version 1.1, June 13, 1989.

Appendix A
Energy Transparency Scaling Relations for IP Parameters

The choice of beam parameters is based on the simplifying assumptions that:

- Horizontal and vertical beam-beam tune shifts of both beams are all equal to a single specified value, ξ
- Both beams exactly overlap transversely at the IP

These assumptions lead to three important relations among energy, intensity, emittance, and β values, from which explicit expressions for emittance and luminosity can be obtained.

A.1. Equal-Energy Beams

The first assumption gives the relationship of the horizontal and vertical β function and emittance values. If the beams are identical, the tune shifts are given by

$$\Delta\nu_i = \frac{r_e \beta_i N}{2\pi \gamma \sigma_i (\sigma_x + \sigma_y)} ,$$

where $i = x, y$ and $\sigma_i = (\varepsilon_i \beta_i)^{1/2}$ (at the IP).

Equating the tune shifts in both transverse planes, $\Delta\nu_x = \Delta\nu_y$, gives the first rule:

$$\frac{\beta_y}{\beta_x} = \frac{\varepsilon_y}{\varepsilon_x} = \frac{\sigma_y}{\sigma_x} = r, \qquad \text{(A-1)}$$

where r is a constant.

A.2. Unequal Beams

Suppose that two unequal-energy beams, designated by the superscript j = (+,-), have beam sizes given by

$\sigma_i^j = (\varepsilon_i^j \beta_i^j)^{1/2}$.

Setting $\sigma_i^+ = \sigma_i^-$ gives the second rule:

$$\frac{\beta_i^+}{\beta_i^-} = \frac{\varepsilon_i^+}{\varepsilon_i^-} = b, \qquad \text{(A-2)}$$

where b is a constant and again i = x,y. The tune shifts are given by

$$\Delta\nu_i^j = \frac{r_e \beta_i^j N^k}{2\pi \gamma^j \sigma_i^k \left(\sigma_x^k + \sigma_y^k\right)},$$

where j = (+, -) and k = (-, +).

Equating the four tune shifts, $\Delta\nu_i^+ = \Delta\nu_i^- = \xi$, gives the third rule:

$$b = \frac{\beta_i^+}{\beta_i^-} = \left(\frac{\gamma^+}{\gamma}\right)\left(\frac{N^+}{N^-}\right) \qquad \text{(A-3)}$$

A.3. Emittance

An explicit formula for emttance is obtained from the tune-shift formula by replacing σ_i^k with σ_i^j:

$$\varepsilon_x^j = \frac{r_e N^k}{2\pi \xi \gamma^j (1 + r)}$$
$$\varepsilon_y^j = r\, \varepsilon_x^j \qquad \text{(A-4)}$$

A.4. Luminosity

For equal beam sizes, the luminosity is given by

$$\mathcal{L} = \frac{c\, N^+ N^-}{4\pi\, s_B\, \sigma_x\, \sigma_y} ,$$

where s_B is the bunch spacing. Substituting $\sigma_x\sigma_y = \beta_y\varepsilon_x$, and replacing N with the beam current, I (= ecN/s_B), we obtain the expression for the luminosity:

$$\begin{aligned} \mathcal{L} &= \frac{\xi\,(1+r)}{2\, e\, r_e} \left(\frac{I\cdot E}{\beta_y^*}\right)_{+,-} \\ &= 2.17 \times 10^{34}\, \xi\,(1+r) \left(\frac{I\cdot E}{\beta_y^*}\right)_{+,-} \quad [cm^{-2}\, s^{-1}] \end{aligned} \tag{A-5}$$

where I is in amperes, E is in GeV, and β_y is in cm. With the assumptions made here, the parenthetical expression in Eq. (A-5) can be evaluated with parameters appropriate to either beam.

Appendix B
Low-Energy Ring with Crab Crossing in the PEP Tunnel

As was mentioned earlier, there would be significant advantages and savings if the low-energy ring could be built inside the existing PEP tunnel. Here we report on a preliminary design in which the two rings have the same circumference and the beams collide at an angle instead of head-on. To avoid synchrobetatron resonances in this scheme, the technique of "crab-crossing" is necessary. Note that head-on collision optics using vertical bends would also be feasible if both rings were in the PEP tunnel; we will study this as well.

A head-on collision scheme poses some difficult (though not intractable) problems for the interaction region (IR) optics. For example, separation magnets must be placed close to the IR to peel the low-energy beam away from the high-energy beam before the high-energy beam enters its first strong focusing magnet; the low-energy beam cannot tolerate the focusing strength. This is a triple disadvantage: the separation fields cause synchrotron radiation to be emitted very close to the detector; the presence of the separation magnets forces the high-energy focusing quadrupoles to be placed further from the IR, making the beta functions larger; and, finally, the length of the separation system limits the closeness of the bunch spacing. The last problem could be especially worrisome; since the luminosity requirement determines the total current, a limit on bunch spacing would limit the bunch population, possibly forcing it to exceed any one of several instability thresholds.

A crab-crossing design, in which the IR optics are decoupled by a finite crossing angle, escapes all these pitfalls. However, some penalties are incurred. The most obvious one is the requirement for large-angle crab cavities, with their unwanted impedances and their possibly difficult voltage tolerances. Another is the need to create a complicated horizontal crossing scheme, since vertical crossing would impose serious limitations on the cavity tolerances.

Several other penalties, which are interrelated, also come into play. In order to keep the weighted transverse impedance of the crab cavities within reasonable bounds, the beta function must be suppressed at the cavities; as a result, β_x at the IP has to be large and the beam must be flat. This loses the advantageous factor of two (1+r) that is available for round beams, so β_y has to be reduced. This, in turn, forces a *very* short crab bunch and correspondingly high voltages. (A surprising consequence is that one needs significantly higher rf voltages in the low-energy ring than in the high-energy ring.)

Compensating advantages of the crab-crossing scheme are that the IR quadrupoles need not be superconducting and that the beams need not be excited vertically—the natural vertical emittance is acceptable and the collision process may behave in the way to which we have become acccustomed.

The design presented here has the same circumference as PEP and is meant to be installed in the PEP tunnel along with the high-energy ring. The crossing plane is horizontal and the crab angle θ_x is about 1.4° (25 milliradians). The tune shifts are the same as those chosen for the round-beam design. The optics at the IR are not radical—they are of the familiar flat-beam type—and they can be realized easily with adequate dynamic aperture. Optically, it seems to be a comfortable design.

The rf system is another matter. The frequency is 706 MHz and every bucket is filled. We are compelled to abandon the familiar frequency of 350 MHz in the interests of closer bunch spacing with correspondingly lower bunch populations and shorter bunches. The klystrons will be physically smaller, but the power density at their windows (and the cavity windows) will be higher.

Table B-1 summarizes the major parameters of the design for the ultimate luminosity of 1×10^{34} cm^{-2} s^{-1}. The crossing configurations of the two beams in the horizontal plane (plan view) and in the vertical plane (elevation) are shown in Fig. B-1.

	Low-energy beam		High-energy beam
Energy, E [GeV]	3		9
Circumference, C [m]		2200.027	
Luminosity, $\mathcal{L}$ [cm^{-2} s^{-1}]		1×10^{34}	
Tune shifts, ξ_x/ξ_y		0.05/0.05	
Beta function at IP, β_x^*/β_y^* [m]		0.50/0.01	
Current, I [A]	3.0		1.0
Natural bunch length, σ_ℓ [cm]	0.50		0.50
Energy spread, σ_p/p	8.1×10^{-4}		6.0×10^{-4}
Bunch spacing, s_B [m]	0.42		0.42
Particles/bunch, N_B	2.7×10^{10}		8.9×10^{9}
Emittance, ε_x / ε_y [m-rad]		$1.3 \times 10^{-8}/2.7 \times 10^{-10}$	
Synchrotron tune, ν_s	0.170		0.047
Momentum compaction, α	3.1×10^{-3}		1.1×10^{-3}
RF voltage, V_{rf} (MV)	34.2		21.3
RF frequency, f_{rf} [MHz]	706		706
Harmonic number, h	5184		5184
Longitudinal threshold, $\lvert Z/n \rvert_{eff}$ [Ω]	0.36		0.67
Energy damping decrement, T_0/τ_E	4×10^{-4}		4×10^{-4}
Crab angle, θ_x [mrad]		25	
Crab cavity frequency, f_x [MHz]		706	
Crab cavity voltage, V_x [MV]	1.4		2.5

Table B-1
Parameters of crossing angle design

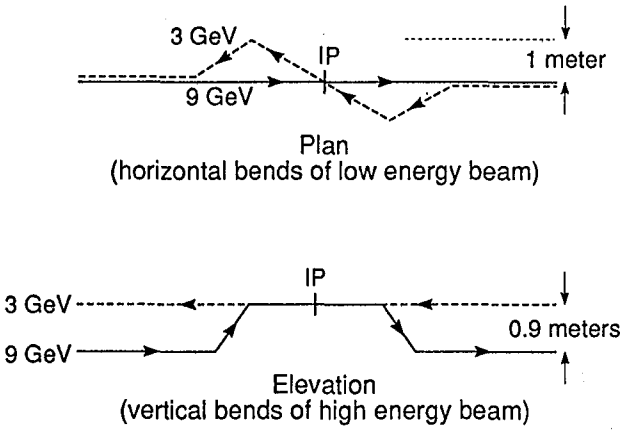

Fig. B–1
Crossing configuration of high and low energy beams in the horizontal plane (plan view) and vertical plane (elevation view), respectively.

The lattice functions (square roots of the horizontal and vertical beta functions, and the dispersion $D_{x,y}$) for half of the low-energy ring are shown in Fig. B-2; the same functions are shown in Fig. B-3 for one-twelfth of the high-energy ring.

Fig. B-2
Lattice functions for one-half of the low-energy ring.
Solid line: $\sqrt{\beta_y}$.
Dashed line: $\sqrt{\beta_x}$.
Dot-dashed line: D_x.
Dotted line: D_y.

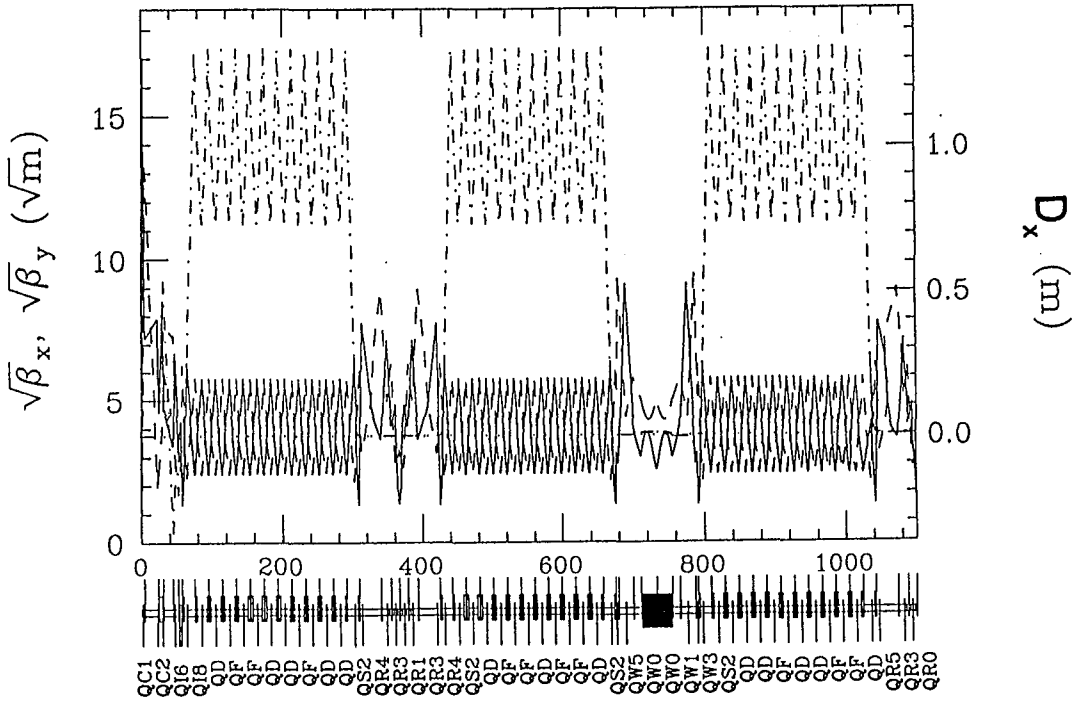

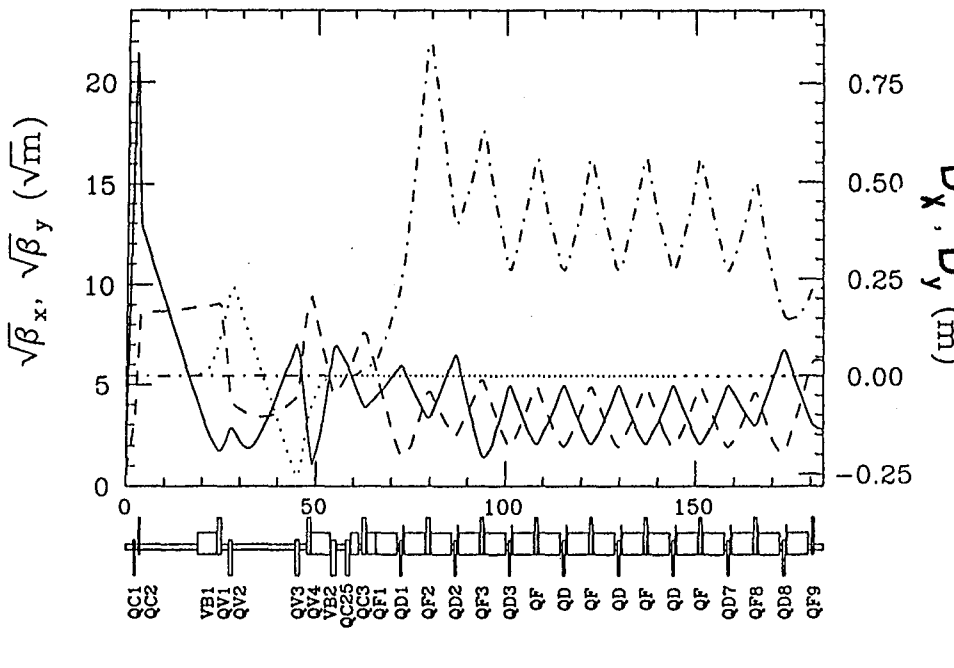

XBL 8910-7790

Fig. B-3
Lattice functions for one-twelfth of the high-energy ring.
Solid line: $\sqrt{\beta_y}$.
Dashed line: $\sqrt{\beta_x}$.
Dot-dashed line: D_x.
Dotted line: D_y.

In the large low-energy ring, one has the normal FODO optics matched to the IP optics and a wiggler region around 720 m from the IP. A closer look at the optics in the low-energy ring near the IP is given in Fig. B-4.

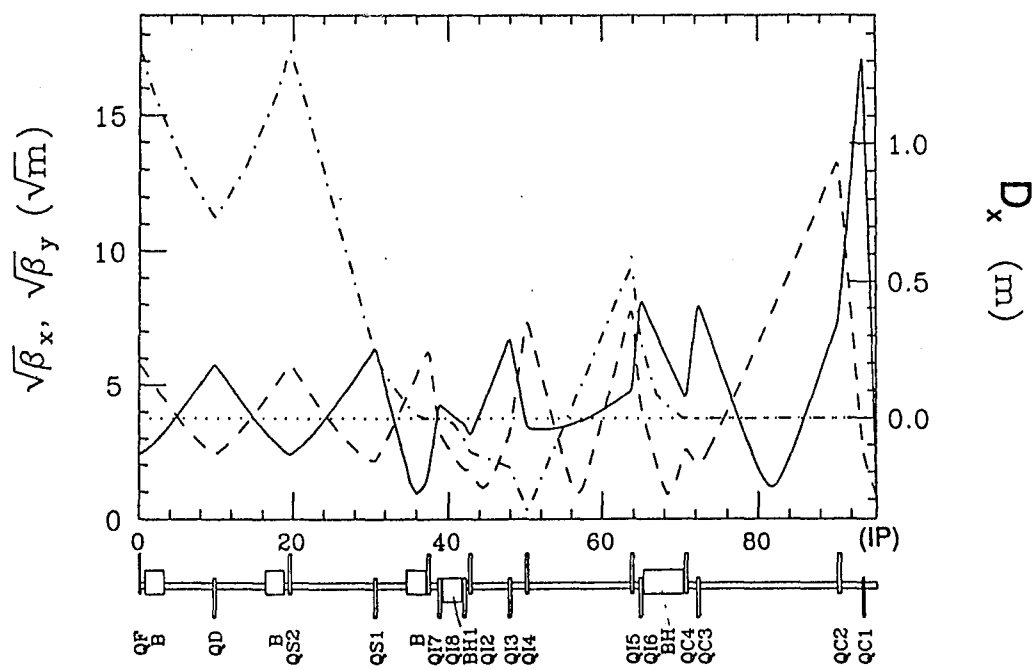

XBL 8910-7791

Fig. B-4
Optics in the low-energy ring near the IP. The bending magnets for the horizontal crossing are labeled BH and BH1
Solid line: $\sqrt{\beta_y}$.
Dashed line: $\sqrt{\beta_x}$.
Dot-dashed line: D_x.
Dotted line: D

Appendix C
Synchrotron Phase Damping

Consider coherent motion of the phase φ and energy deviation δE of the bunch centroid around φ_0 and ΔE_0:

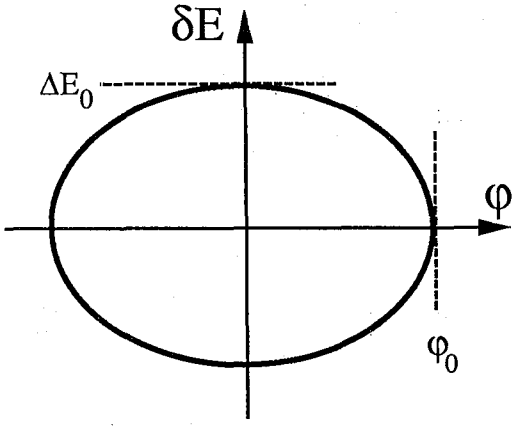

Equations of motion for phase and energy deviation, in the absence of feedback, are

$$\frac{d\varphi}{dt} = -\omega_s \frac{\varphi_0}{\Delta E_0} \delta E \qquad \text{(C-1)}$$

$$\frac{d(\delta E)}{dt} = \omega_s \frac{\Delta E_0}{\varphi_0} \varphi \qquad \text{(C-2)}$$

With feedback, we have an additional term

$$\frac{d(\delta E)}{turn} = \beta\varphi \quad , \qquad \text{(C-3)}$$

so the complete equation of motion in the presence of feedback is

$$\frac{d(\delta E)}{dt} = \frac{\omega_0}{2\pi} \beta\varphi + \omega_s \frac{\Delta E_0}{\varphi_0} \varphi \quad . \qquad \text{(C-4)}$$

In Eq. (C-4), β is the overall phase-to-energy gain of the feedback loop. Let the multibunch coherent motion be characterized by a complex frequency Ω, defined as $\Omega = \omega + ig$, such that

$$\delta E = E_0 e^{-i\Omega t} \quad . \tag{C-5}$$

From Eqs. (C-1), (C-4), and (C-5) we have

$$\Omega^2 = \omega_s^2 + \frac{\omega_s \omega_0}{2\pi} \frac{\varphi_0}{\Delta E_0} \beta \quad , \tag{C-6}$$

and

$$\omega^2 - g^2 + 2ig\omega = \omega_s^2 + \frac{\omega_s \omega_0}{2\pi} \frac{\varphi_0}{\Delta E_0} \left[\mathrm{Re}(\beta) + i\, \mathrm{Im}(\beta) \right] \quad . \tag{C-7}$$

For real β, there is no damping, but there is a coherent frequency shift of

$$\omega = \omega_s \left(1 + \frac{1}{2\pi} \frac{\omega_0}{\omega_s} \frac{\varphi_0}{\Delta E_0} \mathrm{Re}(\beta) \right)^{1/2} \tag{C-8}$$

The case of Re (β) < 0 corresponds to a phase delay. For Im (β) < 0, there is damping induced by the feedback, given approximately by:

$$\mathrm{Im}(\beta) \approx 2 \frac{g}{f_0} \frac{\Delta E_0}{\varphi_0} \tag{C-9}$$

Thus, the real energy gain per turn is given by:

$$\frac{d(\delta E)}{\mathrm{turn}} = \varphi_0 \, \mathrm{Im}(\beta) \approx 2 \frac{g}{f_0} \Delta E_0 \quad . \tag{C-10}$$

LAWRENCE BERKELEY LABORATORY
TECHNICAL INFORMATION DEPARTMENT
1 CYCLOTRON ROAD
BERKELEY, CALIFORNIA 94720